Characteristics of Impingement Diesel Spray

Adhesion on a Flat Wall

A THESIS

Submitted by

MOHD ZAID BIN AKOP

In partial fulfillment of the requirements for the award of the Degree of

DOCTOR OF PHILOSOPHY
IN
MECHANICAL SYSTEM ENGINEERING

Under the guidance of

PROFESSOR MASATAKA ARAI, Ph. D. Eng.

DIVISION OF MECHANICAL SCIENCE AND TECHNOLOGY
GUNMA UNIVERSITY
JAPAN

March 2014

Acknowledgement

Special thanks to my supervisor Professor Dr. Masataka Arai for his great guidance and support. Without his support this study could not have been done properly.

Declaration

I hereby declare that this submission is my own work and that, to the best of my knowledge and belief, it contains no material previously published or written by another person, nor material which has been accepted for the award of any other degree of the university or other institute of higher learning, except where due acknowledgement has been made in the text.

Signature:

Name: Mohd Zaid bin Akop

Student No.: 11812272

Date:

Table of contents

Chapter 1

Impinging diesel spray and its research problem

Chapter 2

Methodology of impinging diesel spray research

Chapter 3

Characteristics of spray impingement

Chapter 4

Impingement area and wall inclination effect on adhered fuel mass

Chapter 5

Weber number correlation on adhesion fuel

Chapter 6

Ambient pressure effect on adhered fuel mass

Chapter 7

Conclusions

List of publications

List of figures

ix

List of tables

List of abbreviations

CO_2	Carbon dioxide
DI	Direct injection
EGR	Exhaust gas circulation
HC	Hydrocarbon
H_2O	Water
HSDI	High spreed direct injection
NA	Natural aspirated
NO_X	Oxides of nitrogen
PDA	Phase doppler anemometer
PDPA	Phase doppler particle analyzer
PIV	Particle image velocimetry
PM	Particulate matter
PCCI	Premixed charge compression ignition
HCCI	Homogeneous charge compression ignition
PDS	Planar droplet sizing
SMD	Sauter mean diameter

Nomenclature

A_d	Impingement disk area	[mm^2]
$A_{d.critical}$	Critical area of disk	[mm^2]
A_{adh}	Adhered area	[mm^2]
$D_{d.critical}$	Critical diameter of disk	[mm]
D_d	Impingement disk diameter	[mm]
D_n	Nozzle hole diameter	[mm]
D_{SMD}	Sauter mean diameter	[μm]
h_{adh}	Average adhered thickness	[mm]
H	Height of post-impingement spray	[mm]
f_{press}	Correction factor for ambient pressure	[-]
k	Modification area factor	[-]
L_w	Impingement distance	[mm]
m_{inj}	Mass of a single shot injection fuel	[mg/injection]
m_{adh}	adhered mass	[mg]
$m_{adh.critical}$	Critical adhered mass	[mg]
N	Number of injections	[-]
P_a	Ambient pressure	[MPa]
P_{inj}	Injection pressure	[MPa]
V_{inj}	Injection velocity	[m/s]
V_{imp}	Impingement velocity	[m/s]
$V_{imp.n}$	Normal impingement velocity	[m/s]
$V_{imp.r}$	Radial impingement velocity	[m/s]
T_a	Ambient temperature	[°K]
$t_{critical}$	Critical thickness of liquid film	[mm]
t_{adh}	Thickness of adhered film	[mm]
t_{asoi}	Time after start of injection	[msec]
t_{ais}	Time after impingement start	[msec]
t_{is}	Time of impingement	[msec]
We	Weber number	[-]
We_{inj}	Weber number of droplet	[-]
We_d	Weber number of droplet at impingement	[-]
$We_{d.n}$	Weber number of droplet at normal impingement	[-]
$W_{s.imp}$	Spray width just before impingement	[mm]
Re	Reynold number	[-]

α_{adh}	Adhered mass ratio	[-]
β_{adh}	Adhered mass ratio with ambient pressure effect	[-]
θ_d	Inclination angle	[deg.]
ρ_{fuel}	Density of fuel	[kgm^{-3}]
ρ_a	Ambient density	[kgm^{-3}]
σ	Surface tension	[kg/s^2]
μ_l	Fuel viscosity	[g/mm-s]
μ_a	Ambient viscosity	[g/mm-s]
τ_{inj}	Injection period	[msec]

Abstract

Many researchers since last decade were looking forward on improving diesel engine performance with keeping low harmful emission. Wall impingement of fuel spray is known as the main contributor to direct injection high-speed diesel combustion, so it becomes an important factor in reducing diesel exhaust emissions. Since the combustion chamber in a diesel engine is too small to mix injected fuel and surrounding gas perfectly, wall impingement of the spray is considered to be inevitable in the engine. Non-evaporated spray research for basic understanding of spray behavior is conducted. The aim of this study is to clarify the fundamental characteristics of non-evaporated impinging spray and adhesion behavior of fuel by measuring the adhering fuel mass on a wall. In this study, a fuel injection system, a high pressure vessel and an image processing unit for impingement spray were used. Experimental investigations were carried out with various injection pressures from 40 MPa to 170 MPa and ambient pressures from 0.1 MPa to 4.0 MPa. The impingement distances were set from 30 mm to 90 mm and various sizes of impingement disk were used. The results show, the adhered fuel mass affected by impingement distances. The adhered mass ratio was inversely proportional to injection pressure. Regardless of injection pressure and impingement distances, it was found that the adhered fuel mass became constant with increasing the diameter of the impingement disk. Thickness of liquid film tended to decrease with increasing of injection pressure. Moreover, the adhered fuel mass ratio decreased with an increase of the inclination angle of disk. General modified adhered mass ratio was introduced to summarize the adhered mass with combinations of various impingement distances, disk sizes, inclination angles and injection pressures. Weber number which was calculated by approaching velocity of droplet to the impingement wall was more dominant factor than the Weber number obtained by droplet absolute velocity. However, the impingement of lower Weber number droplet produced thick film and adhered fuel mass was little influenced by the Weber number. From the results of experimental works, the empirical equations concerning the adhered mass ratio were derived. At higher ambient pressure and higher the injection pressure, adhered mass fuel tended to decrease. As for long impingement distances such as 70 mm and 90 mm, adhered fuel mass in high ambient pressure condition such as 4 MPa was half of that under 1 MPa condition. Finally, it was found that the adhered mass ratio could be correlated by using Weber number and Jet number.

Chapter 1

Impinging diesel spray and its research problems

1.1 Introduction

Over the last decade, study and research on diesel spray have progressed significantly. Many research works have been performed by automotive engineers to improve the performance of diesel engines and to reduce the exhaust emissions as well as fuel consumption.

In a high-speed DI diesel engine, behavior, structure and characteristics of diesel spray have been investigated by many researchers **[1, 2, 3, 4, 5, 6, 7, 8, 9, 10, 11, 12, 13, 14]**. From the viewpoint of spray combustion in the piston cavity, spray impingement on a cavity wall and fuel film adhering to its wall surface have a strong influence on combustion processes, engine performance and also characteristics of diesel exhaust harmful emissions. However, there are a few studies on impinging diesel spray with regard of adhering fuel on the cavity wall. Then it is necessary to understand the effect of fuel adhering when the spray impinges on the cavity wall.

In this chapter, various aspects of impinging diesel spray available in current literatures are reviewed in order to have a better understanding of the impinging diesel spray on the wall. Also, the adhering fuel, which is formed when the spray impinges to a wall, is discussed as an important factor in wall impingement spray. Furthermore, an understanding of the impinging diesel spray mechanisms is crucial for finding the best way on improving engine performance as well as reducing emissions which occurred in the combustion process. The information and knowledge obtained from literatures could give a clear view of the impinging diesel spray in this study.

1.2 General views of diesel spray

1.2.1 Diesel sprays in the combustion process

Figure 1-1 shows the block diagram of the diesel combustion process **[15]**. In the figure, it shows that the primary factor which control the combustion process is coming from the mixing process between injection system, air swirl and

turbulences in the cylinder, and spray characteristics. The spray characteristics control the vaporizing characteristics and the ignition delay characteristics and finally give a great influence on the combustion process and also the exhaust emissions.
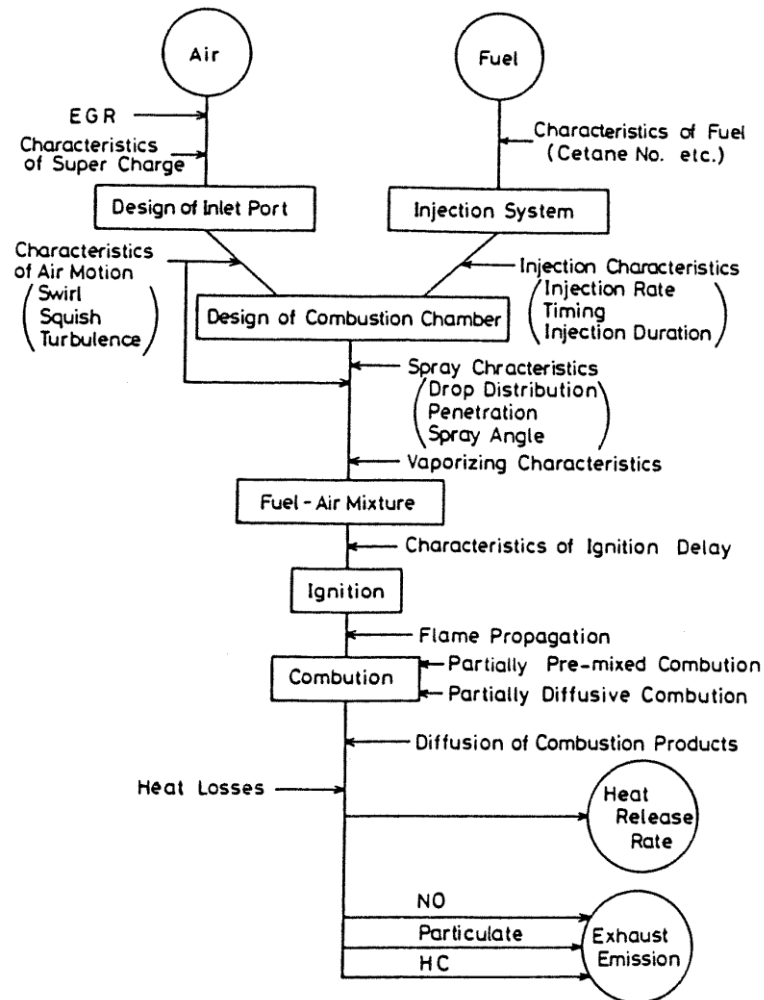
Figure 1-1 Block diagram of diesel combustion **[15]**

Figure 1-2 shows the diesel spray combustion and its behavior in DI diesel engine **[16]**. First process of diesel spray formation was atomization and followed by mixing process between fuel and air. The short break-up length, high swirl, high squish and wide spray which produced from small hole nozzle and high injection pressure, could promote better distribution of spray as well as the rapid atomization of spay. The rapid atomization of spray is needed in order to have good engine performance and also less exhaust emissions from the combustion chamber.
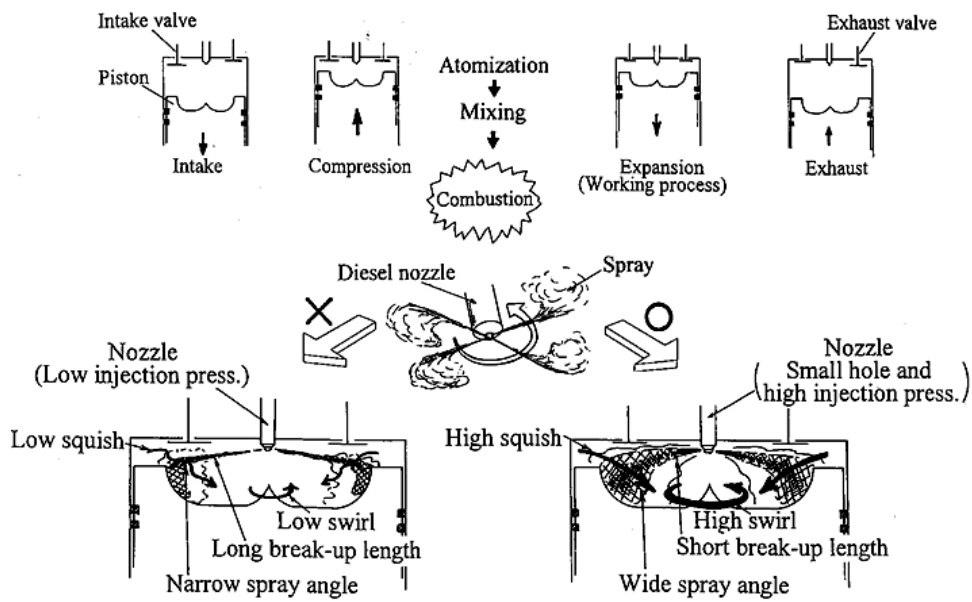
Figure 1-2 Diesel spray combustion in DI diesel engine **[16]**

For better understanding of the spray characteristics, **Fig. 1-3** shows the characteristic parameters of a diesel spray and also well known as macroscopic parameter **[17]**. Those parameters shown in **Fig. 1-3** are the important parameters in free spray and they are related to each others. The movement of the spray tip and break-up length gives clues to understand the disintegrating process of a fuel jet. Spray angle and droplet size are the result of the disintegrating process. A wide of spray angle usually meant the spray having a short breakup length and short core of spray, while narrow spray angle resulted to long breakup length. The adhesion of fuel on the wall normally occurred from the long breakup length condition. As shown in **Fig. 1-2**, a spray with long breakup length resulted in high HC and PM emissions. Diesel spray was a spray which droplet size distribution was in a range around few micrometers to 40 micrometers. The mean droplet size of spray or so called Sauter mean diameter (SMD), represent as the volume-surface mean diameter of spray. The SMD was one of the representative mean diameter and very popular in diesel spray study. It was very important in estimating the size of droplet for better understanding of the evaporation process. Turbulence also counted as one of the important parameters where it was usually activated mixing and evaporation in periphery region of the spray. Further, the intensities of the turbulence was more important in order to promote combustion process inside the spray.
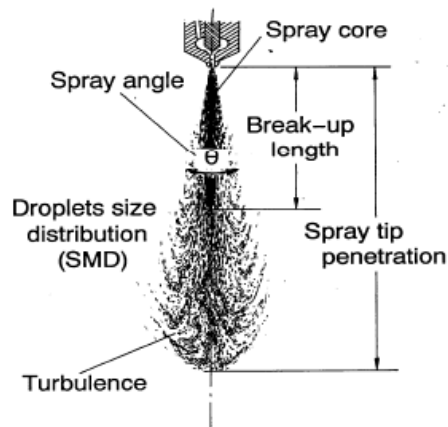
Figure 1-3 Characteristics parameter of diesel spray **[17]**

Structure and shape of impinging spray had been described by Katsura et al. **[18]** as shown in **Fig. 1-4**. They described the impinging spray was separated by two parts namely as unimpinged part and impinged part. An unimpinged part was similar as a free spray structure as shown in **Fig. 1-3** but impinged part was somehow different. The impinged part was divided by several regions. In the wall main jet region, the spray velocity decreased after impingement and also high droplet density appeared along the impingement wall. Stagnate region that occurred at the edge of impinged part due to droplets in the periphery regions, were pushed upward and resulted to loss of momentum. Also, the wall jet vortex phenomena appeared at a peripheral region of the impinging diesel spray. In this region, the density of droplets was large and turbulent mixing occurred between spray and surrounding gas. In this region also, the spray height could be measured for further impingement spray analysis **[18, 19, 20, 21, 22]**.

As described above, both of free spray and impingement spray are heterogeneous in their structures and shapes. In a practical diesel engine, since very short time is allowed for mixing and combustion process between injected fuel and air, the lack of homogeneity in the carburetted mixtures, and the heterogeneity and rapid variations in the temperature do not allow for the ideal combustion process. It would be worse when the adhering fuel deposited on the piston or cavity wall. Adhered fuel caused to the incomplete combustion of hydrocarbons results in the formation of a wide range of harmful gaseous components. Thus, more homogenous spray structure is required for complete combustion in the engine and also for developing advanced combustion system.
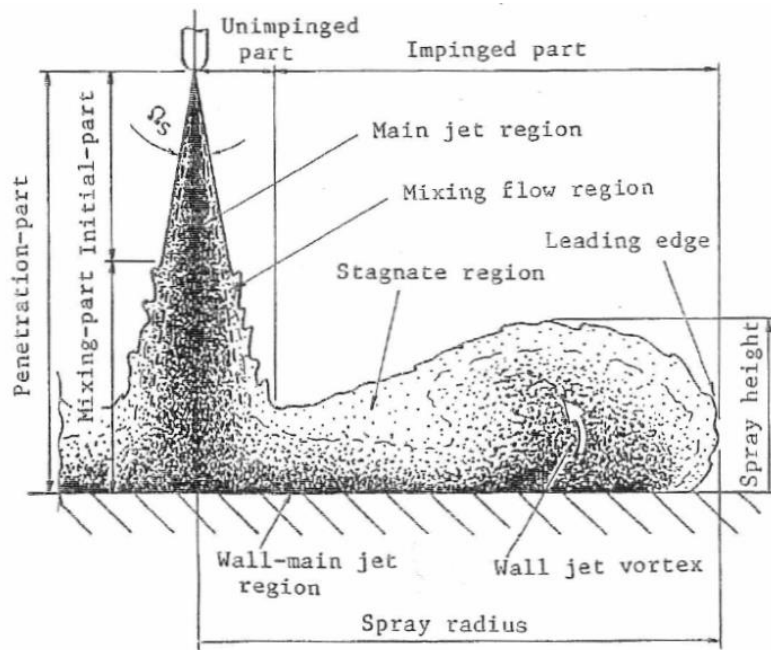
Figure 1-4 Structure and shape of impinging diesel spray **[18]**

1.2.2 Wall impingement and its spray-wall interaction

(a) Wall impingement

Recently the combustion chamber in a diesel engine tends to be small in order to reduce fuel consumption, and injection pressure tends to increase as compared with a conventional diesel engine. Wall impingement of the spray might occur due to downsizing of the engine and high pressure of fuel injection, and unevaporated diesel fuel was adhered on the wall of cavity. The impingement spray causes the emission of hydrocarbon (HC) and soot from the diesel engine. Therefore it is important to understand the spray-wall interaction and adhesion characteristics of impingement diesel spray.

Ko and Arai **[23]** had investigated the characteristics for pre- and post-impingement diesel spray by analyzing the spray penetration and also the spray volume. As shown on **Fig. 1-5**, the horizontal solid lines in the figure indicate the wall distance from the nozzle tip. Obviously we can observe that the penetration rates had the same growth pattern for all wall distance cases except for the free spray cases. At the impingement distances $L_w = 10$ mm, the slope after impingement was steeper than the others impingement distances. It shows, that the shorter impingement distance, the higher momentum of droplets and resulted to the high energy transfer during rebound. Kim et al. **[24]** investigated the

5

penetration length of sprays under non-evaporating condition and injection pressure from 40 MPa to 100 MPa. They found that almost similar trend of spray path penetration as **Fig. 1-5**.

Volume of wall impingement sprays is shown in **Fig. 1-6 [23]**. The spray volumes of L_w = 30, 50 and 70 mm show almost the same values even though there were small differences between these values. Results also show that the spray volume for all impingement cases are higher than free spray case. They concluded that, the volume of spray could be increased more than free spray case if the spray broke up before impinging on the wall. It was also reported by Tsunemoto et al. **[25]** that the spray volume and area which contacting with air were increased by spray impingement. However, in case of projected area, spray did not changed in volume and area that contacting with air. Tanabe et al. **[26]** studied the behavior of impinging spray onto projection of the flat wall. They reported that penetration length and the spray height was increased by increased of nozzle opening pressure.
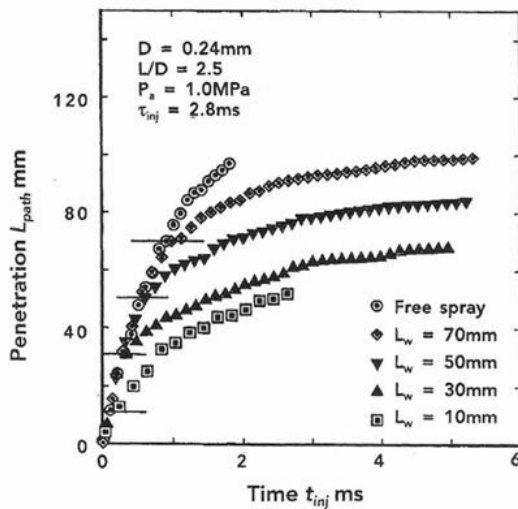
| **Figure 1-5** Penetration of | **Figure 1-6** Volume of wall |
| wall impingement sprays **[23]** | impingement sprays **[23]** |
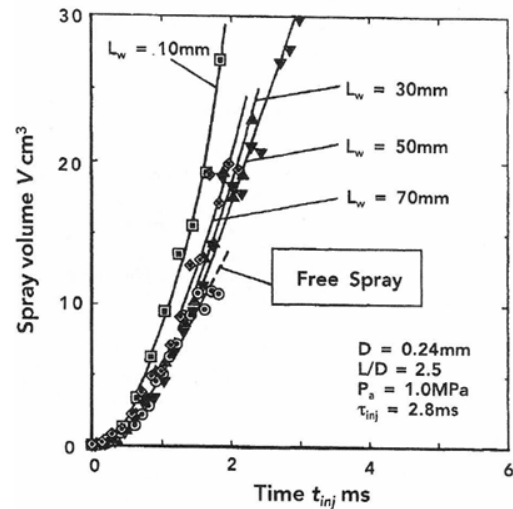
(b) Impingement spray behavior

Montajir et al. **[27]** measured the development of spray near the cavity wall in a combustion chamber geometry. Effects of the spray development in the chamber were investigated based on wall distance from the nozzle tip, shape of the cavity entrance, position where spray impinges on the wall, and so on. They found

that the combustion chamber with round lip and optimum wall distance gives better fuel distribution.
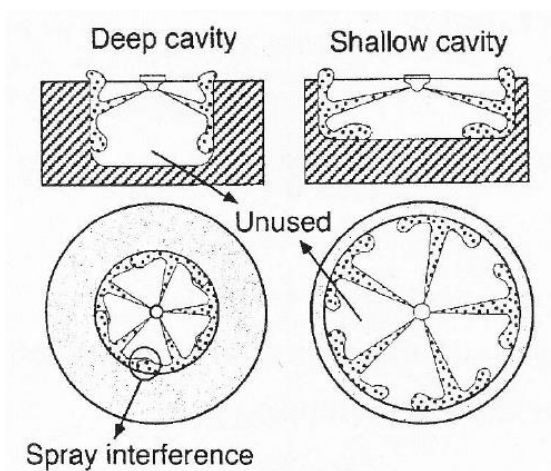
Figure 1-7 Effect of cavity size on spray development **[27]**

As shown in **Fig. 1-7**, they also suggested that, shorter wall distance (deep cavity) could cause to interference between the injected sprays, while too long wall distance (shallow cavity) could create un-used space between two neighboring sprays. Thus, the optimum of wall distance is important in order to get a minimum adherence of spray on cavity wall.

Katsura et al. **[18]** pointed out that by shortening the impingement distance, the droplet density becomes higher and changed accordingly along the wall. Zurlo et al. **[28]** was measured the droplet size distribution of post impingement spray by using polarization ratio measurement technique. They reported that droplet size was smaller when closed to the wall compared to the droplet far from the wall. Another researcher **[29]** investigated the effect of wall distance on the SMD of the post impingement spray. They found that as the impingement distance decreasing, the SMD of the post impingement spray became smaller. By using Exciplex Fluorescence Method, Senda et al. **[30, 31]** proposed 2-D images concerning the concentration distribution of vapor and liquid phases which acquired simultaneously. The observed vapor phase growth upward clearly from the wall to the periphery region while the liquid phase expanded mainly along the wall in the radial direction. Then, it was found that small droplets near the tip of the liquid phase evaporated rapidly due to the hot ambient surroundings, and then the evaporated fuel mixed and diffused with the surroundings.

Arai et al. **[32]** conducted a multi-stage spray with three split sprays at one injection. They suggested the total volume and mean equivalence ratio were affected by the injection interval between split sprays. Almost similar

7

investigation from Arai et al. **[33]** and Nishida et al. **[34]** on the diesel spray with split investigation. They reported that, mass measured from the second stage of injection was large compared to the mass that was measured in interval between the first and second stages of injection.

Since the diesel spray was not necessarily to impinge vertically to the wall of the engine cylinder, effect of the inclination angle of impingement became important for the impingement of a diesel spray. Arai **[35]** reviewed many kinds of diesel spray impingement phenomena including combustion of impingement diesel spray to an inclined wall. As for inclined diesel spray impingement, Fujimoto et al. **[36]** investigated the effect of impingement distance, injection pressure and ambient pressure on characteristics of inclined impinging diesel spray. They found that higher downward flow of spray became appearing when increasing the inclination angle wall.

Ebara et al. **[37, 38]** estimated the spray penetration under the effect of inclined wall impingement. According to them, as the inclination angle increased the spray path penetration became shorter compared to the free spray. They concluded that, mixing process between spray and surrounding was promoted in the cases for larger inclination angles (like normal impingement). However, they were not discussed the effect of inclined wall on the flow of impinged spray along the wall.

Further they enhanced their research on the inclined impingement spray by used of image analysis visualized by YAG laser sheet **[39, 40]**. Skeleton images had been introduced by them in order to discuss the effect of wall distance and inclination angles on high density of the spray zone. **Figure 1-8** are the example of the effect of wall angle on a skeleton spray. Effect of wall distance on the skeleton images was clarified in **Fig. 1-9**. It was observed that liquid column impinged on the wall and high density of spray layer occurred for short impingement distances such as L_w = 10 and 20 mm. They suggested that the high density zone occurred due to roll-up motion of the spray layer on the wall surface. Besides, at L_w = 30 and 50 mm, the high density zone distributed along the some height from the wall. They considered that spray completed the breakup process during impinging on the wall.
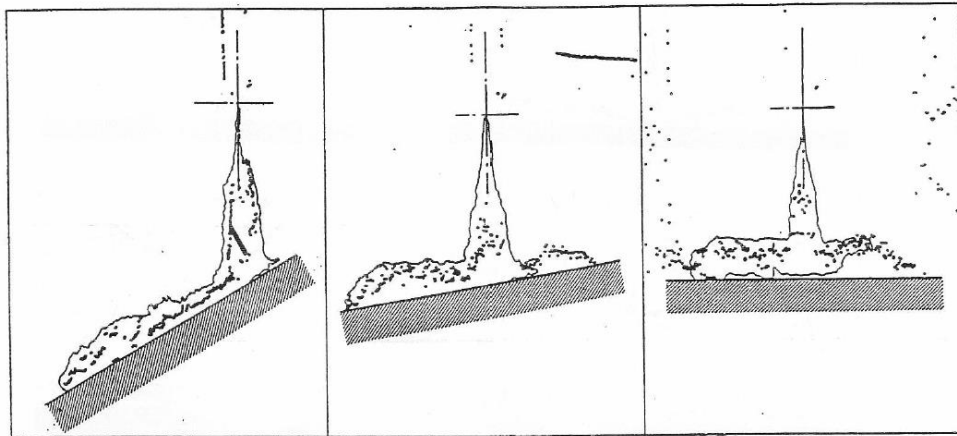
Figure 1-8 Effect of wall angle on a skeleton spray **[40]**

(a) L_w = 10 mm   (b) L_w = 20 mm

(c) L_w = 30 mm   (d) L_w = 50 mm
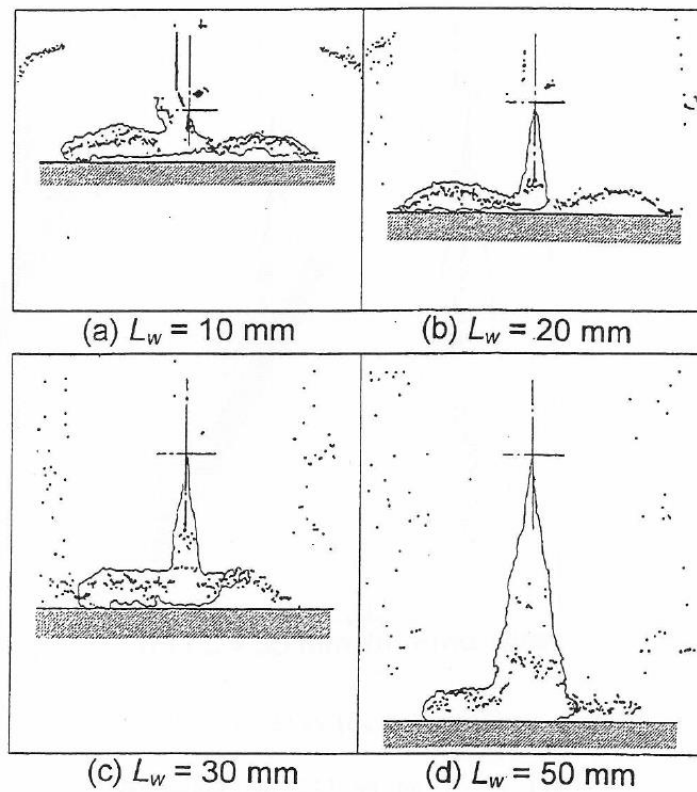
Figure 1-9 Effect of wall distance on a skeleton spray **[40]**

Ishikawa et al. **[41]** pointed out that the impingement location of a diesel spray had a strong influence on engine emissions, because impingement fuel mass and spray behavior after impingement were strongly related to the impingement location. Sakane et al. **[42]** investigated the behavior of non-vaporizing diesel spray impinging on a flat wall by shadowgraphic image analysis. They reported

that the mixing between fuel and surrounding gas was promoted by spray impingement, thus the ambient gas quantity entrained into spray was increased.

(c) Impingement droplet and its Weber number

As a fundamental experimental study, Wachters and Westerling **[43]** investigated the behavior of a water droplet impinging vertically on a flat wall of hot temperature and suggested that the Weber number of the impinging droplet had a direct effect upon the droplet reflection. As based on Wachters and Westerling **[43]** works, Senda et al. **[44, 45]** introduced impingement model which used to predict the secondary atomization of impinging droplet.

Senda et al. **[44]** in their modeling of non-vaporizing spray, they developed the submodel of fuel film formation, fuel film breakup process and dispersion of the spray droplets as shown in **Fig. 1-10**. According to their submodel, fuel film formed in the area of impingement region, and then fuel film formed as the pool. Further, the fuel film broken up into new droplets due to another impinging droplets on the film. As a results, dispersion model for the newly formed droplets was constructed.
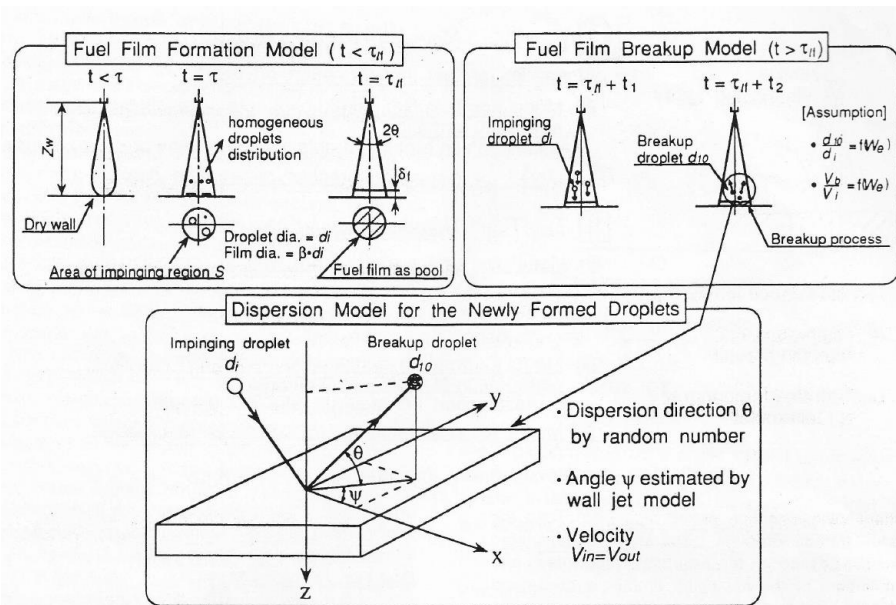
Figure 1-10 Spray impingement model **[44]**

Besides, in their fuel film breakup analysis, breakup model was classified based on Weber number of impinging droplet as shown in **Fig. 1-11**. Here x-axis means the Weber number of impinging and re-bounded droplets. While y-axis

10

means droplet number distribution of re-bounded droplet. Weber number was defined as below;

$$We = \frac{\rho_f \cdot v_i^2 \cdot d_i}{\sigma} \qquad (1\text{-}1)$$

where ρ_f is liquid fuel density, v_i is the impingement velocity of the droplet, d_i is the diameter of the impinging droplet, and σ is the surface tension. In this figure, d_{10} is the arithmetical mean diameter of the breakup droplets, V_b is the total volume of impinging droplet and the V_i is the volume of impinging droplet. As suggested by them, in a case of $We < 80$, the impinging droplets are hardly rebounded from the film surface and caused no breakup on the film surface. While in a case of $80 \leq We < 600$, the impinging droplets breakup into large droplets due to successive droplet impingement. In this Weber number range, the ratio of d_{10} / d_i and V_b / V_i were estimated as 0.3, which means the 30% of impinging droplets volume dispersed as breakup droplets. For We number higher than 600, impinging droplets tends to breakup into small droplets. In this higher Weber number range, the ratio of d_{10} / d_i and V_b / V_i were estimated as 0.1 and 0.5 respectively.

	Breakup Form	d_{10} / d_i	V_b / V_i	Range in We No.
I	non-breakup (into film)	—	—	$We < 80$
II	large breakup	0.3	0.3	$80 \leq We < 600$
III	small breakup	0.1	0.5	$We \geq 600$
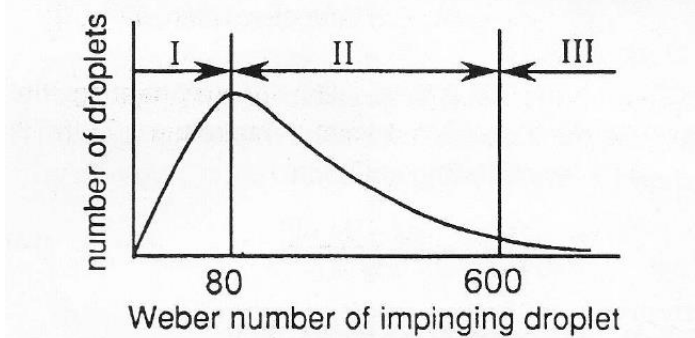
Figure 1-11 Classification of fuel film breakup form by Weber number **[44]**

According to Fujimoto et al. **[36]**, the behavior of impinging spray had a great influence on the dispersion of fuel. It appeared that fuel deposits were formed on the wall surface and caused combustion emission such as unburnt hydrocarbons (HC) and soot. It had been reported by them that the breakup of

impinging droplet and the secondary atomization of fuel film were based on the Weber number of impinging droplet. Naber and Reitz [46], on their spray-wall interaction modeling, introduced three different models of droplet behavior. Each of them was based on the Weber number of impinging and rebounding droplet. They also found that small droplets approaching the wall were deflected away as they followed a wall-jet flow in the surroundings, while large droplets impinged directly on the wall and formed a fuel film.

(d) Spray-wall interaction

Spray-wall interaction was the important phenomena occurred in the impinging diesel spray. However, this phenomena were complicated and till now many investigations and an assumption had been done when they dealt with it. The investigations have been done in experimental works and simulation works. Such as simulation works, most of the researchers enhanced their modeling method in order to close a research gap between experimental and simulation method.

Naber et al. [46] at their early stage of impingement spray study had developed the KIVA code. They clarified the spray-wall interaction process with their developed code. Then, KIVA code had been improved from 2-D to 3-D model which called KIVA II [47]. They simulated the KIVA II code for the spray-wall interaction process on the cold starting engine condition. The result showed that the spray-wall mechanism was differed from that at high impact velocities since the droplets were assumed to be rebounded from the wall.

Senda et al. [44] simulated the spray-wall interaction process for non-evaporative and evaporative spray in diesel engines. They proposed new submodel with included of fuel film formation, breakup process of impinging droplet and dispersion process of breakup droplets. They reported that the new submodel estimated by them was shown better consistency of impinging spray behavior with the experimental results. On the wall impaction of diesel spray, Gavaises et al. [48] proposed the model which covered various cases of normal and inclined angle of the spray impacted on the wall. By used of stochastic particle technique, the 3-D computational fluid dynamics (CFD) code had been developed.

Bai and Gosman [49] developed the model of spray-wall interaction within the framework of Lagrangian approach. Their study was related to characteristics of impinging droplets for pre- and post-impingement of sprays. In their model,

they defined various impingement regimes of spray droplets such as stick, spread, rebound, splash and so on as shown in **Fig. 1-12**. As a result, characteristics of impingement spray such as spray height, spray radius, droplet velocities, adhered fuel ratio, wall film volume and spray tip penetration were well predicted compared to several experimental data.
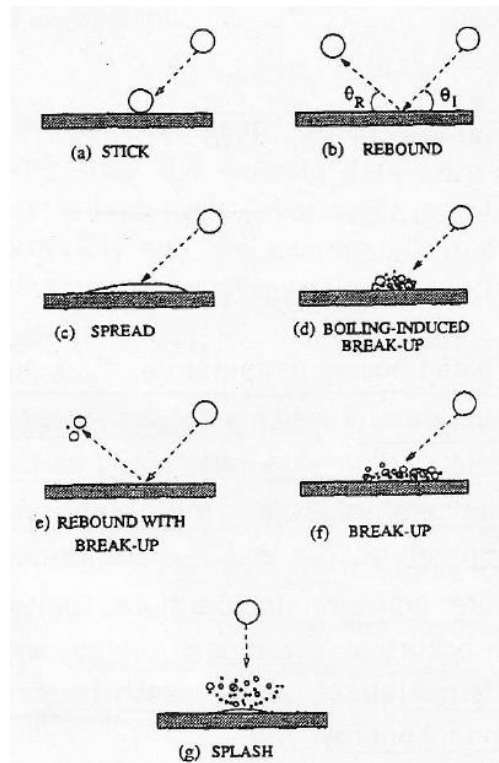
Figure 1-12 Various impingement regimes **[49]**

Senda and Fujimoto **[45]** later improved their model which described earlier. In this model, they introduced the improved model with considering the droplet-droplet interaction near the wall and fuel film. Lee and Ryou **[50]** proposed a numerical model which composed of rebound, deposition and splash of impingement spray regimes. Their results were predicted well with the experimental data. In the similar study, they proposed an improved model which included of the tangential behavior of droplets after impingement **[51]**. As a result, splash behavior was predicted better than previous models.

After all, as discussed literally above on the wall impinging spray phenomena, it shows that the impinging spray characteristics especially on diesel engine was important. Even though, there were many researchers carried out investigations on impinging diesel spray through experiment and modeling

method, there is still a gap that needs to be fulfill and improved in order to have a better understanding of the complex phenomena of impinging diesel spray.

1.2.3 Adhered fuel film and mass of impingement spray

(a) Adhered fuel film

Adhered fuel on the wall could not be avoided since the spray impinged on the cavity wall due to the short distance between nozzle tip and the wall. Amounts of fuel tended to adhere to the wall surface when the spray injected inside the combustion chamber. It is well known that the adhering fuel on the cavity wall or piston wall would form the fuel/liquid film. This formation of adhered fuel film could influence the combustion process which related to engine performance and exhaust emissions. Tsunemoto et al. **[25]** had investigated the behavior of impinging diesel spray using a simulated combustion chamber wall. In their work, diesel spray impinged on piston cavity wall, and liquid film of diesel fuel was formed on the wall. Consequently, increase of smoke level was caused by evaporation of heated liquid film together with the surrounding gas. Thus, it is necessary to understand the characteristics and behavior of fuel adhering on the wall.

Ko **[52]** reported impinging of diesel spray consists of several parameters. He illustrated the main parameters of impinging spray such as adhering fuel, non-adhering fuel, and others as shown in **Fig. 1-13**. According to his report, many research had been done regarding of post-impingement spray which is, related to non-adhering fuel.
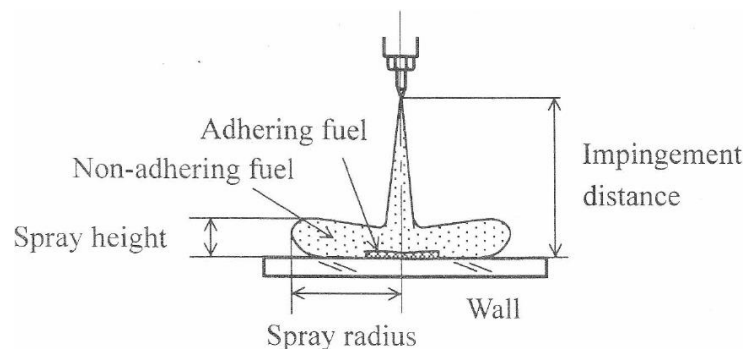
Figure 1-13 Main parameters of impingement spray **[52]**

However, less attempt of research on characteristics of adhering fuel, such as fuel film thickness, formation and breakup of fuel film, and secondary atomized

droplet dispersion on the thin layer of adhering fuel. The reason might be due to insufficient access to the engine wall and also the difficulty in taking some photographic evidence on the piston wall. Thus, by knowing well on the characteristics of adhering fuel especially the relationship between adhering fuel and wall surface will assist the development of diesel engines as well as to improve its performance and exhaust emissions.

Behavior of impingement fuel film on a wall had been investigated by Saito and Kawamura [53]. **Figure 1-14** shows the laser reflection method developed by them as to observe the growth of adhering fuel film on the surface wall.
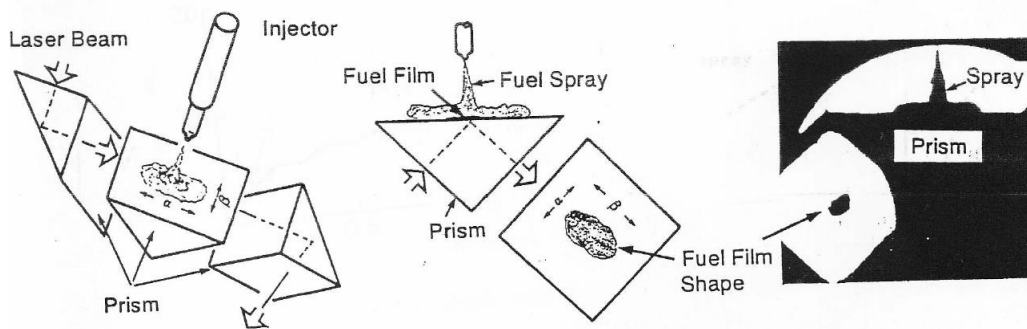
Figure 1-14 Schematic diagram for observation of adhered fuel film [53]
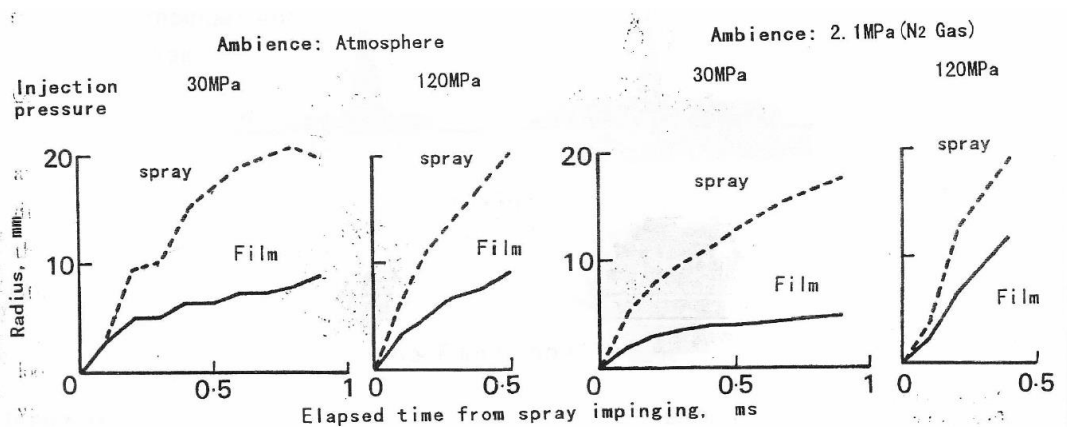
Figure 1-15 Comparison radius of adhered fuel with expanded spray [53]

At ambient pressure of 2.1 MPa and impingement distance of 25 mm, they had found that the spreading area of adhered fuel film was approximately half of the area of spray before impingement as shown in **Fig. 1-15**. **Figure 1-16 (a)** shows that adhered fuel quantity on the impingement wall was over a half of the injected fuel. While in **Figure 1-16 (b)**, the thickness of fuel film became thinner

15

when the injection pressure increase. Also, the thickness of fuel film was lower for lower ambient pressure cases.
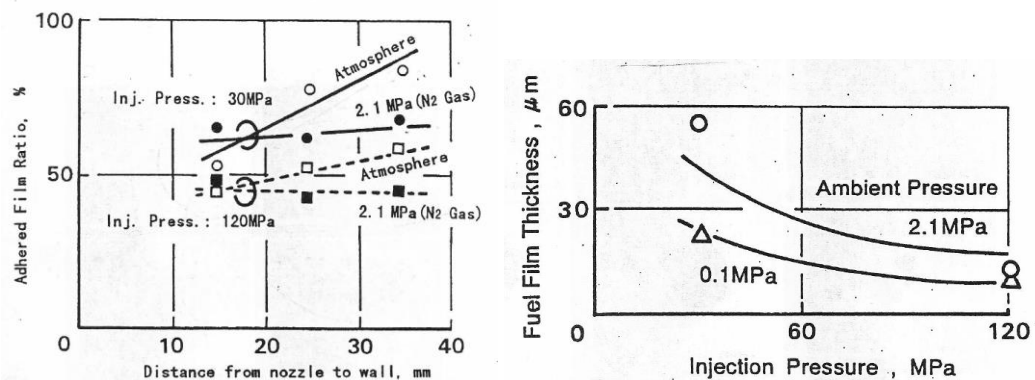
(a) Ratio of adhered fuel quantity　　(b) Thickness of adhered fuel film

Figure 1-16 The results of Saito and Kawamura **[53]**

Ko and Arai **[54, 55]** had investigated the behavior of impingement sprays for various injection pressures, ambient pressures and impingement distances. They had observed the fuel film images which had been taken through the bottom of the transparent wall with 40 mm wide. They defined the fuel film images as shown in **Fig. 1-17**. From the images it shows that the larger fuel film was formed after impingement compared to the spray width at impingement point.

① Impingement spot ② Fuel film diameter
③ Impingement wall width (40mm) ④ Spray diameter
⑤ Slipping phenomena of post-impingement spray
⑥ Wall surface
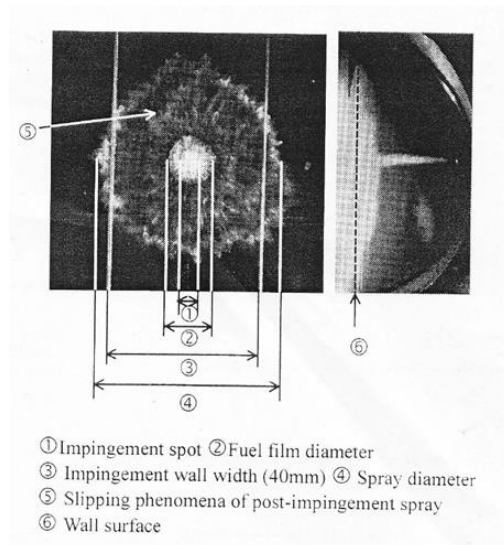
Figure 1-17 Photographs of the impingement spray taken from side and rear view (L_w = 30 mm, P_a = 1.5 MPa, t_{inj} = 2.7 ms) **[54]**
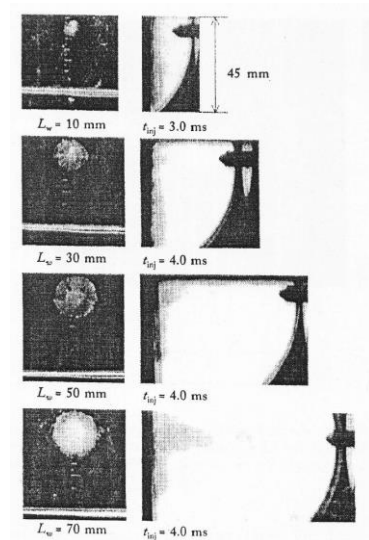
Figure 1-18 Photographs of the impingement spray and the fuel film at P_a = 1.0 MPa **[55]**

16

Figure 1-18 shows the photographs of impingement spray and fuel film which was taken just after end of injection spray at various impingement distances. The fuel film was clearly observed as a circular shape and at the maximum values of diameter. Also, the fuel film diameter became larger as the impingement distance increased.

Then, from the above results, they calculated the fuel film diameter to spray width ratio of various wall distances as shown in **Fig. 1-19**. From the results they obtained that fuel film diameter became larger with increase of wall distance, but the fuel film diameter became smaller as ambient pressure increased. Besides, the spreading ratio D_f/W_s decreased with increased of wall distance.
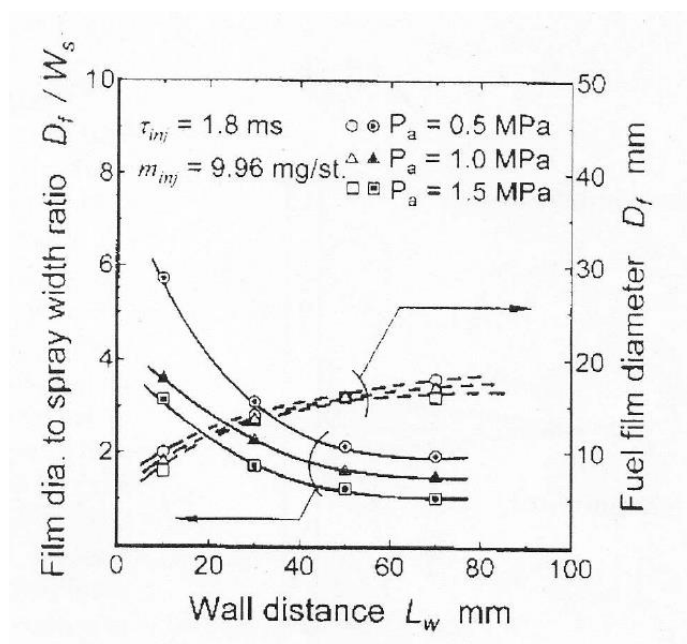
Figure 1-19 Spreading ratio D_f/W_s at various wall distances and ambient pressures **[54]**

(b) Adhered fuel mass and fuel film thickness

Further, Ko and Arai **[54]** measured the adhered fuel mass and calculated the adhered mass ratio. They defined the adhered mass ratio as a ratio of adhering fuel mass to total mass of injected fuel. **Figure 1-20** shows the effect of wall distance on the adhered fuel ratio. It was reported that adhering fuel mass to the wall surface was approximately 30% to 70% of injected fuel. Also they observed that adhered fuel ratio increased linearly with an increase of the impingement distance from 10 mm to 50 mm. However, beyond wall distance of 50 mm, the adhered fuel ratio tended to decrease. Besides, as ambient density becomes higher, the

adhered fuel mass becomes lower. They suggested that as high gas density, droplets easy to move into surrounding gas before arrive on the wall surface. They also concluded that the air fuel ratio for post-impingement spray was strongly affected by adhering fuel mass **[56]**.
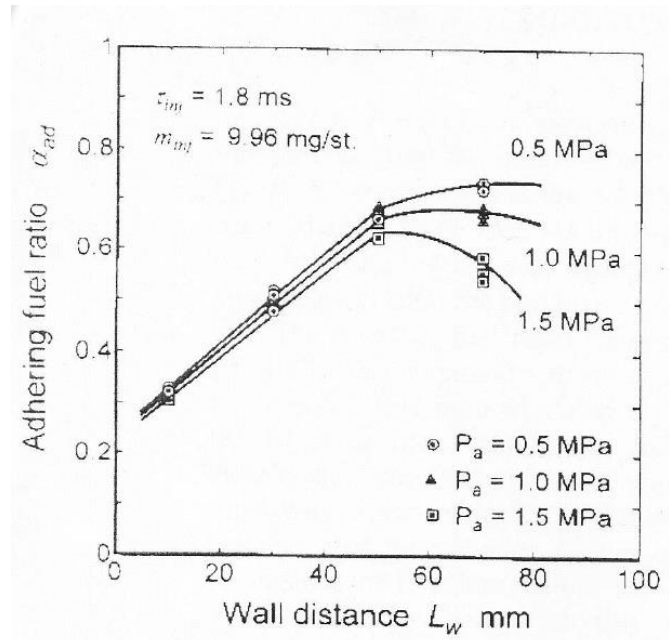
Figure 1-20 Adhering fuel ratios at various wall distances and ambient pressures **[54]**

Figure 1-21 shows the adhered fuel ratio at various impingement distances and ambient pressures **[57]**. The adhered mass ratios changed as time elapsed but it was difficult to measure with variation of time. Thus, the adhered mass ratio measured after end of injection spray. The results shows that adhered mass ratios did not change with increased of ambient pressure at a constant wall distance. But, the adhered mass ratios increased with increased of wall distances at constant ambient pressure. **Figure 1-22** shows the effect of injection pressure on adhering mass ratios at a constant ambient pressure of 18.5 kg/m^3 and wall distance of 24 mm **[57]**. It showed the adhered mass ratios decreased with increased of injection pressure. Hayashi et al. **[58]** had investigated diesel spray impingement on an extruded disk with various sizes of disk from 5 mm to 45 mm. They found that mass of fuel adhering on the disk depended on disk diameter.
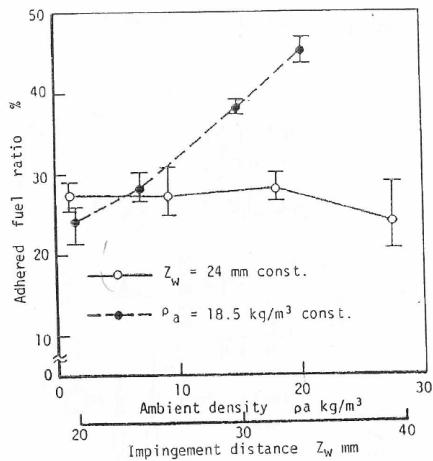
Figure 1-21 Adhering fuel ratios versus various of wall distances and ambient pressures [57]
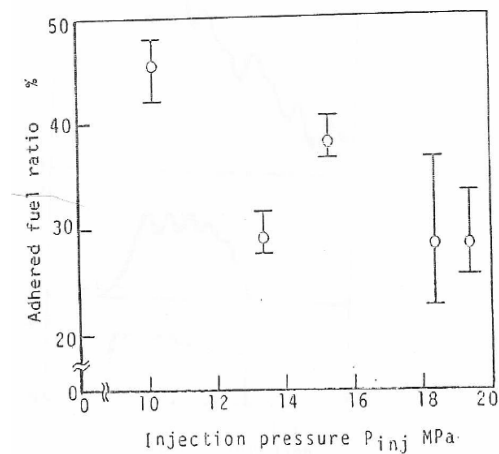
Figure 1-22 Adhering fuel ratios versus injection pressures [57]

Yonezawa and Kawajiri [59] measured the adhered mass ratio at ambient pressure of 0.1 MPa and injection pressure of 0.37 MPa. They found that adhered mass ratio decreased with increased of wall distances from 50 mm to 70 mm. Then, they simulated adhered fuel distribution at an engine intake port as shown in **Fig. 1-23**. A steady state flow model was used to simplify the measurements. Furthermore, **Figure 1-24** shows the comparison of the film thickness between calculated and experimental data. Results show good agreement between them.
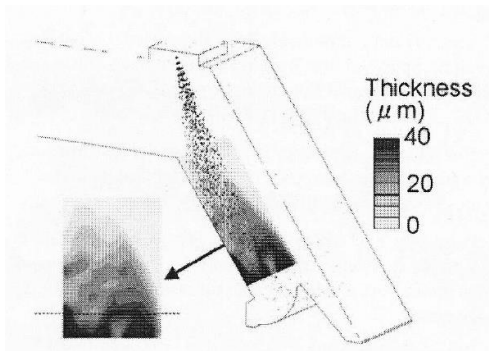
Figure 1-23 Calculated adhered fuel distribution [59]
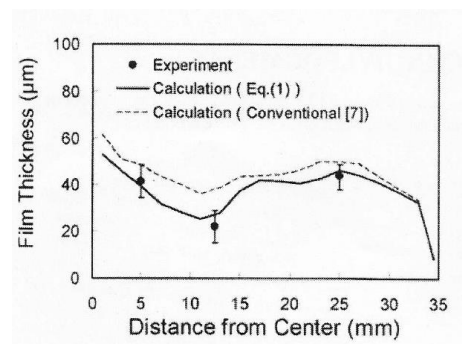
Figure 1-24 Comparison of film thickness [59]

Moller et al. [60] with their prism on the chamber window, and illumination pulsed from Nd: Yag-Laser observed the fuel film of impinging spray at ambient pressure between 0.1 MPa to 2 MPa. They reported that their fuel film was in elliptical shapes for under pressurized condition while in circular shapes under

atmospheric condition. Due to small pressure chamber sizes, there was a possibility of interference of the fuel film movements and it might be affected to the shapes of fuel film.

Liquid film behavior impinging on a flat wall had been investigated by Sato et al. **[61]** at wall distance of 70, 80 and 90 mm and inclination wall of 30, 60 and 90 deg. They explained that fuel film developed in the same direction of the spray movement. Also, thickness of fuel film near to the tip was thicker than far from the tip of injector. However, their experiment conducted under atmospheric pressure and used of gasoline fuel.

Behavior of fuel film of impingement spray was not only investigated by experimental works but also in simulation works which consisted of modeling the fuel film of impingement spray. Stanton and Rutland **[62, 63]** studied the spray-wall interactions and liquid films by multi-dimensional modeling. In their model, they integrated the film thickness and thin film assumptions, and then simplify the related equations. Their model of fuel film and spray-wall interactions were validated through several comparisons with an experimental data. Their models provided good agreement between film thickness, percentage of adhering fuel and so on.

Senda et al. **[64]** proposed the sub-model of impinging spray concerning the fuel film formation. The submodel was incorporated into the KIVA II code. Results showed that fuel film thickness became thinner as radial distance increased. They also assessed the adhering fuel ratio and reported the adhering fuel ratio increased as elapsed time. Also, this model has been extended to port-injected engines with considered of fuel film movement on the wall **[65, 66]**. Kim and Min **[67]**, developed the spray impingement and fuel film formation models with cavitation in HSDI diesel engine by use of CFD code. They considered the surface temperature and fuel film formation conditions. The models calculated the mass conservation, energy conservation and heat transfer to the impinging droplets. As a results, amount of fuel film on the piston wall were reduced by large swirl ratio and high wall temperature.

Although there are many researches conducted as described above, there are some unclear points on adhered fuel film and mass to be discussed further. More various impingement distances needed in order to clarify the effect of impingement distances on adhered fuel film and adhered mass ratio.

20

1.2.4   Impinging spray droplet and mean diameter of spray

Regarding the fundamental study on fuel spray impingement, single droplet impingement on a wall was investigated by many researchers. As well known in free spray and impingement spray phenomena, droplets of spray were so huge in number and consider as complex issues in spray study. Thus, fundamental of droplet study such as single and multiple droplets cases were needed to clarify the characteristics of adhering fuel and fuel film thickness as well as spray-wall interaction.

Since in diesel spray Rioboo et al. **[68]** investigated behavior of droplet impacted on a cold rigid surface. They investigated the disintegration mechanism of the droplet with the various parameters which were impingement velocity, viscosity of the droplet and roughness of the wall. Roisman et al. **[69]** investigated multiple droplets impact on a dry surface experimentally and theoretically. They obtained good agreement between experimental results and theoretical model for disintegration of the multiple droplets. Bai et al. **[19]** summarized behavior of the droplet impacted on the hot surface of the wall. Moreira et al. **[70]** presented an extensive review on the fundamental study of single droplet impact and its relevancy for fuel spray impact. They considered that phenomenological studies of single drop impingement had been essential to understanding the relational character of spray impingement.

Mohammadi et al. **[71]** investigated the atomization of a non-evaporative diesel spray by used of double-nano spark photography. By used of this method, an image of droplet size could be quantified. In early injection period, they observed the droplets flew away from the spray. However, by elapsed time, droplets lost their radial velocity and entrained again into the spray.   The deformation of single droplets impacted onto flat surface was discussed by Moita and Moreira **[72]**. Water and diesel oil were used as the liquid properties in their experimental works. From their results, they reported that droplet might splash from the first contact with surface wall and then secondary droplets might break-up the liquid film.

Instead of investigating the single and multiple droplets in general view of impinging diesel spray, the role of spray droplet size in engine performance and exhaust emissions are more crucial and important. Hiroyasu and Kadota **[73]** in their early stage of fuel droplets study, they measured the fuel droplet size using liquid immersion sampling technique. They discussed the mathematical equations of the distribution size of droplets. It was reported that Sauter mean diameter

increased with increased of back pressure. Laser diffraction technique was used to measure the droplet sizes of a diesel spray [74]. Experiment was conducted under injection pressure of 90 MPa and ambient pressure of 3 MPa. They found that at high injection pressure, Sauter mean diameter increased with increase of ambient pressure, but it decreased with increases of ambient pressure at lower injection pressure. Furthermore, based on above measurement results, they had derived empirical equations for obtaining the Sauter mean diameter (D_{SMD}) [75];

$$\frac{D_{SMD}}{D_n} = MAX \left[\frac{D_{SMD}^{LS}}{D_n}, \frac{D_{SMD}^{HS}}{D_n} \right] \tag{1-2}$$

$$\frac{D_{SMD}^{LS}}{D_n} = 4.12 Re^{0.12} We^{-0.75} \left(\frac{\mu_l}{\mu_a} \right)^{0.54} \left(\frac{\rho_l}{\rho_a} \right)^{0.18} \tag{1-3}$$

$$\frac{D_{SMD}^{HS}}{D_n} = 0.38 Re^{0.25} We^{-0.32} \left(\frac{\mu_l}{\mu_a} \right)^{0.37} \left(\frac{\rho_l}{\rho_a} \right)^{-0.47} \tag{1-4}$$

$$Re = \frac{V_{inj} \cdot D_n}{\nu_l} \tag{1-5}$$

$$We = \frac{V_{inj}^2 \cdot \rho_l \cdot D_n}{\sigma} \tag{1-6}$$

where, MAX [A,B] means the larger value of two. Viscosities of liquid (*l*) and ambient gas (*a*) are shown with μ_l and μ_a, and ρ is density. Weber number and Reynold number represented the non-dimensional values of liquid jet column at injector exit.

In order to access and improve the accuracy of Sauter mean diameter, Domann and Hardalupas [76] proposed the Planar Droplet Sizing (PDS) technique which assisted by intensity ratio and fluorescence light. They measured the droplet size in dense spray condition. From their results, it showed that obtaining Sauter mean diameter by PDS technique was well agreed by Phase Doppler Anemometer (PDA) technique.

By means of Phase Doppler Particle Analyzer (PDPA), the transient overall SMD of impinging spray was measured by Park and Lee [21]. Experiment was performed at an injection pressure of 80 MPa and atmospheric conditions. They defined the overall SMD as the averaged value of all droplets. As shown in **Fig. 1-**

25, the overall SMD decreasing from start of injection until 3.5 ms ~ 4.5 ms of elapsed time regardless of impingement distance. After these times, the overall SMD seemed to be almost constant. However, they have not discussed the effect of impingement distance on overall SMD in detail.
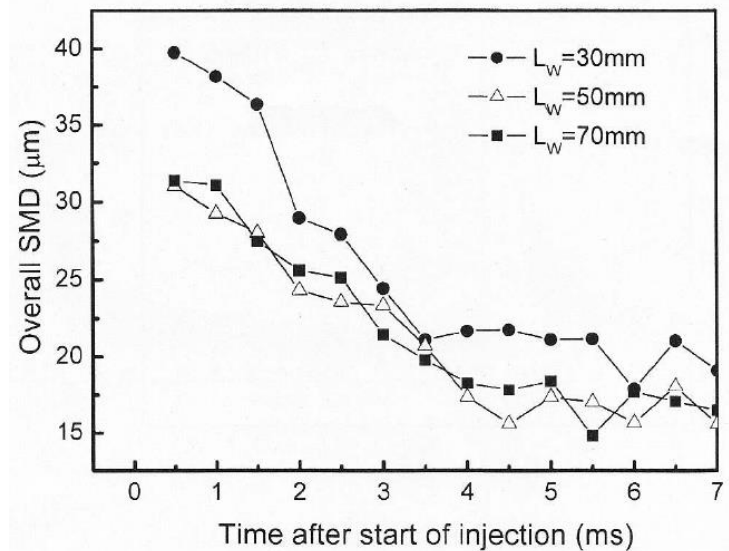
Figure 1-25 Effect of impingement distance from the injector on overall transient SMD **[21]**

Manimaran and Raj **[77]** performed numerical investigations of spray droplet parameters by 3D-CFD computation works. Their CFD code consisted of fuel spray distribution, atomization, evaporation and other parameters. By adjusting the swirl ratio and injection timing, they reported that the droplet parameters affected combustion process and emission formation significantly. Kalantari **[78]** presented a critical summary of existing models for droplet and spray-wall interactions. He evaluated the drawbacks and the strength of the existing models. In general, he found that none of the single droplet models could predict all characteristics of secondary spray which occurred during impinging on the wall. Most of the available models were presented in a few number of secondary spray aspect, while poor estimation on other aspects of secondary spray. Thus, they suggested a simple extrapolation of the results by superposition of individual droplets, even though they declared this is not a proper method.

It was shown that, single drop and multiple drop experimental data were insufficient for describing the spray impingement process. However, these fundamental studies as described above might bring researchers closer to the real

behavior of spray droplet near the wall surface. Also, the relationship of spray droplet size with liquid film was much important.

1.2.5   Injection pressure and gas density surroundings of diesel spray

In the up-to-date high speed diesel engine, injection pressure tends to increase in order to promote atomization of diesel fuel as compared with a conventional diesel engine. Most of the previous studies on impingement spray on the wall were performed under low injection pressure conditions. Therefore, it is necessary to understand the phenomena of impingement spray under high injection pressure conditions for the reduction of pollutant substances from the diesel engine.

Andreassi et al. **[22]** carried out an experimental and numerical analysis of high injection pressure diesel spray impingement. Their experimental and numerical analysis were based on injection pressure up to 120 MPa at various ambient pressures and temperatures. They reported that injection pressure showed a significant effect on radial growth and the splash height of the secondary droplets. They also confirmed that their data had a good agreement between numerical and experimental values.

Minami et al. **[3]** analyzed the fuel spray characteristics with high injection pressure systems. The analyzed the non-evaporating sprays by used of hydraulic pressure intensified type equipment (HPIE) and accumulator type high pressure injection (AHPI). They claimed the injection pressure was reached over than 250 MPa. As shown in their result (**Fig. 1-26)**, the mean droplet size decreased with an increased of injection pressure up to 280 MPa. It was reported that fine droplets were formed under injected spray of high injection pressure.
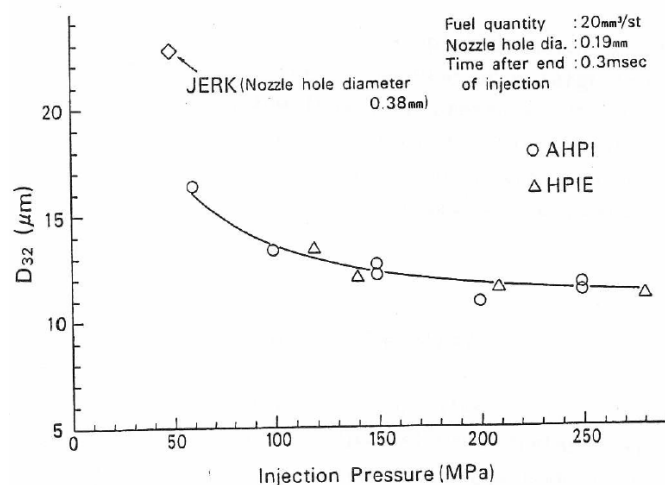
Figure 1-26 Effect of injection pressure on mean droplet size **[3]**

Saito et al. **[79]** with maximum pressure of 120 MPa conducted the impinging spray analysis. They measured several characteristics of impinging diesel spray such as adhered fuel film, spray tip, mean droplet diameter and so on. From the results, it was reported that spray tip increased with increase of injection pressure. While the adhered fuel film becomes thinner as the injection pressure increasing. Droplet behavior in transient diesel spray was investigated based on the effect of high and low injection pressure **[80]**. In this experiment work, high injection pressure was set up at 105 MPa while low injection pressure was set up at 21 MPa. At high injection pressure, spray droplets near the nozzle tip were capable for breakup but it did not happened on lower injection pressure due to low relative speed between droplets and surrounding.

Delacourt et al. **[9]** performed the research on the high pressure impact of spray characteristics up to 250 MPa. By using of direct imaging technique, they reported that their spray tip penetration was well to agree with Hiroyasu and Arai **[4]** equations. Also they found that spray angle was not much affected by injection pressure. It means that spray angle did not change with an increase of injection pressure.

In a direct injection diesel engine, combustion characteristics were influenced not only by injection pressure but also by others parameter such as the ambient gas density. Although high injection pressure was important for faster atomization process, higher gas density surrounding also was required for improving engine performance as well as exhaust emissions **[81]**. Park and Lee **[21]** had clarified the effects of ambient gas density and injection pressure on fuel droplet density near the wall. Roisman et al. **[82]** investigated the relationship between ambient gas density and spray tip penetration of free spray. However, their results were limited within the range of ambient gas density similar to NA diesel engine conditions. Ohta et al. **[11]** investigated behavior of free diesel spray with ambient pressure condition up to 5 MPa. They found that spray tip penetration became shorter as ambient pressure increasing. Similar investigation done by Manaka et al. **[12]** where they found that at a high ambient pressure, momentum of free spray decreased and led to lean homogeneous excess air ratio area. It means that, internal mixing was promoted by the increase of surrounding pressure. As for reduction strategy of NO_X, to reduce the temperature in the combustion process, exhaust gas recirculation (EGR) was adopted. However, increase of soot emission and decrease of performance became concurrently when an absolute amount of combustion air was insufficient as the results of EGR. To compensate insufficient charge of combustion air, high boost air charging system

was usually used. Then not only high performance but also emission reduction, surrounding pressure of diesel spray injection became increasing.

(a)P_a = 0.5 MPa, P_{inj} = 150 MPa, M_{inj} = 31.5 mg

(b)P_a = 4 MPa, P_{inj} = 150 MPa, M_{inj} = 31.5 mg
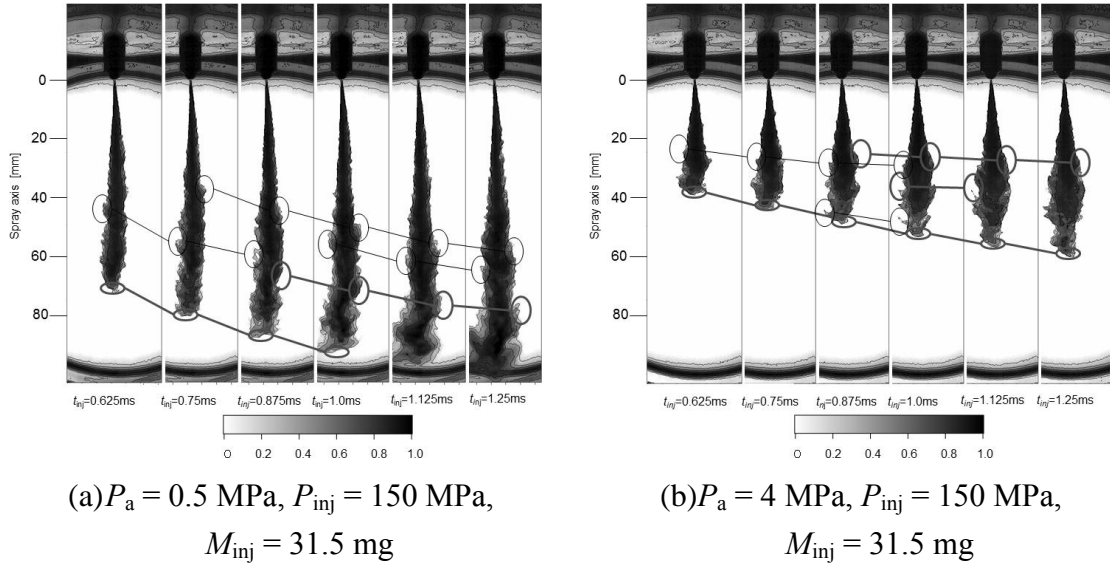
Figure 1-27 Photo density distribution of diesel spray [14]

Recently, Zama et al. [14] investigated the diesel spray under various ambient pressure conditions by using shadow imaging method. **Figure 1-27** shows the photo-density distribution of shadow images at P_a = 0.5 MPa and P_a = 4 MPa. Spray tip and remarkable local patterns on the side-edge of the spray were indicated with circles, and those patterns were sequentially tracked. As shown in **Fig. 1-27 (a)**, movements of the spray tip and spray-edges were almost same. It seemed that they moved with similar axial velocities. Besides, **Figure 1-27 (b)** shows the spray tip penetration increased with elapsed time but spray side-edges were hardly moving. According to the results obtained in various ambient pressure conditions, it was clear that local movement of side-edge spray showed far different from that of spray tip under high gas density condition. Also, the local spray near the side-edge became stagnated with an increase of the density of the ambient gas. Furthermore, they focused on PIV analysis of diesel spray velocity under high ambient density [83]. They reported that velocity in a spray decreased with increasing ambient gas density.

Therefore, it is necessary to understand the phenomena of impingement spray under high ambient and high injection pressure conditions for further reduction of pollutant emissions as well as to obtain more performance of diesel engines. Not only radial development of impingement diesel spray, but the adhered fuel on the impingement wall were also important behavior of

impingement spray. Since the processes of combustible mixture formation from spray spreading on the wall and from fuel film adhering on it were far different, adhered fuel behavior on the wall had to be investigated for understanding whole impingement behavior of diesel spray.

1.2.6 Other characteristics of diesel spray

Most of the main parameters on impinging diesel spray have been discussed literally. Other studies on a diesel spray which have been carried out experimentally and theoretically are discussed as follows.

As for diesel spray impingement, Acroumanis and Chang **[84]** investigated heat-transfer coefficient on a heated flat wall with spray impingement. They measured spray velocity prior to impingement with phase-doppler anemometry (PDA) and wall temperature by sensitive thermocouple. They clarified that the heat transfer rate was dependent on spray velocity prior to impingement. However, in their experiment, diesel fuel was injected to the atmospheric surroundings. In other words, ambient condition of the spray differed from that of diesel engine.

Georges and Buchlin **[85]** measured the liquid sprays with laser velocimeter. They also developed a 1-Dimensional mathematical modeling and compared it with the measurement data. As a first attempt in their modeling, the measurement data were well predicted with modeling approach. Samenfink et al. **[86]** performed the analysis of deposition and secondary droplet characteristics. They focused on droplet wall interaction and fraction of liquid remained on the wall film. The results of their study could be served as the basis for development of a 2-D model of interaction between droplets and liquid film.

Interimpingement diesel spray was investigated by Chiba et al. **[8]**. They showed that mutual interaction of spray-to-spray collision in diesel spray resulted in strong effect on the spray behavior after collision. It was reported by them, spray behavior after mutual interaction between fully developed sprays was similar to gas jet interaction. However, when the fully developed spray and undeveloped spray interacted together, spray behavior after the collision was different from the original spray behavior. They suggested that the spray after the collision was much controlled by collision angle, the collision position of the spray and momentum of spray density.

Ko et al. **[87]** in their first attempt conducted the impinging diesel spray on the recessed wall as shown in **Fig. 1-28**. In this figure, they defined recess diameter as D_r, spray width as W_s and H as maximum spray height rebounded from

the wall. With this new concept of impingement spray, they discussed the width-to-diameter ratio W_s/D_r precisely. Their results showed that spray impinging on the recessed-wall is reflected from the wall to the direction of spray axis. Also, the width-to-diameter ratio controlled the behavior of spray than the recess diameter itself. They also found that adhering fuel ratio of the recessed-wall is smaller than of the flat wall.
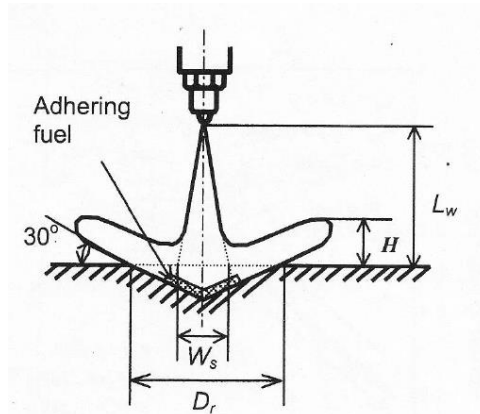
Figure 1-28 Parameters of spray impinging on a recessed-wall **[87]**

New type of combustion system for a direct injection diesel engine was developed by Ronghua et al. **[88]**. They investigated the macrospray characteristics of the fuel jet impinging on the slanting wall. The schematic diagram of this new combustion system is shown in **Fig. 1-29**. From this figure we can assume that the injected spray will collide with the slanting wall at very short distance. This might expand the spread area with the piston cavity. Under various test conditions, they reported that spray colliding near to the slanting wall tended to spread widely and more uniform than a free spray. However, this type of spray combustion had not been applied in practical diesel engine.
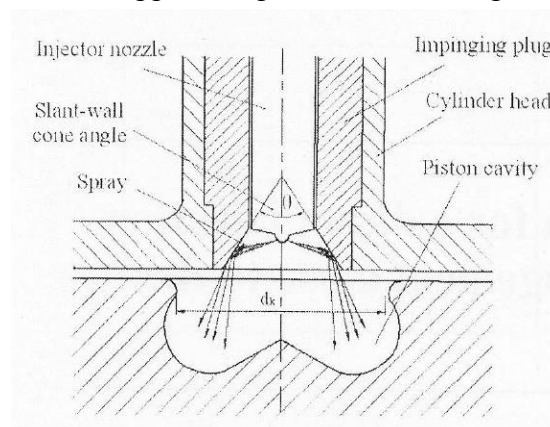
Figure 1-29 Schematic diagram of the new combustion system with an
impingement cavity **[88]**
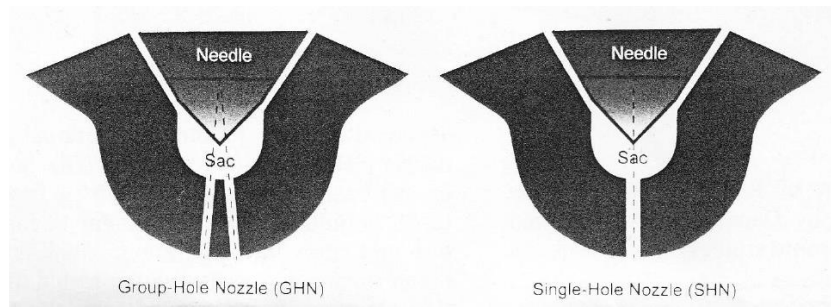
Figure 1-30 Schematic diagram of GHN and SHN **[89]**

Moon et al. **[89]** performed a study on penetration and evaporation of diesel spray by a group of two closely spaced orifices or mostly known as a group-hole nozzle. **Figure 1-30** shows the schematic diagram of group hole nozzle (GHN) and single hole nozzle (SHN) used in this experiment. The total hole area of GHN is same as SHN. The results were compared with the conventional single hole nozzle of sprays under various wall impinging conditions. From their results, it was reported that the momentum interaction of the two jets from GHN nozzle caused the higher penetrating rate after impinging than the SHN sprays.

1.2.7 Non-evaporated and evaporated spray

Terminology of the non-evaporated and evaporated diesel spray are well known to the researcher in this field. Some researchers defined the non-evaporated diesel spray as the spray conducted under cold pressure vessel conditions while evaporated diesel spray conducted under hot pressure vessel conditions **[90]**. Some researchers defined the non-evaporated as the condition under room temperature and cold wall **[54, 55]** while evaporated condition conducted under elevated wall temperature **[91]**. Senda et al. **[44]** in their model of spray impingement defined non-evaporated spray when saturated temperature of fuel droplet higher than wall surface temperature and vice versa for the evaporated spray. As well known, momentum of spray did not changed even though it was evaporated but momentum transfer mechanism from fuel to surrounding was changed according as the fuel phase such as spray, vapor and adhering mass. Also the spatial movement of evaporated spray and movement of adhered fuel was primary controlled by momentum conservation theory of spray.

Spray momentum that was given by the injection did not change under the conditions of room temperature and high temperature. Then mixing process of fuel spray and air was not so different when the mixing phenomena was controlled

by momentum conservation theory. Also spray dispersion of non-evaporating spray was the base of evaporated fuel dispersion under elevated temperature condition. As for fuel adhesion, liquid phase fuel adhesion might sometimes occur for evaporating spray. And evaporation of some part adhered liquid fuel was happened after spray in the space was completed evaporated. Then adhered mass measurement under non-evaporated condition was very important for combustible mixture formation.

In order to observed and measured several characteristics of diesel spray such as spray tip penetration, spray angle, spray width, break-up length, Sauter mean diameter, adhered fuel mass on the wall and so on, many researchers adopted the non-evaporated condition. Hiroyasu and Kadota **[73]** determined the fuel droplet size distribution by non-evaporated condition. The Sauter mean diameter was obtained by various techniques through the non-evaporated condition **[75, 28, 71]**. However, for better understanding on the vaporization of fuel spray, evaporated test condition was also needed. Since the fuel was injected inside the pressure chamber and was vaporized, then the understanding of evaporated diesel spray was important for controlling the air fuel mixture ratio for better combustion process.

Diesel combustion activities consist of several complex processes such as the turbulent spray formation, the vaporization of droplets and the combustion of fuel vapor. The analysis of these processes is essential to the development of new concepts and of physical spray models for diesel engines. The vaporization and combustion of spray droplets are strongly affected by the characteristics of non-evaporating spray such as Sauter mean diameter, spray penetration, spray width, height of post-impingement spray, adhered fuel on the wall and so on. Therefore the investigation of wall impingement phenomena under non-evaporation condition is very important even though evaporation is not included.

1.3 Purpose of this research study

1.3.1 Overview of recent studies

In the literature, general views of diesel spray such as combustion process, wall impingement, spray-wall interaction, adhered fuel film and mass have been widely discussed. The physical parameters in impinging spray such as impingement distance, wall surface area, injection pressure, ambient pressure are the parameters that are responsible for causing different behavior that appears

during the early stage of diesel combustion. By referring to these parameters, at early stage of combustion, the cavity wall or piston surface wall will have increasing tendencies of adhered fuel on a wall due to low wall temperature. This adhering tendencies will lead to fuel film formation on the wall surface and it will caused to incomplete combustion. However, the aspects of fuel film formation from the adhering fuel mass are still complex and not well understood.

Investigation of impinging diesel spray in terms of the combustion process, exhaust emission, engine performance and others were conducted more than 30 years ago. Many investigations have been conducted experimentally and theoretically in order to understand the behavior of impinging spray and the interaction between wall surface and adhering fuel. Since the investigation of impinging diesel spray is very difficult to access in real engine, most of the researchers had investigated the impinging spray phenomena inside the simulated pressure chamber.

Recently, Kiplimo et al. **[92]** investigated the effect of spray impingement, injection parameters, and EGR on combustion and emission characteristics of the PCCI diesel engine. In their study, they used two types of engine, namely as test engine and optical engine. The test engine was close to the real engine with PCCI strategies and specifically to measure the exhaust emission and combustion characteristics. While the optical engine was specifically designed for capturing the image and real behavior of spray inside the combustion chamber. Kay et al. **[93]** with his research team also simulated the transient fuel spray impingement inside the high-pressure and high temperature constant volume rig assisted with large optical access. Herfatmanesh et al. **[94]** used single-cylinder optical engine for investigating the effects of two-stage injection on fuel injection quantity, combustion and emission. In their results, they could observe the combustion image sequence of variable split strategies. From the study above, it shows that until now the research of impinging spray inside the simulated pressure chamber are still important and reliable.

In order to understand the mechanism of impinging diesel spray, both real engine and fundamental studies on impinging diesel spray are significant. Fundamental studies on impinging diesel spray especially on adhering fuel characteristics are very important. An extensive studies has been done on the non-vaporization and vaporization spray **[1-4, 15-16, 18, 30, 31]** that can serve as part of the fundamental knowledge in adhering fuel caharacteristics.

Nevertheless, the understanding for the impinging spray is essential for development of new diesel engine, which should be integrated with feature of the

lower exhaust emissions, and fuel economy without compensating the engine performance. Although diesel engine has been improved over the past years, there is still a gap and potential for further improvement and optimization of efficiency and pollutant emissions.

1.3.2   Objectives of this study

The aims of this study are to provide detailed information on fundamental characteristics of non-evaporated condition of impinging spray, adhering fuel on a wall and adhesion behavior of fuel. As well known, in the small type of high speed DI diesel engine, the distance is short between injector and piston wall. Here bore size of around 80 mm – 140 mm and cavity diameter of around 60 mm – 120 mm are assumed as the target engine of research. Thus, when fuel injected into the combustion chamber, fuel tended to adhere on the wall, and so the adhered fuel causes to unburnt hydrocarbon and soot particles in real engine. Accordingly, based on the research done on the spray-wall interaction, the adhering fuel on the dry wall surface is considered as an important factor of impinging spray. Thus, in this work, adhered fuel mass on dry wall surface is measured as the main parameter and several effects on it are investigated as follows.

(1)   Effect of injection pressure and impingement distance

The effect of injection pressure and impingement distance on the adhering mass ratio are introduced at the start of this study. Various injection pressure and impingement distance are considered. Different size of impingement disk is used as an impingement wall. The effect of injection pressure and impingement distance on the wall area are discussed. Also, impingement behavior and height of post-impingement spray are discussed.

(2)   Impingement area and wall inclination effect

This study focuses extensively investigating the effects of impingement disk area and wall inclination angle on the adhered fuel mass of impinging diesel spray. Firstly, the experiment is conducted in cases of normal wall and various impingement disk sizes. In the next step, it is conducted under inclined wall. The critical area of disk is introduced. Spray width and critical thickness of liquid film are discussed. Moreover, modified adhered mass ratio is introduced in order to

explain the general trend of adhered fuel mass. Also, PIV analysis on inclined wall is discussed as to clarify the velocity field near the wall.

(3) Weber number correlation on adhesion

Based on the previous effects, impingement velocity and Weber number of droplet are calculated. The effect of Weber number of impinging droplet on adhered mass, modified adhered mass ratio concerning diameter of impingement disk and inclined angle is discussed. Also, empirical relationships among adhered mass ratio, thickness of adhered fuel film and Weber number are derived.

(4) Ambient pressure effect

Through this study, various ambient pressure is chosen. At first, the effect of Weber number of droplet at impingement on ambient pressure is discussed. Then effect of adhered mass ratio on ambient pressure at various impingement distance is discussed. The shadowgraph images on ambient pressure effect are analyzed. From the results, the height of impingement spray is measured. Moreover, relationship between Weber number of impinging droplet with adhered mass ratio and modified adhered mass ratio are discussed. From the above results, ambient pressure effect is considered using Jet number and empirical equations of adhered mass ratio are introduced.

1.3.3 Outline of the thesis

The outline of this thesis is as follows.

Chapter 1
This chapter gives an overview of the diesel spray especially on the impinging diesel spray. The reviews of previous research works in the literature relating to impinging diesel spray, wall impingement and adhering fuel are also available. Finally, objectives of this study are given.

Chapter 2
The methodology and experimental apparatus are described in this chapter. Related content such as experimental conditions, test procedure, experimental

parameter and data analysis are showed. Further, the basic performance of the injector is introduced here.

Chapter 3

In this chapter, characteristics of spray impingement are discussed in details through the effects of injection pressure and impingement distance. In addition, the effect of injection pressure and impingement distance on the wall area are identified. Also, the critical velocity effect on the adhered mass ratio is clarified. Morevover, impingement behavior and height of post-impingement spray are discussed.

Chapter 4

This chapter shows the experimental results regarding the effects of impingement area and inclination wall on adhered mass fuel. Various sizes of disk and inclined angles are tested in order to observe the behavior of impinging spray. Concept of impingement mass of spray and critical disk diameter are introduced. The effect of injection pressure on thickness of the liquid film is estimated. Moreover, general trend of adhered fuel mass is explained by using of modified adhered mass ratios concept which combined with disk diameter and inclination angle effect. Also, PIV analysis on inclined wall is discussed as to clarify the velocity field near the wall.

Chapter 5

In this chapter, effect of Weber number of impinging droplet, impingement disk size, and inclination angle of disk on adhering fuel mass is discussed. The transient Weber number is discussed on the adhered fuel ratio. Also, the empirical relationships among adhered mass ratio, thickness of adhered fuel film and Weber number are derived.

Chapter 6

The experimental results of ambient pressure effects on adhered mass fuel are showed. Concerning the trend of adhered mass ratio, shadowgraph image and Weber number of impingement spray droplet are discussed. Finally, ambient pressure effect is considered using Jet number and empirical equations of adhered mass ratio are introduced.

Chapter 7

This chapter summarizes the conclusions that are obtained through this study.

References

[1]   Kuniyoshi, H., Tanabe, H., Sato, G.T. and Fujimoto, H., Investigation on the Characteristics of Diesel Fuel Spray, *SAE paper*, no. 800968, pp. 1-19, 1980.

[2]   Arai, M., Tabata, M., Hiroyasu, H. and Shimizu, M., Disintegrating Process and Spray Characterization of Fuel Jet Injected by A Diesel nozzle, *SAE paper*, no. 840275, pp. 1-14, 1984.

[3]   Minami, T., Yamaguchi, I., Shintani, M., Tsujimura, K. and Suzuki, T., Analysis of Fuel Spray Characteristic and Combustions Phenomena under High Pressure Fuel Injection, *SAE paper*, no. 900438, pp. 1-12, 1990.

[4]   Hiroyasu, H. and Arai, M., Structures of Fuel Sprays in Diesel Engines, *SAE paper*, no. 900475, pp. 1-12, 1990.

[5]   Takahashi, H., Yanagisawa, H., Shiga, S., Karasawa, T. and Nakamura, H., Analysis of High Pressure Diesel Spray formation in the Early Stage of Injection, *Proc. of ICLASS 1994,* pp. 262-269, 1994.

[6]   Arai, M. and Amagai, K., Experimental Study on a Diesel Spray of Multi-Stage Injection, *Proc. of International Symposium COMODIA*, pp. 219-224, 1994.

[7]   Smallwood, G.J. and Gulder, O.L., Views on the structure of Transient Diesel Sprays, *Atomization and Spray*, vol. 10, pp. 355-386, 2000.

[8]   Chiba, T., Saito, M., Amagai, K. and Arai, M., Characteristic of Interimpingement Diesel Spray, *Atomization and Spray*, vol. 12(4), pp. 431-449, 2002.

[9]   Delacourt, E., Desmet, B. and Besson, B., Characterisation of Very High Pressure Diesel Sprays Using Digital Imaging Techniques, *Fuel*, vol. 84, pp. 859-867, 2005.

[10]   Nishida, K., Gao, J., Manabe, T. and Zhang, Y., Spray and mixture properties of evaporating fuel spray injected by hole-type direct injection diesel injector, *Int. J. Engine Res.* vol. 9, pp. 347-360, 2008.

[11]   Ohta, T., Furuhata, T., Saito, M. and Arai, M., Behavior of Diesel Free Spray in High Ambient Pressure Conditions, *Proc. of ILASS-Asia 2008,* pp. 15-20, 2008.

[12]   Manaka, Y., Ohta, T., Saito, M., Furuhata, T. and Arai, M., Effect of High Ambient Pressure on Behavior and Structure of Diesel Spray, *Proc. of ICLASS 2009,* pp. 1-6, 2009.

[13]   Goldsworthy, L. C., Bong, C. and Brandner, P. A., Measurements of Diesel spray dynamics and the influence of fuel viscosity using PIV and shadowgraphy, *Atomization and Spray*, vol. 21(2), pp. 167-178, 2011.

[14]   Zama, Y., Ochiai, W., Furuhata, T. and Arai, M., Study on Behavior of Diesel Spray under High Ambient Density Condition, *Proc. of ILASS-Asia 2011,* pp. 1-8, 2011.

[15]   Hiroyasu, H. and Arai, M., Diesel Engine Combustion and its Modeling, *JSME paper*, pp. 53-75, 1985.

[16]   Arai, M., Spray and Spray Combustion (Formation of Diesel Spray and its Ignition Delay, *Engine Technology*, vol. 2, no. 6, pp. 82-87, 2000.

[17]   Arai, M. et al., Disintegrating Process and Spray Characterization of Fuel Jet injected by a Diesel Nozzle, *SAE Paper*, no. 840275, 1984.

[18]   Katsura, N., Saito, M., Senda, J. and Fujimoto, H., Characteristics of a Diesel Spray Impinging on A Flat Wall, *SAE paper*, no. 890264, pp. 191-207, 1989.

[19]   Bai, C., Rusche, H., and Gosman, A., Modelling of gasoline spray impingement, *Atomization and Sprays*, pp. 1–28, 2002.

[20]   Wang, Z.C., Du, H., Liu, J., Han, L. and Liu, S., Spray Wall-Impingement from a Single Hole Nozzle under Common Rail Condition, *Advanced Materials Research*, vol. 347-353, pp. 770–773, 2011.

[21]   Park, S.W. and Lee, C.S., Macroscopic and Microscopic characteristic of a fuel spray impinged on the wall, *Experiments in Fluids 37*, Springer-Verlag, pp. 745-762, 2004.

[22]   Andreassi, L., Ubertini, S. and Allocca, L., Experimental and numerical analysis of high pressure diesel spray-wall interaction, *Int. Journal of Multiphase Flow,* vol. 33, pp. 742-765, 2007.

[23]   Ko, K. and Arai, M., The Characteristics of Post-Impingement Diesel Spray, Part 1: Penetration and Volume, *Atomization and Spray*, vol. 12(4), pp. 403-417, 2002.

[24]   Kim, K., Kim, D., Jung, Y., and Bae, C., Spray and Combustion characteristics of gasoline and Diesel in a Direct Injection compression ignition engine, *Fuel*, vol. 109, pp. 616-626, 2013.

[25]   Tsunemoto, H. et al., Process of Mixture Formation of Impinging Spray on the Wall in a Hole Type Nozzle, *JSAE*, vol. 27, no. 2, pp. 39-45, 1996.

[26] Tanabe, H., Takahashi, M., Sato, G.T., Sato, S., and Onishi, S., Experimental Study on Unsteady Fuel Spray Impinging onto a Projection on a Wall, *COMODIA 94*, pp. 379-384, 1994.

[27] Montajir, R.M., Tsunemoto, H., Ishitani, and Minami, T., Fuel spray behavior in a small DI diesel engine: effect of combustion chamber geometry, *SAE Paper*, no. 2000-01-0946, 2000.

[28] Zurlo, J.R., and Chigier, N., Impinging Diesel Spray Dynamics, *Atomization and Sprays*, vol. 1, pp. 303–318, 1991.

[29] Park, D. et al., Effect on Diesel Spray for Variation of Ambient Pressure and Impingement Land Position, *KSAE*, vol. 5, no. 3, pp. 95-105, 1997.

[30] Senda, J. et al., Visualization of Evaporative Diesel Spray Impinging upon Wall Surface by Exciplex Fluorescence Method, *SAE Paper*, no. 920578, pp. 1–10, 1992.

[31] Senda, J., Kanda, T., Kobayashi, M., and Fujimoto, H., Quantitative Analysis of Fuel Vapor Concentration in Diesel Spray by Exciplex Fluorescence Method, *SAE Paper*, no. 970796, pp. 283–295, 1997.

[32] Arai, M. et al., Post-Impingement Penetration of Single and Two-Stage Injection Diesel Spray, *ILASS-Asia 98*, pp. 73-78, 1998.

[33] Arai, M. and Amagai, K., Experimental Study on a Diesel Spray of Multi-Stage Injection, *COMODIA 94*, pp. 219-224, 1994.

[34] Nishida, K. et al., Wall Impingement Behavior of the Diesel Spray with Split Injection, *JSAE*, vol. 30, no. 3, pp. 17–24, 1999.

[35] Arai, M., Physics behind diesel spray characteristics and Its Combustion, *Proc. Engine Combustion Process, Current Problems and Modern Techniques, 11th Congress, Ludwingsburg, Germany,* pp. 417-436, 2013.

[36] Fujimoto, H., Senda, J., Nagae, M., Hashimoto, A., Saito, M., and Katsura, N., Characteristics of a diesel spray impinging on a flat wall, *International Symposium COMODIA-1990*, pp. 193–198, 1990.

[37] Ebara, T. and Arai, M., Estimation of Spray Penetration under a Wall Effect, *ILASS-Japan*, pp. 213-218, 1996.

[38] Ebara, T., Amagai, K., and Arai, M., Penetration Model of a Diesel Spray along a Wall , *COMODIA 98*, pp. 423-428, 1998.

[39] Ebara, T. and Arai, M., Image Analysis of a Diesel Spray Impinging on a Wall, *ICLASS 97*, pp. 537-544, 1997.

[40] Ebara, T., Amagai, K., and Arai, M., Movement and Structure of Diesel Spray Impinging on an Inclined Wall, *SAE Paper*, no. 970046, 1997.

[41] Ishikawa, N., Fujino, R., Minami, T., and Yokota, K., Observation of Spray Impingement Behaviour in a Small D.I. Combustion Chamber, *JSAE,* vol. 29, no. 2, pp. 23-28, 1998.

[42] Sakane, A. et al., Behavior of Diesel Spray Impinging on a Wall, *JSME,* vol. 54, no. 503, pp. 1861-1865, 1987.

[43] Wachters, L.H.J. and Westerling, N.A., The heat transfer from a hot wall to impinging water drops in the spheroidal state, *Chem. Eng. Sci.,* vol. 21, no. 11, pp. 1047-1056, 1966.

[44] Senda, J., Kobayashi, M., Iwashita, S. and Fujimoto, H., Modeling of diesel spray impinging on flat wall, *SAE Technical Paper*, no. 941894, 1994.

[45] Senda, J., and Fujimoto, H., Multidimensional modeling of impinging sprays on the wall in diesel engines, *ASME Paper*, vol. 52, no. 4, 1999.

[46] Naber, J.D. and Reitz, R.D., Modeling spray/wall impingement, *SAE Paper*, no. 880107, 1988.

[47] Gonzalez, M., Borman, G., and Reitz, R.D., A Study of Diesel Cold Starting using both Cycle Analysis and Multidimensional Calculations, *SAE Paper*, no. 910180, 1991.

[48] Gavaises, M., Theodorakakos, A., and Bergeles, G., Modeling wall impaction of diesel sprays, *Journal of Heat and Fluid Flow*, 1996.

[49] Bai, C.X., and Gosman, A.D., Development of a methodology for spray impingement simulation, *SAE tech paper*, no. 950283, 1995.

[50] Lee, S., and Ryou, H., Modeling of Spray-Wall Interactions Considering Liquid Film Formation, *ICLASS 2000*, CD Paper, 2000.

[51] Lee, S.H., and Ryou, H.S., Development of a New Spray/Wall interaction Model, *International Journal of Multiphase Flow*, vol. 26, pp. 1209-1234, 2000.

[52] Ko, K., Characteristics of the Diesel Spray Impinging on a Wall, PhD Thesis., Gunma University, Japan, 2002.

[53] Saito, A. and Kawamura, K., Behavior of Fuel Film on a Wall at Fuel Spray Impinging, *Proc. of ICLASS 1997,* pp. 54-61, 1997.

[54] Ko, K. and Arai, M., Diesel Spray and Adhering Fuel on an Impingement Wall, *SAE paper*, no. 2002-01-1628, pp. 115-128, 2002.

[55] Ko, K. and Arai, M., Diesel Spray Impinging on a Flat Wall, Part 1: Characteristics of Adhered Fuel Film in an Impingement Diesel Spray, *Atomization and Spray*, vol. 12(5&6), pp. 737-751, 2002.

[56] Ko, K. and Arai, M., Diesel Spray Impinging on a Flat Wall, Part 2: Volume and Average air-fuel ratio of an Impingement Diesel Spray, *Atomization and Spray*, vol. 12(5&6), pp. 753-768, 2002.

[57] Katsura, N. et al., Characteristics of a Diesel Spray Impinging on A Flat Wall (2nd Report), *JSME*, vol. 56, no. 521, pp. 227-233, 1990.

[58] Hayashi, Y., Wakabayashi, C., Furuhata, T. and Arai, M., Behavior of Diesel Spray Impingement on an Extruded Column, *Proc. of 18th International Combustion Engine Symposium*, vol. 71, pp. 1-6, 2005.

[59] Yonezawa, T., and Kawajiri, K., Study of Adhesion Fuel Behavior Formed by Spray-Wall Impingement in PFI Engine, *SAE International*, no. 2010-01-0782, 2010.

[60] Moller, J., Chaves, H., and Obermeier, F., Fuel Deposition on Wall Impingement of a Spray, *SAE Paper*, no. 961207, 1996.

[61] Sato, T., Nakase, Y., Takahashi, Y and Kubota, M., Liquid Film Behavior of PFI Spray Impinging on a Flat Wall, *ICLASS-2006*, 2006.

[62] Stanton, D.W., and Rutland, C.J., Multi-Dimensional Modeling of Heat and Mass Transfer of Fuel Films Resulting from Impinging Sprays, *SAE*, no. 980132, 1998.

[63] Stanton, D.W., and Rutland, C.J., Multi-dimensional modeling of thin liquid films and spray-wall interactions resulting from impinging sprays, *International Journal of Heat and Mass Transfer*, pp. 3037-3054, 1998.

[64] Senda, J. et al., Modeling Spray Impingement Considering Fuel Film Formation on the Wall, *SAE Paper*, no. 970047, 1997.

[65] Senda, J. et al., Measurement and modeling on wall-wetted fuel film profile and mixture preparation in intake port of SI engine, *SAE Paper*, no. 1999-01-0798, 1999.

[66] Senda, J. and Matsuda, T., Modeling on interaction processes of engine sprays and chamber wall, *JSME Paper*, vol. 12, no. 39, 2003.

[67] Kim, M. and Min, K., Calculation of fuel spray impingement and fuel film formation in an HSDI diesel engine, *KSME International Journal*, vol. 16, no. 3, pp. 376-385, 2001.

[68] Rioboo, R., Tropea, C., and Marengo, M., Outcomes from a drop Impact on solid surfaces, *Atomization and Sprays*, vol. 11, no. 2, pp. 155–165, 2001.

[69] Roisman, I.V., Prunet-Foch, B., Tropea, C., and Vignes-Adler, M., Multiple Drop Impact onto a Dry Solid Substrate, *Journal of Colloid and Interface Science*, vol. 256, no. 2, pp. 396–410, 2002.

[70] Moreira, A.L.N., Moita, A.S., and Panao, M.R., Advances and challenges in explaining fuel spray impingement: How much of single droplet impact research is useful?, *Progress in Energy and Combustion Science*, vol. 36, pp. 554–580, 2010.

[71] Mohammadi, A., Miwa, K., Ishiyama, T., and Abe, M., Investigations of Droplets and Ambient Gas Interaction in a Diesel Spray using a Nano-Spark Photography Method, *SAE Paper*, no. 981073, 1998.

[72] Moita, A.S., and Moreira, A.L.N., The deformation of single droplets impacting onto a flat surface, *SAE*, no. 2002-01-2749, 2002.

[73] Hiroyasu, H. and Kadota, T., Fuel Droplet Size Distribution in Diesel Combustion Chamber, *JSME Paper*, vol. 19, no. 135, 1976.

[74] Tabata, M., Arai, M., and Hiroyasu, The Sauter Mean Diameter of a Diesel Spray in an Elevated Pressure Environment, *ICLASS-88*, 1988.

[75] Hiroyasu, H., Arai, M. and Tabata, M., Empirical equations for the sauter mean diameter of a diesel spray, *SAE Paper*, no. 890464, 1989.

[76] Domann, R., and Hardalupas, Y., Quantitative Measurement of Planar Droplet Sauter Mean Diameter in Sprays using Planar Droplet Sizing, *Particle & Particle Systems Characterization*, vol. 20, pp. 209-218, 2003.

[77] Manimaran, R., and Raj, R.T.K, Numerical Investigations of Spray Droplet Parameters on Combustion and Emission Characteristics in a Direct Injection Diesel Engine using 3-Zone Extended Coherent Flame Model, *Advances in Modern Mechanical Engineering*, 2012.

[78] Kalantari, D., Evaluation of some of the existing models for droplet and spray/wall interactions, *Tech Science Press*, vol. 92, no. 2, pp. 169-182, 2013.

[79] Saito, A. et al., Analysis of Impinging Spray Characteristics under High-Pressure Fuel Injection (1st Report, Measurement of Impinging Spray Characteristics), *JSME,* vol. 59, no. 566, pp. 356-361, 1993.

[80] Hung, C.C., Martin, J.K. and Koo, J.Y., Injection Pressure Effects upon Droplet Behavior in Transient Diesel Spray, *SAE*, no. 970053, 1997.

[81] Osada, H., Aoyagi, Y. and Kazuaki, S., Goto, Y. and Suzuki, H., Reduction of NOx and PM for a heavy duty diesel using 50% EGR rate in single cylinder engine, *SAE International Journal*, no. 2010-01-1120, pp. 65-80, 2010.

[82] Roisman, I.V., Araneo, L. and Tropea, C., Effect of ambient pressure on penetration of a diesel spray, *Int. J. Multiphase flow*, vol. 33, pp. 904-920, 2007.

[83] Zama, Y., Ochiai, W., Furuhata, T. and Arai, M., Velocity measurement inside a diesel spray by using time-resolved PIV under high ambient density condition, *Proc. of ICLASS*, 2012.

[84] Arcoumanis, C., and Chang, J., Heat transfer between a heated plate and an impinging transient diesel spray, *Experiments in Fluids*, vol. 119, pp. 105–119, 1993.

[85] Georges, M., and Buchlin, J.M., Detailed Single Spray Experimental Measurement and One-Dimensional Modelling, *Int. J. Multiphase flow*, vol. 20, no. 6, pp. 979-992, 1994.

[86] Samenfink, W. et al., Droplet interaction with shear-driven liquid films: analysis of deposition and secondary droplet characteristics, *Int. J. Heat and Fluid Flow*, vol. 20, pp. 462-469, 1999.

[87] Ko, K. et al., Diesel Spray Impingement Behavior and Adhering Fuel on a Recessed Wall, *SAE paper*, no.2003-01-1834, 2003.

[88] Ronghua, H., Xiaobei, C., and Guang, H., New Type of Combustion System for a Direct Injection Diesel Engine, using spray Impingement close to the Slanting Wall, *Proceedings of the Institution of Mechanical Engineers*, 2004.

[89] Moon, S., Zhang, W., Nishida, K., Matsumoto, Y. and Gao, J., Development and Evaporation of group-hole nozzle sprays under various surrounding and impinging conditions of Direct-Injection Diesel Engines, *Int. J. Engine Res.*, vol. 12, 2010.

[90] Mirza, M.R., Baluch, A.H.., and Chaudry, I.A., Structure of evaporating diesel sprays, *J. Eng & Appl. Scie.*, 2007.

[91] Guerrassi, N. and Champoussin, J.C., Experimental study and modelling of diesel spray/wall impingement, *SAE Paper*, no. 960864, 1996.

[92] Kiplimo, R., Tomita, E., Kawahara, N., and Yokobe, S., Effects of spray impingement, injection parameters, and EGR on the combustion and emission characteristics of a PCCI diesel engine, *Applied Thermal Engineering*, no. 37, pp. 165–175, 2012.

[93] Kay, P.J., Bowen, P.J., Gold, M.R., and Sapsford, S.M., Transient fuel Spray Impingement at Atmospheric and Elevated Ambient Conditions, *Exp Fluids*, no. 53, pp. 873–890, 2012.

[94] Herfatmanesh, M.R., Lun, P., Attar, M.A., and Zhao, H., Experimental Investigation into the Effects of Two-Stage Injection on Fuel Injection Quantity, Combustion and Emissions in a High-Speed Optical Common Rail Diesel Engine, *Fuel*, no. 109, pp. 137–147, 2013.

Chapter 2

Methodology of impinging diesel spray research

2.1 Importance of the adhered fuel mass research

Many researchers since last 30 years ago were looking forward on improving diesel engine performance with keeping low harmful emission. Various types of diesel spray research have been conducted as discussed in Chapter 1. Research method is covered in variety ways such as experimental research, modeling work, numerical simulation and also practical spray analysis in engine. Those methods are related and supported each others in term of data validation. Thus, the concluded data and results might be useful in the application to practical engine development.

Wall impingement of fuel spray is known as the main contributor to direct injection high-speed diesel combustion, so it becomes an important factor in reducing diesel exhaust emissions. In small type high speed DI diesel engine, the injected fuel spray impinges on a wall of the combustion chamber because of short distance between an injection nozzle and a cavity wall. From the viewpoint of Boot et al. [1] and Han et al. [2], the fuel impingement on a cylinder wall or a piston surface occurs and causes the HC emission. Recently Arai [3] pointed out the importance of diesel spray handling and that the task of diesel spray injection was fuel preparation at desired timing and desired space in combustion cavity.

The vaporization and combustion of diesel spray are strongly affected by the characteristics of non-evaporating spray. For understanding the mechanism of non-evaporated diesel spray condition on adhering fuel, spray-wall interaction, spray modeling, and further the development of the advanced combustion system, the behavior of impingement spray should be clarified experimentally and theoretically. Adhering fuel mass on the piston/cavity wall seems as the important factor in non-evaporated impinging diesel spray. The adhesion behavior influences the combustion process and results in harmful emissions. As the spray impinged on piston cavity wall, liquid film of diesel fuel is formed. Consequently, the smoke level increases due to evaporation of heated liquid film together with surrounding gas [4].

In diesel engines, great numbers of fuel droplets are involved during atomization. The droplets evaporate and burn in the combustion chamber space.

However, some of the droplets find their way to impinge the wall surface in the combustion chamber as illustrated in **Fig. 2-1 [5]**. The interaction between fuel spray and a surface within an engine leads to the adhering of liquid fuel films **[6]**. This liquid film formation is one of the factors that caused deposit formation on the wall surface in the combustion chamber.
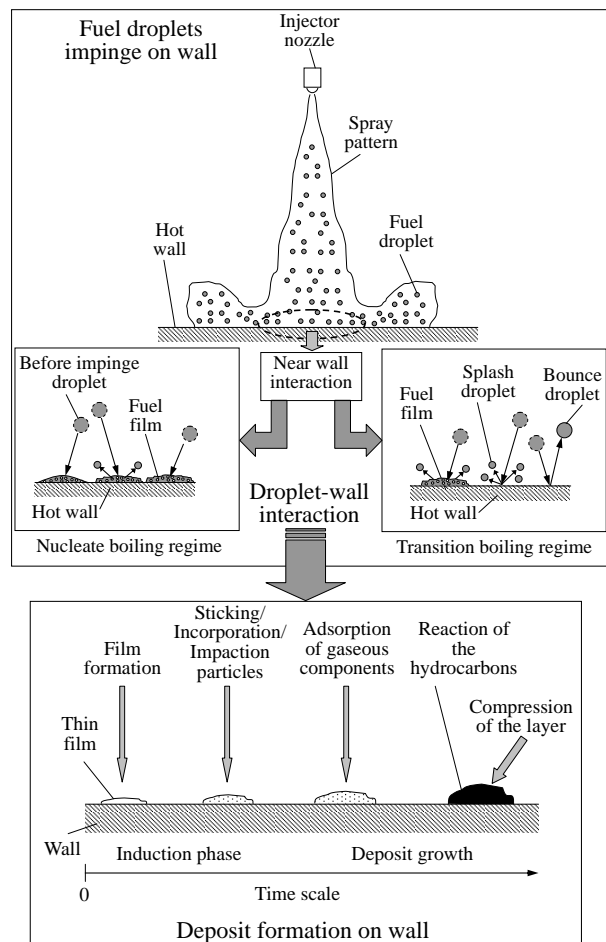
Figure 2-1 Deposit formation mechanism in an engine **[5]**

In some cases for diesel engines, fuel spray impingement on a hot wall surface in a combustion chamber cannot be avoided. Werlberger and Cartellieri **[7]** observed in their small bore DI diesel engine experiments, more than 50 percent of the fuel impinged upon the piston bowl at high load engine operation. The tendency of fuel spray impingement on a piston wall in an engine increases due to following reasons:

1) Higher injection pressure that increased spray penetration and also when the spray impingement was used as a design consideration to promote spray

atomization **[8]**.

2) Engine operation with longer ignition delay compared to the injection period **[9]**.

3) Engines that have a short distance between the injection nozzle and the piston head such as for small and high speed engines **[10]**.

2.2 Methodology of adhered fuel mass measurement

Figure 2-2 shows the general method of impinging diesel spray investigation in this study. In practical direct injection diesel engine, as shown in **Figs. 1-2** and **1-7 (**Chapter 1), multi-hole nozzle injector was used. Then spray-to-spray interaction might be affect the combustion process. However when interaction between spray-to-wall was investigated, spray-to-wall interaction of a single spray was fundamental and also important for multi-spray behavior including spray-to-spray interaction. Then, this investigation only involves a single hole injector system for the whole experiment. Since the impinging spray on the wall was the complex phenomena, using of single hole injector system could simplify the experimental analysis **[11, 12, 13]**. The diesel spray will impinge on the dry surface of the wall. Similar to the phenomena occurred in real engine, when the fuel remained on the surface of the wall it will be burned by the following combustion phase, and then the next spray will be impinged again on the dry surface. Although the wetted surface was also important in diesel spray impingement, the impinging spray effect on the dry surface of the wall could not be avoided as many researchers also focused on the dry wall surface **[14, 15, 16, 17, 18]**. As the spray impinged on the dry surface wall, the adhered fuel mass was measured as the main parameter in this study. Then adhered mass ratio was analyzed.

Almost similar method has been adopted earlier by several researchers in impinging diesel spray research but their focused of study were different **[12, 19, 20, 21, 22]**. Their research works had been discussed literally in Chapter 1. Generally, there were four findings in these impinging diesel spray investigation as shown in **Fig. 2-2** (inside dash box). They were the (a) effect of injection pressure and impingement distance, (b) impingement area and wall inclination effect, (c) Weber number effect of adhesion and (d) ambient pressure effect. These effects were influenced by the diesel spray characteristics such as injection velocity, injection mass, Sauter mean diameter, spray penetration and impingement velocity. Each of the effects will be discussed in details in Chapters 3, 4, 5 and 6. Details on

experimental apparatus and procedure will be explained in a next section of this chapter.

```
            ┌─────────────────────┐
            │  Impinging diesel   │
            │ spray investigation │
            └──────────┬──────────┘
                       │
            ┌──────────┴──────────┐      ┌─────────────────────────────────┐
            │    Single hole      │      │ Diesel spray characteristics:   │
            │  nozzle injection   │─────▶│  • Injection velocity           │
            └──────────┬──────────┘      │  • Injection mass               │
                       │                 │  • Sauter mean diameter         │
            ┌──────────┴──────────┐      │  • Spray penetration            │
            │    Dry surface      │      │  • Impingement velocity         │
            └──────────┬──────────┘      └─────────────────────────────────┘
                       │
            ┌──────────┴──────────┐
            │   Adhered fuel      │
            │      mass           │
            └──────────┬──────────┘
                       │
            ┌──────────┴──────────┐
            │   Adhered mass      │
            │      ratio          │
            └──────────┬──────────┘
```
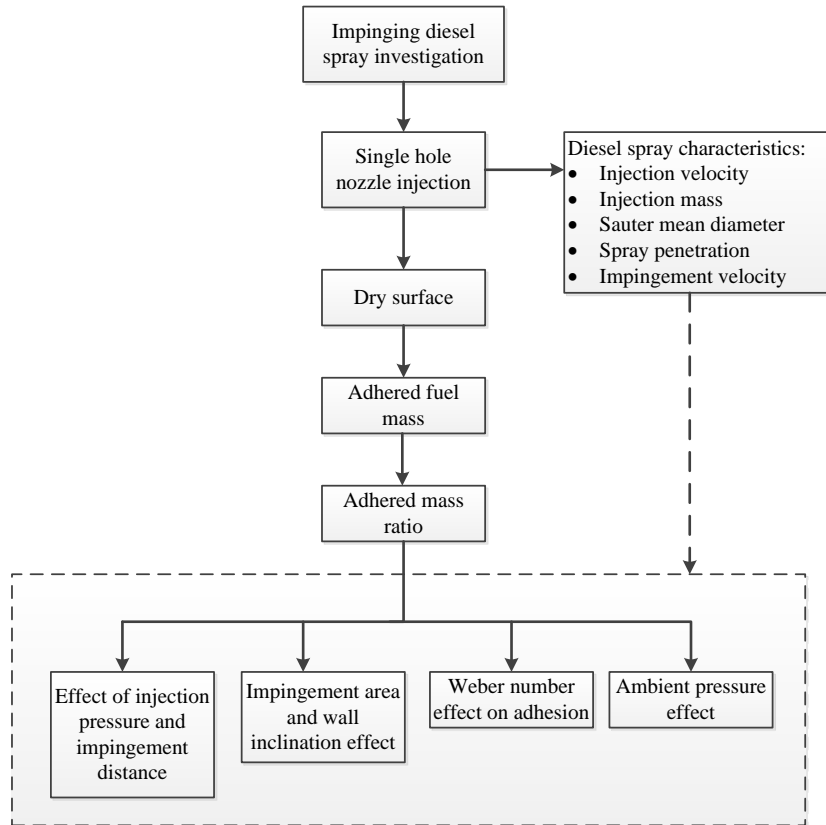
Figure 2-2 General method of impinging diesel spray investigation

2.3 Experimental apparatus and setup

2.3.1 Experimental apparatus for normal and inclined wall experiments

In this study, there are two types of experiments were conducted; a normal wall impinging spray and an inclined wall of impinging spray. Purpose of both the experiments was the measuring of adhering fuel mass on the wall. A real photograph for both experiments apparatus is shown in **Fig. 2-3**. A schematic diagram of the experimental apparatus for normal and inclined wall impingement are shown in **Fig. 2-4** which is similar as shown in real picture of **Fig. 2-3**. Similar apparatus was used in both experiments. It consisted of a fuel injection system, a high pressure vessel and an image processing unit for impingement spray. The high pressure vessel with a size of 220 mm $\times$ 200 mm $\times$ 280 mm was used. The high pressure vessel was filled with N_2 gas of room temperature which to control

the ambient density inside the pressure vessel. Diesel fuel of JIS No.2 was used as a test fuel. The test fuel was injected into the vessel with a single shot fuel injection system, and a spray impinged on an impingement disk placed in a vessel. In order to observe the behavior of an impingement spray, a shadow imaging technique was applied. A metal halide lamp was used as the light source, and sequential shadow images of diesel spray were captured with a high speed digital camera (Phantom, PCI-512).
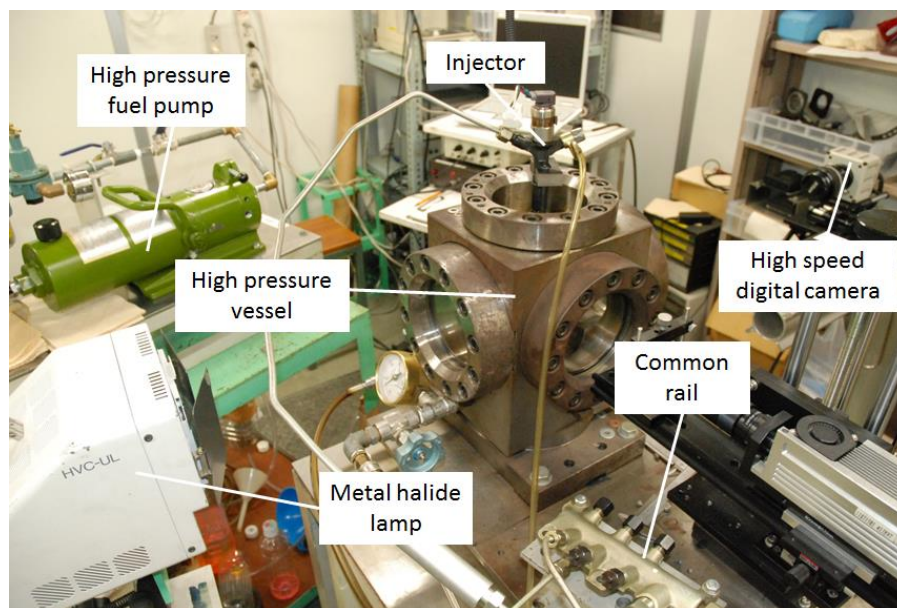
Figure 2-3 Photograph of impinging diesel spray test bench
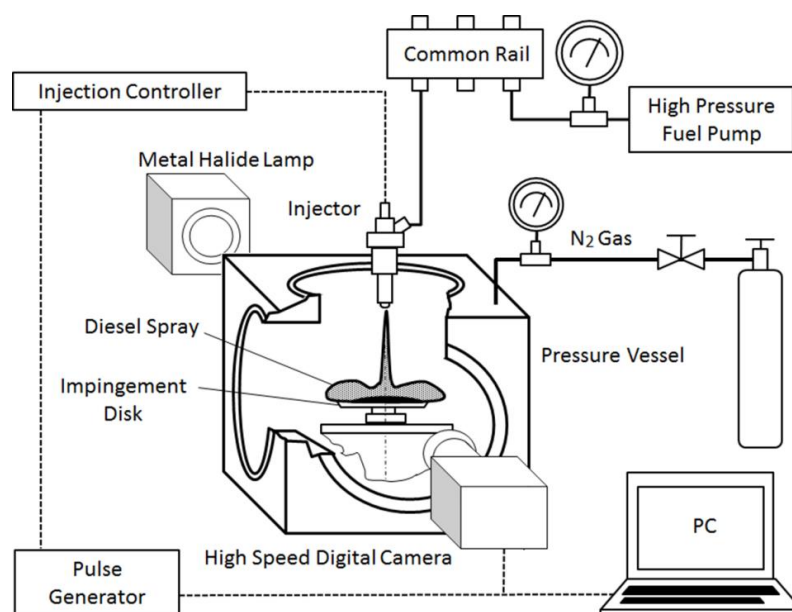
Figure 2-4 Schematic diagram of the normal wall impingement apparatus

2.3.2 Normal and inclined wall setup

Figures 2-5 and 2-6 show the impingement disk setup for normal wall and inclined wall impingement respectively. On both wall setups, an aluminum flat disk was used as an impingement wall, which had 45 degree cut edge in order to prevent the adhered mass attached to side wall of the disk. Various sizes of impingement disk were used in this experimental work as shown in **Table 2-1**. The experiments had been carried out with the condition that the spray axis coincided with the center of impingement disk even though for the inclination wall position.
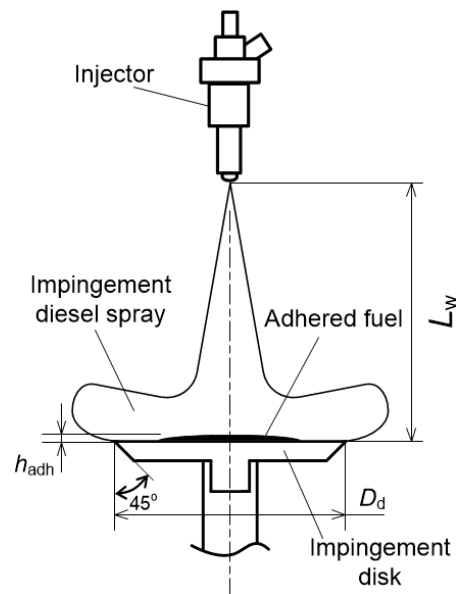
Figure 2-5 Diesel spray and normal set-up of impingement disk
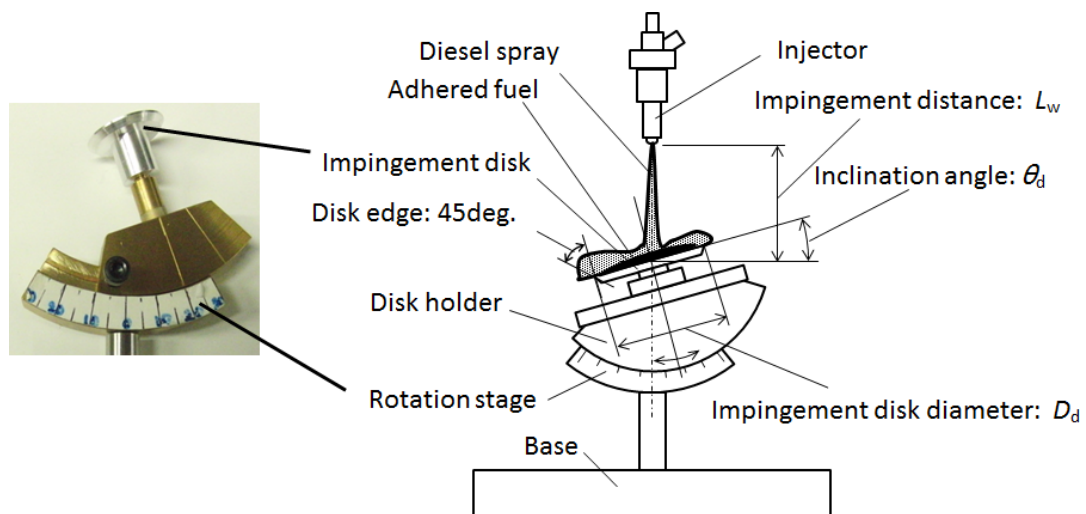
Figure 2-6 Diesel spray and inclined set-up of impingement disk

Vertical impingement of diesel spray was investigated as the fundamental study of impingement spray. However the diesel spray impinged vertically to the wall occurred rarely in a diesel engine. Therefore, research of diesel spray impinged to an inclined wall was important to clarify the general behavior of impingement spray. For inclination wall conditions as shown in **Fig. 2-6**, disk holder and rotation stage were fabricated, and used as to hold and rotate the impingement disk to the specified inclination angle. Using this system, impingement axis of diesel spray could be kept on the center of impingement disk. The inclination angle θ_d was set-up from 0 to 50 degrees as listed in **Table 2-1**. When the inclination angle increased over 50 deg., some of adhered fuel dripped from the disk. Therefore the inclination angle for inclined wall experiment was limited by 50 deg.

2.4 Experimental condition and procedure

(1) Main experimental conditions

Table 2-1 shows the main experimental conditions for both types of experiments. The diameter of the nozzle hole was 0.17 mm. Its diameter was in a range of multi-hole injector which around 1 liter per cylinder. The injection period of 3.2 msec were adopted in this research. Injection pressures were 40, 80, 100, 120, 130, 150 and 170 MPa with injection mass of 18.2, 24.5, 26.8, 28.7, 29.6, 31.5 and 32.8 mg respectively to each injection pressure. Recently, high injection pressure was applied in the diesel engine in order to atomize the liquid fuel into small droplets and enable rapid vaporization in the combustion chamber **[23]**. Thus, it is good to have the high injection pressure condition such as 170 MPa in order to observe the behavior of adhering fuel due to fully atomization of the injection spray.

Table 2-1 Main experimental conditions

Injector	Nozzle type	Single hole nozzle / common rail injection							
	Diameter of nozzle hole D_n mm	0.17							
Injection liquid	Fuel oil	Diesel fuel (JIS No.2)							
	Density at 300K ρ_l kg/m^3	828							
	Surface tension σ kg/s^2	0.0278							
	Viscosity μ_l g/mm-s	3.1×10^{-3}							
Injection condition	Injection period τ_{inj} msec	3.2							
	Injection pressure P_{inj} MPa	40	80	100	120	130	150	170	
	Injection mass m_{inj} mg (P_a = 0.1 MPa)	18.2	24.5	26.8	28.7	29.6	31.5	32.8	
Ambient condition	Temperature T_a K	300							
	Pressure P_a MPa	0.1	0.5	0.7	1	2	4		
	Density ρ_a kg/m^3	1.16	5.8	8.12	11.6	23.2	46.4		
	Viscosity μ_a g/mm-s	1.8×10^{-5}							
Impingement condition	Impingement distance L_w mm	30, 50, 70, 90							
	Impingement disk diameter D_d mm	6	14	20	25	30	35	40	50
	Impingement disk area A_d mm^2	28	154	314	491	707	962	1257	1964
	Inclination wall angle θ_d deg.	0, 10, 20, 30, 40, 50							
	Impingement disk surface roughness RA μm	Approx. 1.6							
	Impingement disk material	A 5056							

The ambient gas temperature in the high pressure vessel was 300 K (i.e. room temperature). The ambient pressure in the vessel was set on from 0.1 MPa to 4 MPa. Here, at P_a = 1 MPa and 300 K, ambient gas density of 11.6 kg/m^3 was equivalent to a compressed gas density of 3 MPa at 800 K. This pressure and temperature were similar to a combustion chamber condition at ignition timing of conventional natural aspirated (NA) diesel engine. In an ultra-high boost engine, compressed gas density in combustion chamber became 4 or 5 times higher than that of NA engine. Therefore in order to clarify the impingement behavior of a diesel spray in ultra-high boost engine, high ambient pressure conditions such as 2 MPa and 4 MPa were included in the test conditions. The impingement distances L_w from the nozzle tip to the wall were varied from 30mm to 90mm. The impingement distance of L_w = 30 mm and 50 mm were set to clarify impingement behavior of small size conventional diesel engine. At these distances for small size of diesel engine, the spray penetration might impinge on the cylinder wall and piston cavity. While impingement distances of L_w = 70 mm and 90 mm were set to examine impingement behavior of medium size diesel engine and early injection of PCCI condition. As early injection timing of PCCI condition, means the in-cylinder temperature and surrounding pressure were low. In other word, the fuel vaporization rate will reduce and the liquid penetration length will increase, and

there might be increased of adhering fuel mass on the wall. Thus, longer impingement distance in this study could be presented for this condition.

Eight different sizes of impingement disk were adopted as shown in **Table 2-1**. The fundamental behavior of adhering fuel is related to the nature of the affinity and it was greatly affected by the surface material. Then in this study, the aluminum which is corresponded to the material of the small type engine piston was used as the impingement wall surface material. The surface roughness of the wall was approximately 1.6 µm. The diameters D_d of impingement disk were 6, 14, 20, 25, 30, 35, 40, and 50 mm. A photograph of each disk diameter is shown in **Fig. 2-7**. Various sizes of disk diameter prepared in this study in order to obtain the behavior of adhered mass as discussed later in Chapter 4. Smaller size of disk was prepared to investigate the critical diameter of impingement disk that could capture the whole adhered fuel. The physical meaning of the critical diameter of disk was the fuel adhesion that remained on the disk.

There is no flat disk impingement in a practical cavity of diesel engine, however, flat wall impingement could considered to appear as the fundamental behavior of wall impingement, and also it was a simple case for phenomenological analysis.
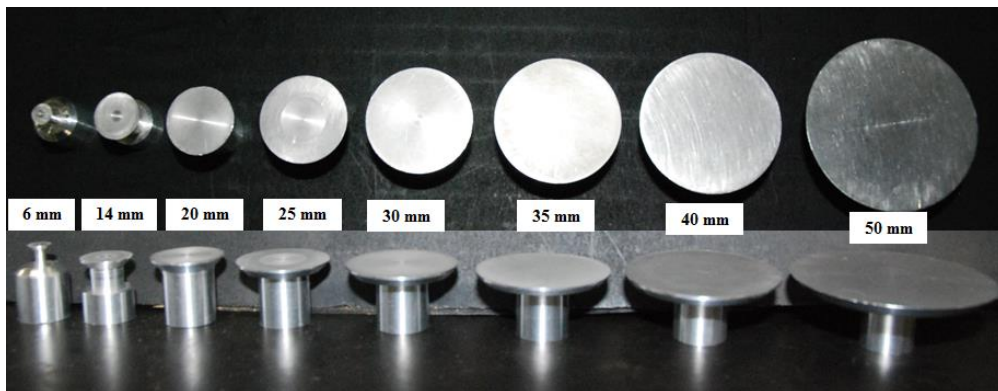
Figure 2-7 Photograph of various size of disk diameter

Further, **Table 2-2** below shows the experimental conditions based on different investigation category. These experimental conditions basically adopted from **Table 2-1** but specifically re-arranged in order to give overall understanding on the investigation that has been done. The investigation of this study has been divided to four categories which mainly discussed on the adhering of fuel mass (Experiments No. 1 to No. 4). Later, details explanation on each category will be discussed in four separate chapters.

Table 2-2 Experimental conditions (based on different investigation conditions)

Experiment	Investigation	Disk diameter	Injection pressure	Ambient pressure	Impingement distance	Inclination angle
		mm	MPa	MPa	mm	deg.
No. 1 (Chapter 3)	Characteristics of spray impingement	20, 30, 40	40, 80, 100, 120, 130, 150, 170	1, 3	30, 50, 70, 90	0
No. 2 (Chapter 4)	Impingement area and wall inclination effect	6, 14, 20, 25, 30, 35, 40, 50	40, 100, 130, 150, 170	1	30, 50, 70, 90	0, 10, 20, 30, 40, 50
No. 3 (Chapter 5)	Weber number effect on adhesion fuel		40, 100, 130, 170			
No. 4 (Chapter 6)	Ambient pressure effect on adhered fuel mass	50	40, 80, 100, 130, 150	0.1, 0.5, 0.7, 1, 2, 4	30, 50, 70, 90	0

(2) Procedures

The measurement procedure of adhering fuel mass is illustrated in **Fig. 2-8**. The mass of dry impingement disk was measured before fuel injection. Then, the impingement disk was set normally to the injector. After spray impinged on the disk, the disk was removed from the high pressure vessel and adhered fuel mass was measured together with the mass of disk by using a precision balance with sensitivity of 0.01 mg.

Impingement diesel spray

Adhered fuel

Mass measurement of disk

Single shot diesel spray impingement

Mass measurement of adhered fuel and disk
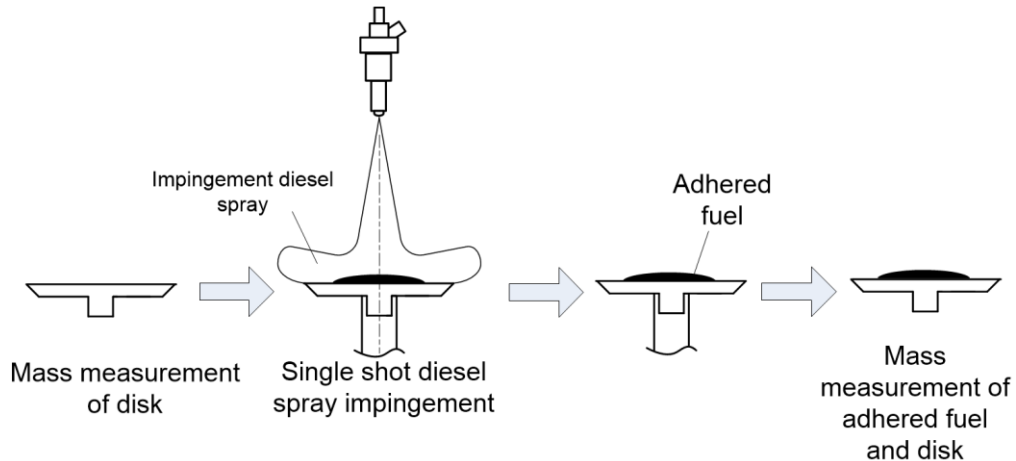
Figure 2-8 Measurement procedure

Adhered fuel mass m_{adh} was derived by the difference of the disk masses of before and after impingement as shown in **Equation (2-1)**. Adhering mass ratio α_{adh} was defined as **Equation (2-2)**. Adhered fuel mass was sampled three times or more in each experimental condition, and then an average of them was taken.

The total mass of injected fuel was measured by using the small bottle with tissues inside the bottle in order to capture the injected fuel. It was measured with a little effect of ambient density. Similar measurement procedure as shown in **Fig. 2-8** but was replaced by the small bottle. The total mass of injected fuel was measured for each injection pressure condition and was sampled more than 5 times, and then average of them was taken. The data error range for both measurements were observed less than 8%.

m_{adh} = [Mass of the disk after spray impingement] – [Mass of the dry disk]   (2-1)

α_{adh} = m_{adh} / [Total mass of injected fuel]   (2-2)

(3) Experimental parameter and data analysis

Figure 2-9 shows definitions of injection velocity, mean diameter and Weber number of spray droplet. Droplet near the spray tip was represented by injection velocity (V_{inj}), Sauter mean diameter (D_{SMD}) of spray and Weber number (We_{inj}) of droplet. The injection velocity was calculated using the injection rate during a steady state period of spray. The Sauter mean diameter (D_{SMD}) of spray was derived from typical empirical equations of diesel spray [24]. The equations were derived as follows.

$$\frac{D_{SMD}}{D_n} = MAX \left[\frac{D_{SMD}^{LS}}{D_n}, \frac{D_{SMD}^{HS}}{D_n} \right]$$ (2-3)

$$\frac{D_{SMD}^{LS}}{D_n} = 4.12 Re^{0.12} We^{-0.75} \left(\frac{\mu_l}{\mu_a} \right)^{0.54} \left(\frac{\rho_l}{\rho_a} \right)^{0.18}$$ (2-4)

$$\frac{D_{SMD}^{HS}}{D_n} = 0.38 Re^{0.25} We^{-0.32} \left(\frac{\mu_l}{\mu_a} \right)^{0.37} \left(\frac{\rho_l}{\rho_a} \right)^{-0.47}$$ (2-5)

Where, MAX [A,B] means the larger value of two. Viscosities of liquid (l) and ambient gas (a) are shown with μ_l and μ_a, and ρ is density. Weber number and Reynold number are represented the non-dimensional value of injected fuel, and representative diameter was nozzle hole diameter. Based on the injection velocity and the mean diameter, Weber number of droplet was derived as follows.

$$We_{\text{inj}} = \frac{\rho_l V_{inj}^2 D_{SMD}}{\sigma} \qquad (2\text{-}6)$$

Where, σ is the surface tension of liquid. The Sauter mean diameter (D_{SMD}) of spray was the volume-surface mean diameter of spray. In this study, it could be assumed that spray-wall interaction was to be discussed using the average Weber number based on D_{SMD}. Sauter mean diameter was convenient to understand the evaporation feature of spray because it represents the mean surface area of spray droplets. It might be doubtful to represent the impingement behavior of spray. However, D_{SMD} was used in the study, because there were many research works on diesel spray D_{SMD} and it became convenient to compare the previous works of various diesel spray researches.

Droplet near the wall surface was represented by impingement velocity (V_{imp}), normal impingement velocity ($V_{\text{imp.n}}$), Weber number (We_d) of droplet at impingement and Weber number ($We_{d.n}$) of droplet at normal impingement. Impingement velocity of droplet was an absolute velocity close to the wall surface. This velocity was obtained based on the spray tip movement at each impingement point. High-speed camera was used to observe the movement of spray tip. Weber number (We_d) of droplet at impingement was described as follows.

$$We_{\text{d}} = \frac{\rho_l V_{imp}^2 D_{SMD}}{\sigma} \qquad (2\text{-}7)$$

Normal impingement velocity ($V_{\text{imp.n}}$) was an approaching velocity of droplet to the impingement wall. Since the droplet impact energy to the wall was directly concerned by this approaching velocity, it might be more important than the absolute velocity. It was calculated using impingement velocity and inclination wall angle.

$$V_{\text{imp.n}} = V_{\text{imp}} \cdot \cos \theta_{\text{d}} \qquad (2\text{-}8)$$

Based on **Equation (2-8)**, Weber number ($We_{d.n}$) of normal impingement was derived as follows.

$$We_{\text{d.n}} = \frac{\rho_l V_{imp.n}^2 D_{SMD}}{\sigma} \qquad (2\text{-}9)$$
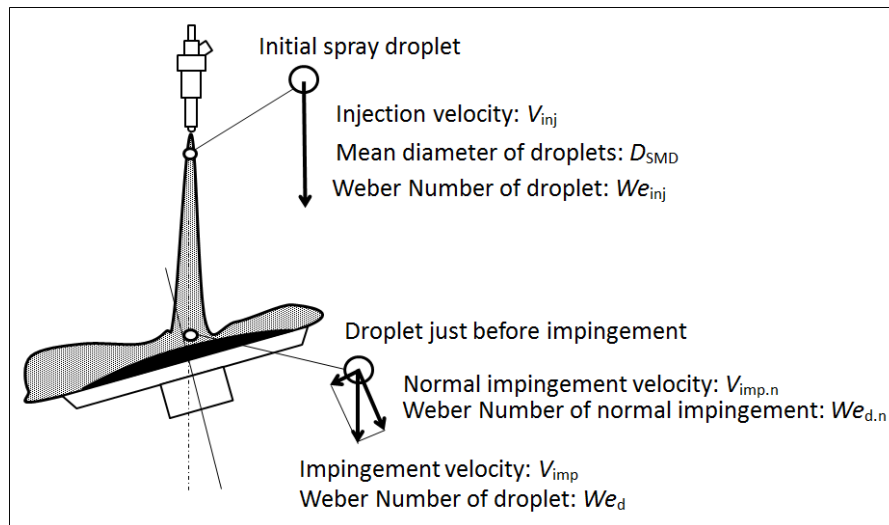
Figure 2-9 Definitions of injection velocity, mean diameter and Weber number of droplet

2.5 Basic performance of the single hole injector

(1) Injection rate of fuel

Figure 2-10 shows the injection rate history of 3.2 ms injection period. The injection rate was measured using the Bosch type (long tube method) injection rate meter. Since the spray behavior such as penetration, adhering fuel mass and others were affected by injection rate history **[25]**, the injection rate data were important as a start of this study.

$P_{inj} = 150$ MPa

$\tau_{inj} = 3.2\ ms$
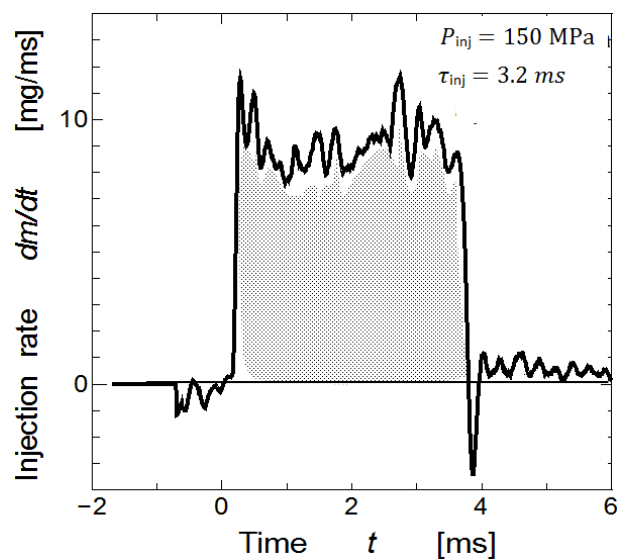
Figure 2-10 Time history of injection rate

Injection pressure was 150 MPa. Injection mass of test fuel was 31.5 mg with a little influence of ambient pressure because effective injection pressure (P_{inj} − P_a) was mainly dominated with absolute injection pressure. Constant injection rate was almost attained except the short periods of injection start and end. Since the constant injection rate obtained, the injection mass of fuel was reliable for this study.

(2) Injection mass of fuel

Figure 2-11 shows the relationship of injection mass of fuel and the injection pressure under injection period of 1.5 msec and 3.2 msec. As referred in **Fig. 2-11**, for both injection periods, the injection fuel mass increased by an increase of injection pressure. The injection fuel mass of 3.2 msec-spray increased steeper than 1.5 msec-spray. However, the same trend of increment of injection fuel mass which was proportional to square root of pressure difference ((P_{inj} − P_a)$^{0.5}$) between injection pressure and ambient pressure was maintained. Owing to the high ambient pressure, the injection fuel mass in high ambient pressure condition (P_a = 4 MPa) was slightly lower than that in 1 MPa condition. Injection mass was proportional to the period of injection duration. It means the other evidence of steady state injection was continued and injection rate did not changed. The total mass of injected fuel changed with injection and surrounding pressures.
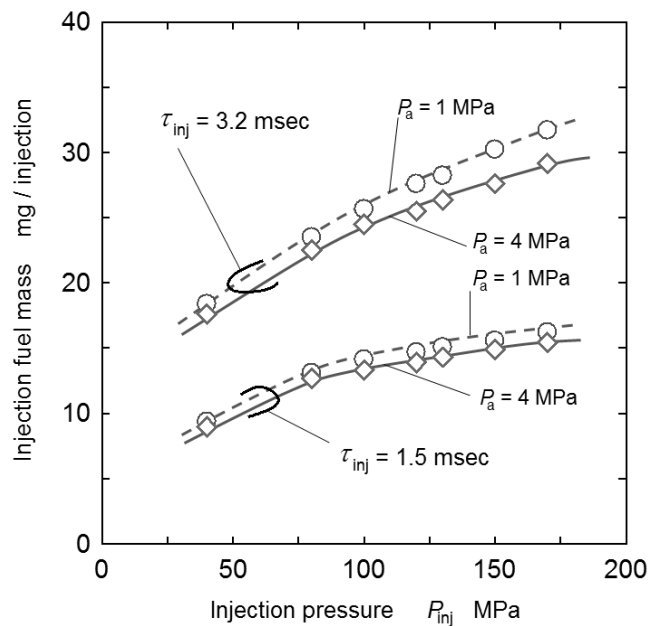
Figure 2-11 Injection mass of fuel

(3) Spray tip velocity and D_{SMD} from injection rate

Figure 2-12 shows the spray tip velocity at various injection pressure from 40 MPa to 170 MPa and ambient pressure of 1 MPa. The spray tip velocity was calculated based from the spray penetration of the free spray which measured from the shadow graph images.
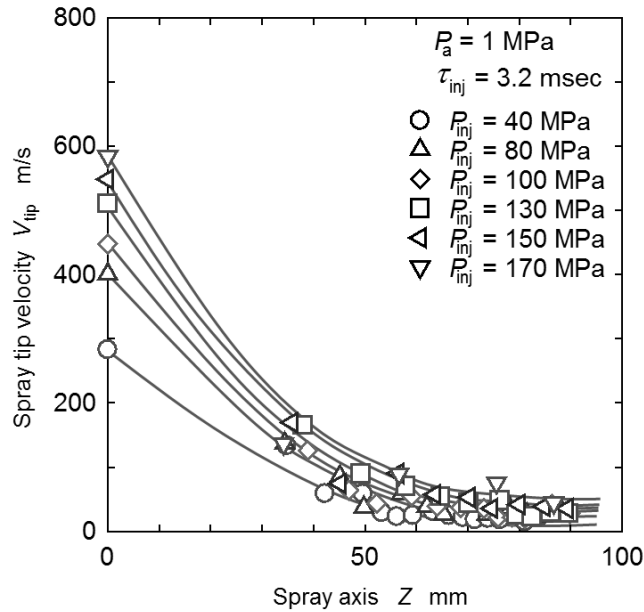
Figure 2-12 Spray tip velocity

The results show the spray velocity decreased with increases of axis distance which is the distance from the nozzle tip to the impingement wall. Also the spray velocity decreased with decreases of injection pressure. In this study, this kind of result was used as to estimate the impingement velocities at various impingement distances.

Figure 2-13 shows the calculated Sauter mean diameter at various ambient pressures and injection pressures. Almost all the obtained D_{SMD} was the under high speed regime shown by **Equation (2-5)**, except low injection pressure with low ambient pressure. The result shows the D_{SMD} decreased with increases of injection pressure regardless of ambient pressure. The decreasing trends were almost similar for all ambient pressures cases. The D_{SMD} obtained larger value at ambient pressure of 4 MPa, while lower at ambient pressure of 0.1 MPa. As the ambient pressure increased, the spray velocity decreased and resulted to increase of droplet size. Also, when at high ambient pressure, coalescence of droplets due to small penetration of spray resulted to large droplet size. The similar result was

also obtained by Hiroyasu et al. **[26]**. Further, this result was used later in Chapters 5 and 6 for detailed discussion on the Weber number correlation on adhered fuel mass.
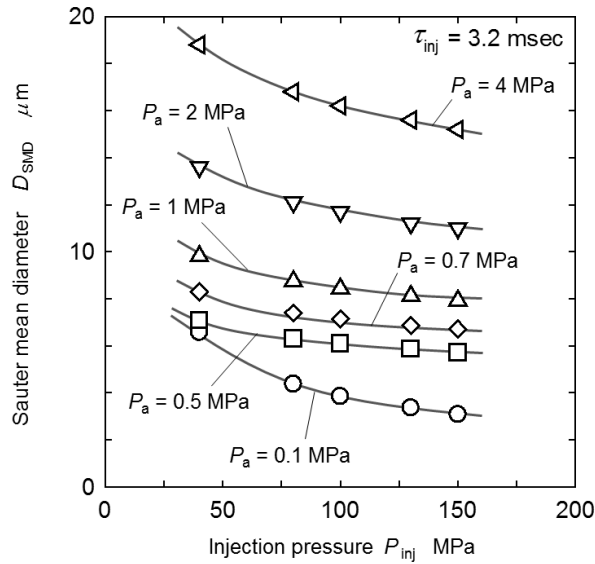
Figure 2-13 Calculated Sauter mean diameter

2.6 Injection period and injection shot number

Effects of injection period and injection shot number on the total adhering mass of fuel were investigated as the start of experiment of this research. The summary of the results are shown in **Fig. 2-14**.
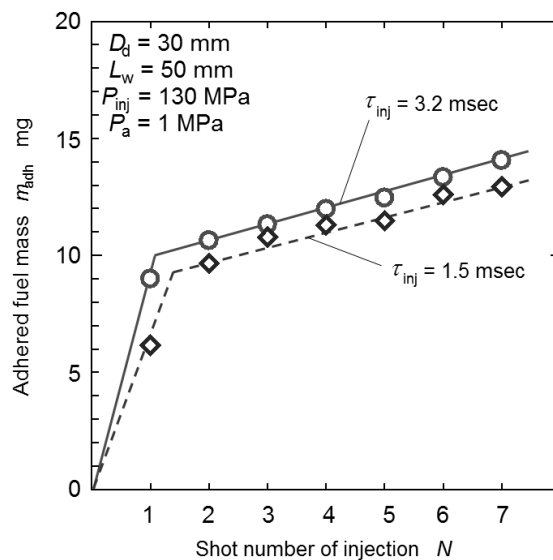
Figure 2-14 Effects of injection period and injection shot number on adhered mass of fuel

57

Experiment conditions were based on an impingement disk of 30 mm, impingement distance of 50 mm, injection pressure of 130 MPa and ambient pressure of 1 MPa. Both of the injection period of 1.5 msec and 3.2 msec showed the same trend of adhering fuel mass.

The adhered fuel mass increased with shot number N of injection. As for $N = 2$ to $N = 7$ shots of injection, there was only a small increase of fuel mass on the disk compared to a single shot injection. Referring to the literature of Ko and Arai [12], due to repetition and continuous injection, the fuel film was formed on each injection and a strong splash occurred with the breakup of fuel film. While it did not occur during the single shot injection. The single shot injection was conducted on the dry wall surface. It means the single shot injection represented for the dry wall impingement condition. While two or more than two shots of injection represented the wet wall impingement condition. Since only small increased of adhered fuel mass appeared on the wet wall condition, the dry wall condition was much important for analyzing the adhesion behavior on the wall surface.

As for fuel adhering phenomena in a real engine, only a single shot impingement occurred at every engine cycle. Sometimes, two and three injections happened when a pilot or a split injection was adopted. In this study, as a fundamental study of adhering fuel research, the single shot case was used for the main study of fuel adherance.

2.7 PIV analysis

2.7.1 Experimental setup and PIV procedure

Schematic view of experimental set-up for PIV flow analysis is shown in **Fig. 2-15**. This setup was similar with main experimental setup as explained earlier in **Section 2.3.1**. However, additional apparatus was used in this PIV configuration. For velocity measurement inside a diesel spray, continuous laser was utilized as a light source, and a laser-light sheet was formed. Then tomographic image of a diesel spray was obtained. The thickness of laser-light sheet was adjusted and set on 1mm. The digital high-speed camera (Vision Research, Phantom V711) was arranged in perpendicular position to the laser-light sheet, and sequential images of a diesel spray were captured.

Time-resolved PIV analysis was applied to measure velocity field inside an impingement spray. For PIV analysis, correlative tomographic images with narrow time interval were required. Consequently, the frame rate was set to be a

spray displacement around 5 pixels on sequential images. Since an ultra-high frame rate of 150,000 f.p.s was needed for PIV analysis, image size was restricted by the performance of digital high-speed camera. Spatial resolution was fixed constant at 0.08 mm/pixel regardless of inclination angle of the disk. A droplet with velocity of 100 m/s moved 0.67 mm at one frame interval (1/150,000 sec.). Then the relatively thicker laser light sheet (1mm) and high frame rate of the camera were helpful to catch droplets traveling random directions including normal direction of observation plane.

According to the insufficient spatial resolution (0.08 mm/pixel) of an image, each droplet in a spray could not be resolved on an image. Inside diesel spray, number density of the droplets was very high. Consequently, cloud of spray droplets could be captured as photo-density distribution in a spray image. Thus velocity distribution of droplet cloud could be obtained with PIV analysis based on direct cross-correlation method with sub-pixel accuracy. Spray droplet clouds did not behave as a continuous fluid. Then conventional error removal and interpolation technique for PIV data was not applied, because those techniques were based on a concept of continuous fluid.

In this PIV analysis, interrogation spot size was 21 pixels×21 pixels which coincided with 1.84 mm×1.84 mm of real image, and interrogation spot area of 50% was overlapped with the adjacent interrogation area. It means that grid space in PIV analysis was 0.92 mm. In order to measure velocity near the disk, velocity measurement point nearest the disk was set at 0.2 mm from the disk.
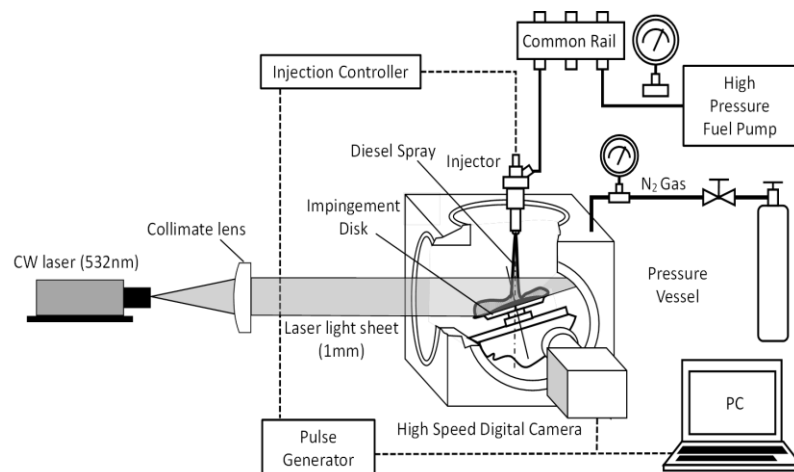
Figure 2-15 Experimental setup with PIV consideration

2.7.2 Wall impingement and bar impingement

As shown in **Fig. 2-16** (A), post-impingement diesel spray was rolling up after impingement. Post-impingement spray was developing all three dimensional (3D) directions on the impingement surface, and its spreading part located at front of the camera became shading the tomographic image that should be captured. Therefore, it was difficult to capture high quality PIV image of post-impingement diesel spray.

In order to reduce the effect of the rolled-up post-impingement spray on the tomographic image, slender bar shown in **Fig. 2-16** (B) was adapted as an impingement wall. Width of the bar was 5mm, and its width corresponded with the half of spray width. The bar was placed on the flat wall. After impingement to the bar, the spray located at the front of camera hardly rolled up, and it did not shade the 2D tomographic image of the post-impingement spray on the bar. However, three dimensional (3D) flow structure of the post-impingement spray spreading radially was slightly maintained due to the width of the bar and 3D motion of the spray on the flat wall located under the bar. By adapting the slender bar, tomographic image of the post-impingement spray could be captured more clearly than that of flat disk case.
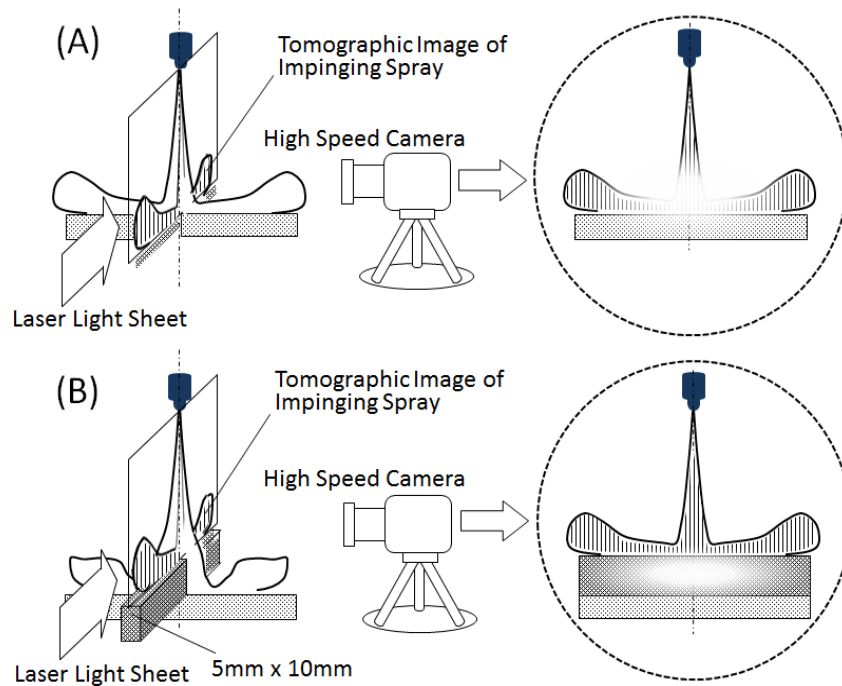
Figure 2-16 3D and 2D construction of impingement diesel spray

Figure 2-17 shows velocity fields of diesel spray impinging on the flat disk and the slender bar for 20 deg. of inclination angle. The vector map was obtained from the tomographic image (t_{imp} = 0.18 ms). Spray peripheries of the post-impingement sprays of flat wall and bar impingement were almost the same, and were shown with dash lines. As shown in both of these vector maps, no obvious differences of flow pattern at the tips and upper parts of post-impingement spray were observed. However, no information in the vicinity of the wall was obtained from **Fig. 2-17 (a)**, whereas velocity distribution near the wall (H < 0.2 mm) was clearly obtained when the post-impingement image was captured by the slender bar impingement system. It means that velocity information of whole post-impingement spray could be obtained by using bar impingement. Then it was concluded that the slender bar impingement system shown in **Fig. 2-16** (B) could provide more detail flow information inside post-impingement spray, and the result for bar impingement could be used as a substituted result of flat wall impingement.

(a) Flat wall impingement
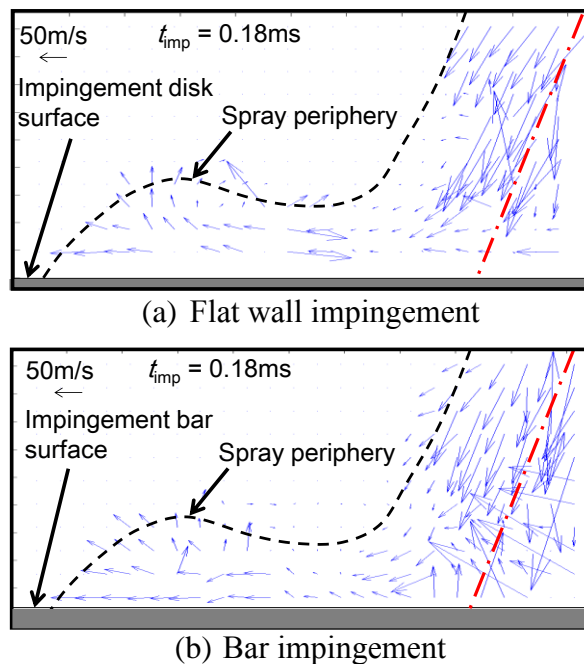
(b) Bar impingement

Figure 2-17 Flow patterns of diesel spray to flat wall impingement and bar impingement

2.8 Summaries

For the fundamental research on the impinging diesel spray, adhered fuel mass was the important factor considered in this study. Measurement of the adhered fuel mass was discussed in this chapter in detailed. Experimental

apparatus was described accordingly. The experimental procedure for measuring adhered fuel mass was explained. Range of experimental conditions such as impingement distance, injection pressure, ambient pressure, disk size and inclination angle were discussed and fixed. Also, the basic performance of the single hole injector was discussed for clear understanding on the injection characteristics. Finally, PIV configuration and analysis on impinging spray were explained briefly.

References

[1]   Boot, M., Rijk, E., Luijten, C., Somers, B., and Albrecht, B., Spray impingement in the early direct injection premixed charge compression ignition regime, *SAE Technical Paper*, 2010.

[2]   Han, M., Assanis, D.N., and Bohac, S.V., Sources of Hydrocarbon Emissions from Low-Temperature Premixed Compression Ignition Combustion from a Common Rail Direct Injection Diesel Engine, *Combustion Science and Technology*, vol. 181, no. 3, pp. 496–517, Feb. 2009.

[3]   Arai, M., Physics behind diesel spray characteristics and Its Combustion, *Proc. Engine Combustion Process, Current Problems and Modern Techniques, 11th Congress, Ludwingsburg, Germany,* pp. 417-436, 2013.

[4]   Tsunemoto, H. and Ishitani, H., The Behavior of Impinged Fuel Sprays on Simulated Combustion Chamber Walls in Direction Injection Diesel Engine, *JSAE Rev.*, vol. 3, pp. 9-14, 1982.

[5]   Arifin, Y.M., Diesel and Bio-diesel Fuel Deposits on a Hot Wall Surface, PhD Thesis., Gunma University, Japan, 2009.

[6]   Mathews, W.S., Lee, C.F., and Peters, J.E., Experimental investigations of spray/wall impingement, *Atomization and Spray*, vol. 13, pp. 223-242, 2003.

[7]   Werlberger, P. and Cartellieri, W.P., Fuel injection and combustion phenomena in high speed DI diesel engine observed by means of endoscopic high speed photography, *SAE paper*, no. 870097, 1987.

[8]   Eckhause, J.E. and Reitz, R.D., Modelling heat transfer to impinging fuel sprays in direct-injection engines, *Atomization and Spray*, vol. 5, pp. 213-242, 1995.

[9]   Taylor, C.F., The internal-combustion engine in theory and practice: Volume II, London: The MIT press, 1980.

[10] Andreassi, L., Ubertini, S. and Allocca, L., Experimental and numerical analysis of high pressure diesel spray-wall interaction, *Int. Journal of Multiphase Flow,* vol. 33, pp. 742-765, 2007.

[11] Park, S.W. and Lee, C.S., Macroscopic and Microscopic characteristic of a fuel spray impinged on the wall, *Experiments in Fluids 37*, Springer-Verlag, pp. 745-762, 2004.

[12] Ko, K. and Arai, M., Diesel Spray Impinging on a Flat Wall, Part 1: Characteristics of Adhered Fuel Film in an Impingement Diesel Spray, *Atomization and Spray*, vol. 12(5&6), pp. 737-751, 2002.

[13] Katsura, N., Saito, M., Senda, J. and Fujimoto, H., Characteristics of a Diesel Spray Impinging on A Flat Wall, *SAE paper*, no. 890264, pp. 191-207, 1989.

[14] Bai, C.X., and Gosman, A.D., Development of a methodology for spray impingement simulation, *SAE tech paper*, no. 950283, 1995.

[15] Randy, L., Vander, W.G., Berger, G.M., and Mozes, S.D., The combined influence of a rough surface and thin fluid film upon the splashing threshold and splash dynamics of a droplet impacting onto them, *Experiments in Fluids*, pp. 23-32, 2006.

[16] Stow, C.D., and Hadfield, M.G., An experimental investigation of fluid flow resulting from the impact of a water drop with an unyielding dry surface, *Proc R Soc Lond A*, pp. 419-441, 1981.

[17] Naber, J.D. and Reitz, R.D, Modeling spray/wall impingement, *SAE Paper*, no. 880107, 1988.

[18] Bai, C., Rusche, H., and Gosman, A., Modelling of gasoline spray impingement, *Atomization and Sprays*, pp. 1–28, 2002.

[19] Ko, K. and Arai, M., Diesel Spray Impinging on a Flat Wall, Part 2: Volume and Average air-fuel ratio of an Impingement Diesel Spray, *Atomization and Spray*, vol. 12(5&6), pp. 753-768, 2002.

[20] Ko, K. and Arai, M., The Characteristics of Post Impingement Diesel Spray, Part 1: Penetration and Volume, *Atomization and Spray*, vol. 12(4), pp. 403-417, 2002.

[21] Ko, K. and Arai, M., Diesel Spray and Adhering Fuel on an Impingement Wall, *SAE paper*, no. 2002-01-1628, pp. 115-128, 2002.

[22] Senda, J., Ohnishi, M., Takahashi, T., Fujimoto, H., Utsunomiya, A., and Wakatabe, M., Measurement and modeling on wall wetted fuel film profile and mixture preparation in intake port of SI engine, *SAE tech paper*, no. 1999-01-0798, 1999.

[23]   Agarwal, A.K, Srivastava, D.K., Dhar, A., Maurya, R.K., Shukla, P.C., and Singh, A.P., Effect of fuel injection timing and pressure on combustion, emissions and performance characteristics of a single cylinder diesel engine, *Fuel*, pp. 374-383, 2013.

[24]   Hiroyasu, H. and Arai, M., Structures of Fuel Sprays in Diesel Engines, *SAE paper*, no. 900475, pp. 1-12, 1990.

[25]   Azetsu, A.,Wakisaka, Y., Fukuchi, Y. and Oikawa, C., Effect of fuel injection rate shaping on spray combustion (1st Report: An electronically controllable fuel injection system for variable injection rate shaping and analysis of spray), *JSME*, vol. 64, no. 624, pp. 371-377, 1998.

[26]   Hiroyasu, H., Arai, M. and Tabata, M., Empirical equations for the sauter mean diameter of a diesel spray, *SAE Paper*, no. 890464, 1989.

Chapter 3

Characteristics of spray impingement

3.1 Introductory remarks

Since the combustion chamber in a diesel engine is too small to mix injected fuel and surrounding gas perfectly, wall impingement of the spray is considered to be inevitable in the engine. Therefore it is important to understand the basic behavior of impingement spray and the fuel dispersion after impingement. Especially normal impingement on the flat wall is the fundamental of inclined wall impingement and also the fundamental of impingement phenomena on a wall with curvature. In this chapter, the effects of impingement distance, injection pressure and ambient pressure on adhering fuel mass of a normally imping diesel spray on a flat wall were investigated experimentally. The investigation in this chapter is focused on the non-evaporating spray. Though the evaporation process of fuel injected in combustion chamber has greatly effect on engine performance and exhaust emission, it is determined by the behavior of the non-evaporating spray in combustion chamber. Therefore, understanding fundamental characteristics of non-evaporating spray has the very important meaning to characterize an evaporating spray.

Recently, injection pressure tended to increase in order to promote atomization of diesel fuel as compared with a conventional diesel engine **[1]**. In this study, due to the importance of injection pressure and impingement distance, effects of injection pressure and impingement distance on adhering fuel were discussed in detail. In addition, the experiment in this study was carried out under room temperature, therefore results obtained in this study could be directly useful for the case of cold starting diesel engine.

3.2 Adhered fuel mass

Various evaluation indexes concerning adhered fuel are shown in **Fig. 3-1**. The various evaluation indexes were based on P_{inj} = 130 MPa, D_d = 30 mm, and P_a = 1 MPa with various impingement distances. Evaluation indexes were adhered fuel mass (m_{adh}), adhered mass ratio (α_{adh}) and average adhered thickness (h_{adh}). The physical meaning of average adhered thickness was an average thickness of

fuel film which remained on the disk. It was derived by adhered fuel mass over the area of the disk (A_{adh}) and density of fuel (ρ_{fuel}) as shown in **Equation (3-1)**.

$$h_{adh} = m_{adh} / (\rho_{fuel} . A_{adh}) \qquad (3\text{-}1)$$

Figure 3-1 shows that the adhering fuel mass on a dry surface was from 3 mg to 12 mg under a single shot injection. While the adhered mass ratio was from 0.12 close to 0.45. Behaviors of all three indexes were the same because there were linear relationships among them. Over the impingement distance of 70 mm, the adhered fuel mass and the other two indexes tended to increase slowly up to an impingement distance of 90 mm.
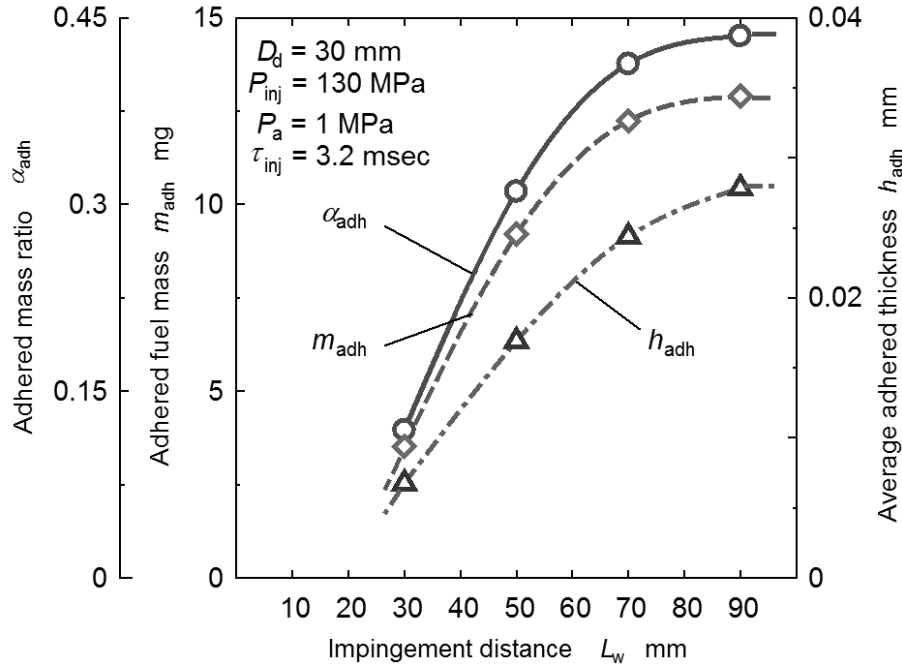
Figure 3-1 Various evaluation indexes of adhered fuel

Average adhered thickness was estimated to be 0.007 mm (7 μm) to 0.028 mm (28 μm). These results were in good agreement with those suggested by Ko and Arai **[2]**, who reported that the adhered thickness of the fuel film was in the range from 10 μm to 30 μm. At the impingement distance of 30 mm, the adhered thickness approached to 0.01 mm (10 μm) which was in the range of droplet size of diesel spray. Thin fuel film thickness such as 10 μm seemed to allow direct interaction between impinging droplets and the impingement wall surface even though the droplet impinged on the surface of fuel film. However, as the

impingement distance increased up to 90 mm, the adhered thickness grew to 0.03 mm (30 µm) which was much larger than the droplet size of the diesel spray. The thick fuel film appeared to be suitable to capture fuel droplets impinging on the fuel film surface. The adhered thickness estimated here could be further discussed by using the concept of non-dimensional thickness of adhered fuel film to the mean diameter of spray as explained later in Chapter 5.

3.3 Impingement distance and adhered mass ratio

Figure 3-2 shows the relationship between impingement distance and adhered mass ratio for an impingement disk diameter of 20 mm. As for the cases of injection pressure of 40 MPa, adhered mass ratio increased with an increase of impingement distance up to 70 mm. However, at an impingement distance over 70 mm, adhered mass ratio tended to decrease. Beyond the 70 mm condition, it seemed that the momentum of spray droplets became small due to momentum exchange between the droplets and surrounding gas. They moved with the entrained gas stream, therefore, spray droplets were less like adhering to the disk. This phenomena also found in Katsura et al. **[3]** experimental works where the result shows that small droplets are deflected away from the wall and taken away by the gas flow near the wall. In addition, the injection pressure of 40 MPa was lower than injection pressures of other conditions (80 MPa to 170 MPa). Regardless of impingement distance, it suggested that a non-splash effect occurred due to the low momentum of diesel spray itself.
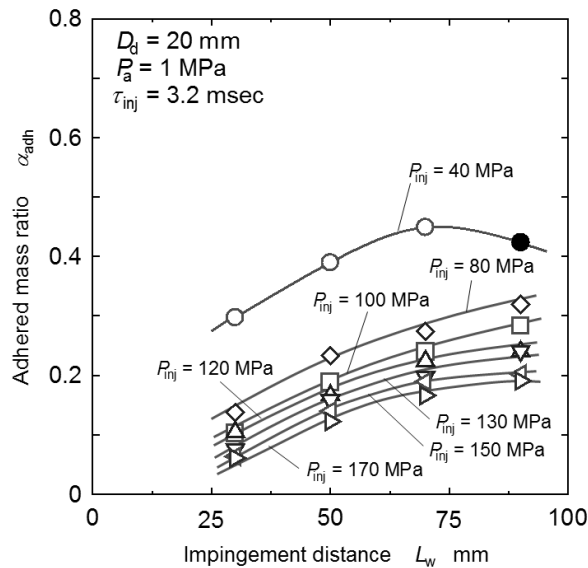
Figure 3-2 Effects of impingement distance and injection pressure on adhered mass ratio of 20 mm impingement disk

On the other hand, as for injection pressures over 80 MPa, the adhered mass ratio increased gradually with an increase of impingement distance. It seemed that the momentum of spray droplets was maintained up to 70 mm due to injection pressure higher than 40 MPa. It also suggested that strong impingement and splash of fuel film occurred. Since the splash effect was stronger than the adhering mechanism, adhered mass ratio at injection pressure over 80 MPa were less than that of injection pressure of 40 MPa. These trends seems similar to Ko and Arai [4] experimental works. According to their results, the adhering fuel ratio tended to decrease when impingement distance reached up to 70mm. However, in their study, the impingement distance was limited only to 70mm and the injection period was 1.8 msec which is slightly shorter period than this experimental work.

As referred to **Fig. 3-2**, there were two types of fuel adherance trends. The first one is shown by the blank symbol (plotted by ○) and named as the 'A' trend. It meant that adhered mass ratio increased with an increase of impingement distance. The second is shown by the filled symbol (plotted by ●) and named as 'B' trend. It meant the decreasing manner of adhered mass ratio with an increase of impingement distance. These definitions of 'A' and 'B' were also applied in later figures of this chapter.

The adhered mass ratio for a 30 mm disk impingement is shown in **Fig. 3-3**. For injection pressure of 40 MPa, adhered mass ratio increased when impingement distance increased from 30 mm to 50 mm. From the data in **Fig. 3-1**, an average adhered thickness at $L_w = 50$ mm was 58 μm and it seemed to be a sufficient thickness to capture fuel droplets into the fuel film, because of the low droplet velocity of the 40 MPa spray. The adhered thickness estimated here could be further discussed by using the concept of non-dimensional thickness of adhered fuel film to the mean diameter of spray as explained later in Chapter 5. Furthermore, adhered mass ratio decreased with further increase of impingement distance (70 mm and 90 mm). On the other hand, for injection pressures of 80 MPa and 100 MPa, it continued to increase up to an impingement distance over 70 mm. Then, it tended to decrease under impingement distances longer than 70 mm. When injection pressure was set beyond 120 MPa, adhered mass ratio increased continuously up to 90 mm impingement.

The case of an impingement disk size of 40 mm, the adhered mass ratio is shown in **Fig. 3-4**. Trends of adhered mass ratio indicated by 'A' and 'B' were similar to the cases of the 30 mm impingement disk but these trends appeared more clearly in **Fig. 3-4** (40 mm disk) than **Fig. 3-3** (30 mm disk). Average adhered fuel thicknesses found in **Fig. 3-1** were around 6 μm at $L_w = 30$ mm ($D_d =$

40 mm and P_{inj} = 170 MPa) and around 23 μm at L_w = 90 mm (D_d = 40 mm and P_{inj} = 170 MPa).   These fuel film thicknesses were thin enough for direct interaction of impinging droplets and the wall surface under fuel film. It suggested the possibility of the re-bound of droplet or fuel film splash that will be explained later in this chapter.

Figure 3-3 Effects of impingement distance and injection pressure on adhered mass ratio of 30 mm impingement disk
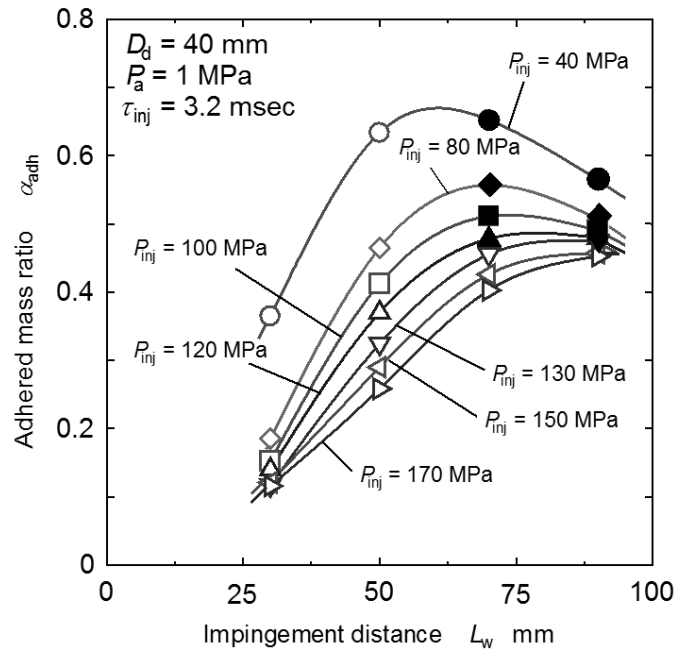
Figure 3-4 Effects of impingement distance and injection pressure on adhered mass ratio of 40 mm impingement disk

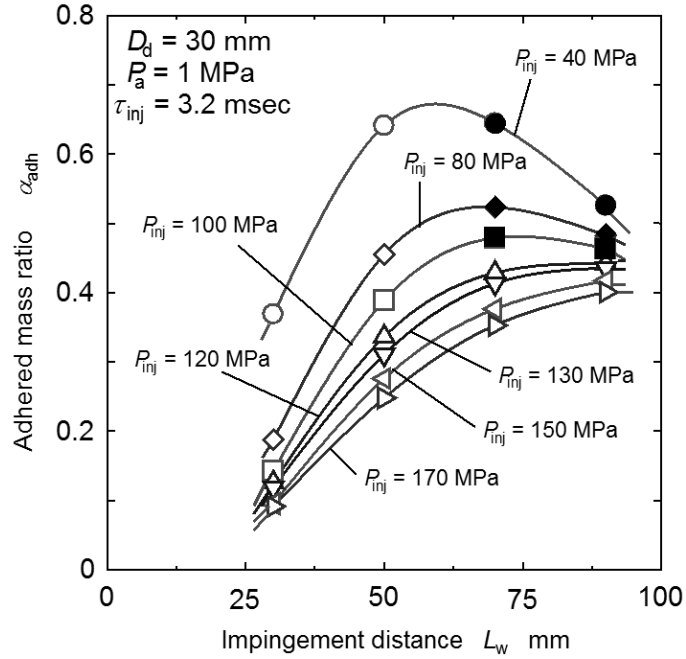'A' and 'B' trends indicated different mechanisms of fuel adherance. The 'A' trend showed the tendency for adhered mass ratio to increase with an increase of impingement distance regardless of injection pressure. It meant that fuel adhering by 'A' mechanism was not significantly dependent on injection pressure. Re-bound of spray droplets and splash of adhered fuel were considered as the main mechanism of less adhering fuel. Furthermore, short impingement distances such as $L_w = 30$ mm had stronger influences on less adherance than injection pressure. In the 'B' trend, adhered mass ratio tended to decrease with an increase of impingement distance. Owing to the slow velocity of long spray penetration, spray droplets moved with the entrained gas stream and less adherance was formed with a greater increase of impingement distance.

3.4 Impingement velocity effect

From the results of **Figs. 3-2 to 3.4**, it might be suggested that the 'A' trend showed a velocity domain dependance, while the 'B' trend might depend on the lower value than a critical velocity of velocity dependance domain. **Figure 3-5** show the another expression of the results shown in **Fig. 3-3**. Here, impingement velocity was selected as the main parameter of the phenomena. Injection velocity was set by injection pressure whereas impingement velocity was dominated with injection pressure and impingement distance. Then this velocity had a direct effect on impingement phenomena and it was the reason why it was selected as the main parameter. This classification was clearly shown in **Fig. 3-5**. Critical velocity divided 'A' and 'B' trends was at around 40 m/s. Even though critical velocity was one of the dominant parameter that affected adhered fuel mass but it was insufficient to explain the overall phenomena. There were some complicated trend as shown in **Fig. 3-5**. For example at the velocity of 40 m/s, trends of 'A' and 'B' were weird. Even though same impingement velocities, adhered mass ratios showed different behavior according as injection pressure and impingement distance. The complicated trend was regarding another controlling factor of changing of adhered mass ratio. The factor of critical velocity alone was not enough to justify the mechanism changed of adhered mass ratio. It might be effect of droplet diameter and others. Then more detail discussion was performed in Chapter 5 by introducing the Weber number of impinging droplet.
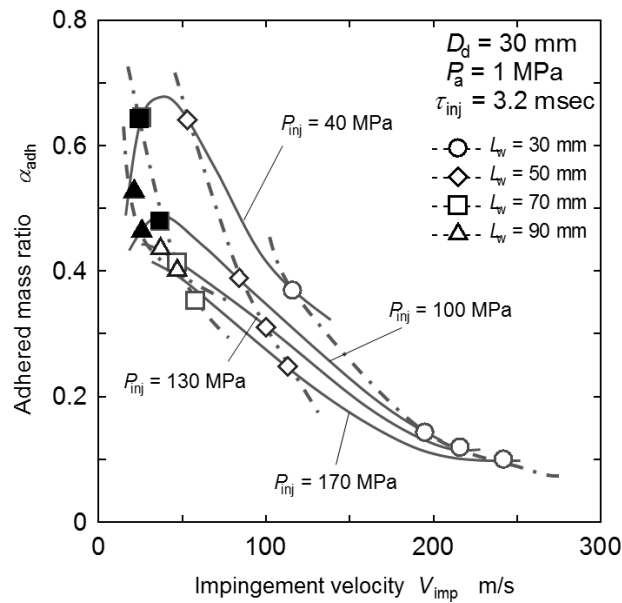
Figure 3-5 Relationship between adhered mass ratio and impingement velocity

3.5 Impingement surface area and adhered mass ratio

Figures 3-2, **3-3** and **3-4** were re-arranged using the surface area of each impingement disk. **Figure 3-6** shows the effect of disk area on adhered mass ratio in the case of the 30 mm impingement distance. At an impingement disk area of 314 mm^2 (D_d = 20 mm), adhered mass ratio was slightly lower than that of impingement disk area of 707 mm^2 (D_d = 30 mm).
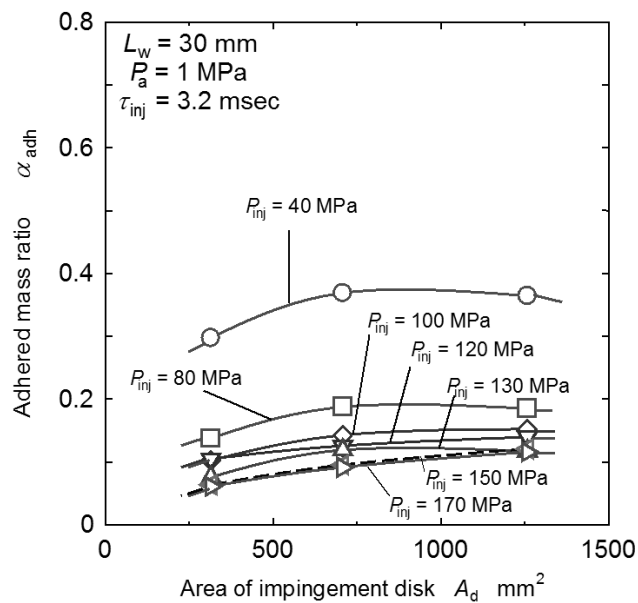
Figure 3-6 Effects of impingement disk area and injection pressure on adhered mass ratio of 30 mm impingement distance

While for an area of 1257 mm^2 ($D_d = 40$ mm), the adhered mass ratio was most likely the same as that of 707 mm^2 even though the impingement area increased by almost two times. There is little difference of adhering mass ratio obtained for each area of impingement disks. This resulted the average adhered thickness of fuel being inversely proportional to the area of impingement disk. It was considered that diesel spray impinged only on the center area of the impingement disk as shown later in **Figs. 3-9 to 3-11**. Fuel adherance seemed to occur mainly on this center area and the adhered fuel film seemed to be stretched by radial movement of the post impingement spray. It might cause an apparent decrease in average adhered thickness.

The adhered mass ratio increased with decrease of injection pressure for all of the impingement area conditions. Based on the injection pressure, the initial velocity of a 40 MPa injection diesel spray had 0.7 times lower velocity than of 80 MPa diesel spray. It suggested that the amount of adhered fuel for an injection pressure of 40 MPa was higher due to insufficient injection velocity for splash and re-bound.
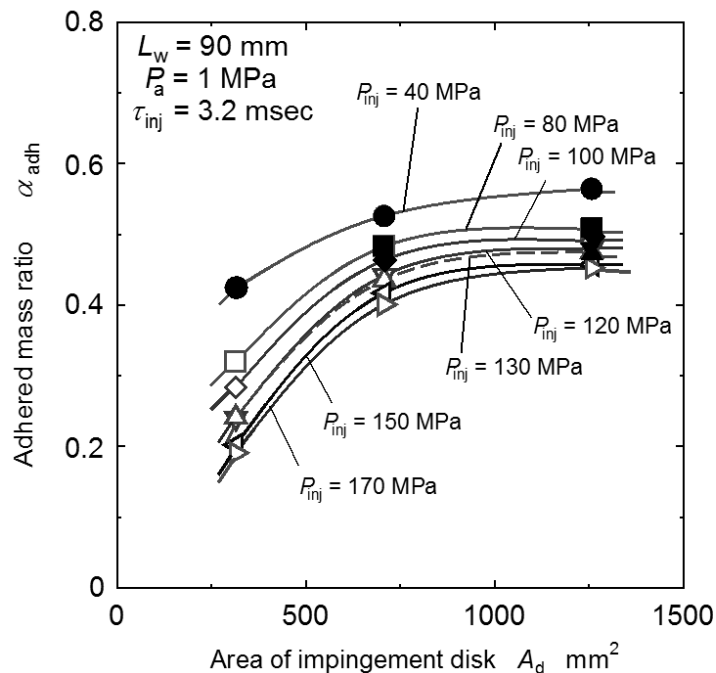
Figure 3-7 Effects of impingement disk area and injection pressure on adhered mass ratio of 90 mm impingement distance

Figure 3-7 shows the effect of disk area on adhered mass ratio in the case of an impingement distance of 90 mm. It appears that adhered mass ratio proportionally increased with area from 314 mm^2 to 707 mm^2. It shows that the

average adhered thickness of fuel between these areas is constant. However, adhered mass ratios were close to constant for disk areas from 707 mm^2 and 1257 mm^2. Thus, the average adhered thickness of fuel between these areas were inversely proportional to the area of the impingement disk.

3.6 Ambient pressure and adhered mass ratio

In this section, the effect of ambient pressure on the adhered fuel mass was discussed. **Figure 3-8** shows the comparison of adhered masses between ambient pressures of 1 MPa and 3 MPa. For an impingement distance of 30 mm, ambient pressures of 1 MPa and 3 MPa showed no difference in results for adhering mass ratio even though 170 MPa injection showed less adherance than 40 MPa. Sprays impinging on the wall located at 30 mm from the nozzle had sufficient velocity to splash fuel film from the wall, and it caused less adhering though the injection pressure effect was clearly maintained.
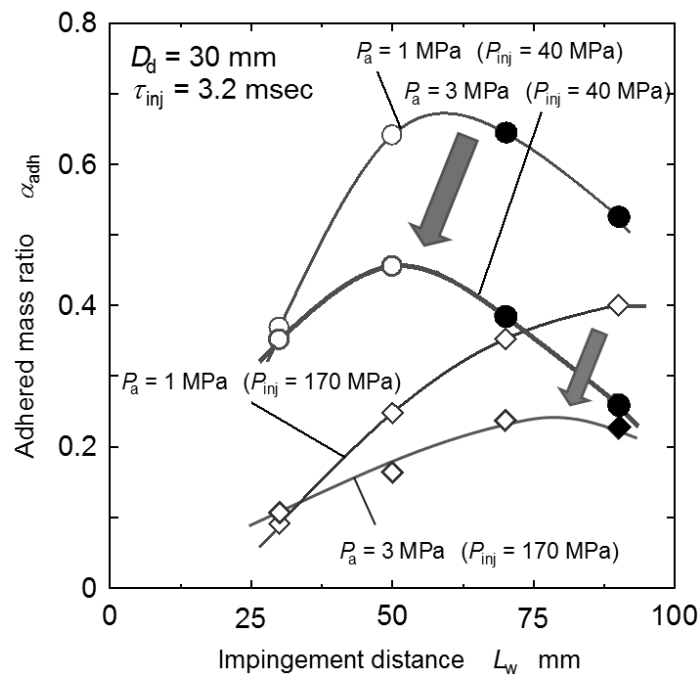
Figure 3-8 Pressure effect on adhered mass ratio

When the impingement distance was longer than 50 mm, the ambient pressure effect was clearly observed. High ambient pressure caused a quick decay of impingement velocity and it caused less adhering. Owing to the high gas density of the high ambient pressure condition, droplets in the spray tended to move with entrained gas. This caused less impingement and less adherance to the

wall. The peak of adhering mass ratio was usually observed at the impingement distance where fuel adherance occurred with sufficient velocity but its velocity did not have enough potential to splash the fuel film from the wall. Its peak position appeared at a shorter impingement distance with the change of ambient pressure from 1 MPa to 3 MPa. In this chapter, only ambient pressure effect of 1 MPa and 3 MPa were discussed, details explanation on ambient pressure effect will be discussed later in Chapter 6.

Table 3-1 shows the relationship between ambient pressure and impingement distance on the spray velocity. These velocity data were calculated through the shadowgraph images at each respective impingement points of 30 mm, 50 mm, 70 mm and 90 mm. At an injection pressure of 40 MPa, the nozzle tip velocity was 283 m/s for ambient pressures of 1 MPa and 3 MPa. While, at an injection pressure of 170 MPa, the nozzle tip velocity was 584 m/s, almost 2 times higher than nozzle tip velocity at an injection pressure of 40 MPa. Using these velocity results, the following discussion could be possible on the adherance mechanism.

When the impinged distance increased from 30 mm to 90 mm, the spray velocity decreased continuously at each impingement point regardless of injection and ambient pressures. As discussed previously in **Fig. 3-8**, at an injection pressure of 40 MPa, the adhered mass ratio reached its maximum and declined above an impingement distance of 50 mm. While at the injection pressure of 170 MPa, the adhered mass ratio took its maximum at an impingement distance of 90 mm. These phenomena were corresponding to the velocities shown in **Table 3-1**. Where its velocity (at $L_w = 70$ mm and $P_{inj} = 40$ MPa) was almost the same as the velocity at an impingement point of 90 mm ($P_{inj} = 170$ MPa). It meant that the adhered mass ratios tended to decline when the impingement velocity decreased beyond a critical velocity. Besides, impingement velocity (at $L_w = 90$ mm, $P_{inj} = 170$ MPa and $P_a = 1$ MPa) was 30 m/s which lower than the critical velocity of 40 m/s as discussed earlier in **Fig. 3-5**. However, impingement velocity at this condition was classified under 'A' trend. It shows the discrepancy trend appeared here where the critical velocity was not only factor influencing the changed of adhered mass ratio. It might be another factor controlling the changed of adhered mass ratio such as effect of droplet diameter and others. Then more detail discussion was performed in Chapter 5 by introducing the Weber number of impinging droplet.

**Table 3-1** Spray velocity

Injection Pressure P_{inj}, MPa	Ambient pressure P_a, MPa	Injection velocity V_{inj}, m/s	Velocity at impingement point V_{imp}, m/s			
			30mm	50mm	70mm	90mm
40	1	283	136	65	29	18
	3	283	35	17	11	5
170	1	584	227	100	53	30
	3	584	85	39	20	12

3.7 Impingement behavior and height of post impingement spray

Figures 3-9, **3-10** and **3-11** show shadowgraphic images corresponding to impingement distances of 30 mm, 50 mm and 70 mm, respectively. In those shadowgraphic images, series A and B represent images of ambient pressures of 1 MPa and 3 MPa under injection pressure of 40 MPa. While series C and D represent images under injection pressure of 170 MPa.

As shown on **Fig. 3-9** (A, B, C and D), the spray arrived on the disk earlier than 1 msec due to the short impingement distance. Typical impingement phenomena were clearly observed at 3 msec after the injection start. The spray strongly impinged on the disk and expanded to the lateral side direction of the disk. Series A shows that the spray expanded to the side faster than series B due to the low ambient pressure effect. While at higher injection pressure (C and D), the spray expanded to the side faster than series A and B. It was clearly observed that the rolling up motion of impinged sprays of series C and D was stronger than series A and B. Owing to this motion, thickness or height of post impingement spray that was moved radial and upward directions on impingement disk increased with the elapsed time.

Figure 3-10 shows impingement phenomena at 50 mm distance. At 1 msec after the start of injection, the spray of series A arrived to the disk, but not series B. As elapsed time increased, the spray expanded in the lateral direction. A similar trend occurred for series C and D, but sprays of series C and D expanded to a lateral direction faster due to higher injection pressure. When impingement distance increased to 70 mm, as shown in **Fig. 3-11**, the spray did not arrive to the wall at the elapsed time of 1 msec. Further, at the elapsed time of 3 msec, the spray of series B did not arrive at the wall. The spray seemed to arrive with slow velocity and impinged weakly on the disk. While at higher injection pressure, sprays of series C and D became expanded in lateral direction.
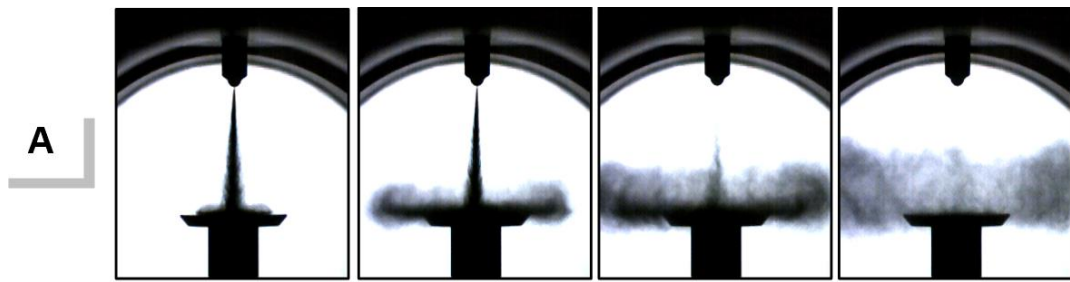
t_{asoi} = 1.0 msec t_{asoi} = 3.0 msec t_{asoi} = 5.0 msec t_{asoi} = 8.0 msec

(a) L_w = 30 mm, D_d = 30 mm, P_{inj} = 40 MPa, P_a = 1 MPa
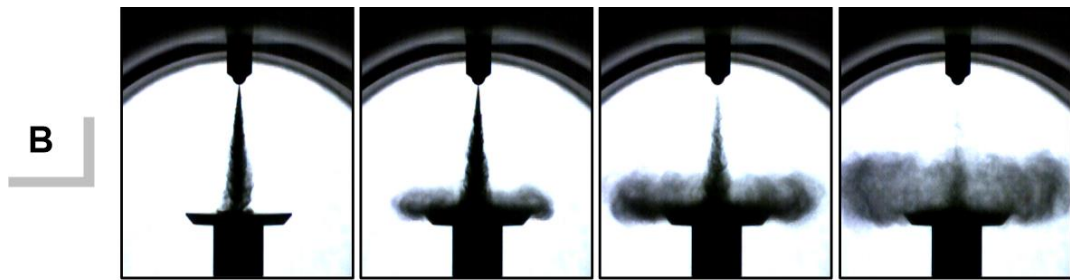
t_{asoi} = 1.0 msec t_{asoi} = 3.0 msec t_{asoi} = 5.0 msec t_{asoi} = 8.0 msec

(b) L_w = 30 mm, D_d = 30 mm, P_{inj} = 40 MPa, P_a = 3 MPa
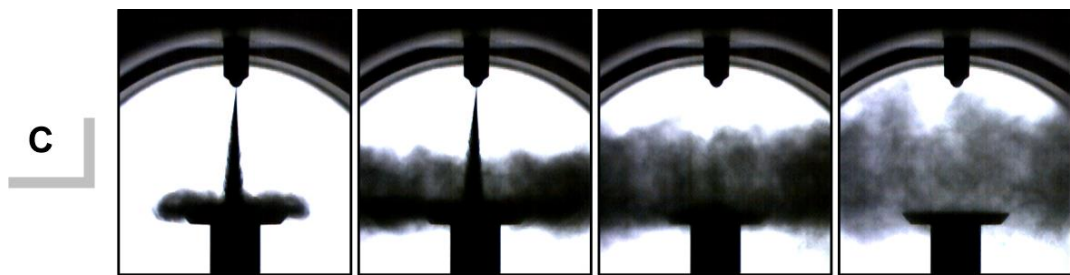
t_{asoi} = 1.0 msec t_{asoi} = 3.0 msec t_{asoi} = 5.0 msec t_{asoi} = 8.0 msec

(c) L_w = 30 mm, D_d = 30 mm, P_{inj} = 170 MPa, P_a = 1 MPa
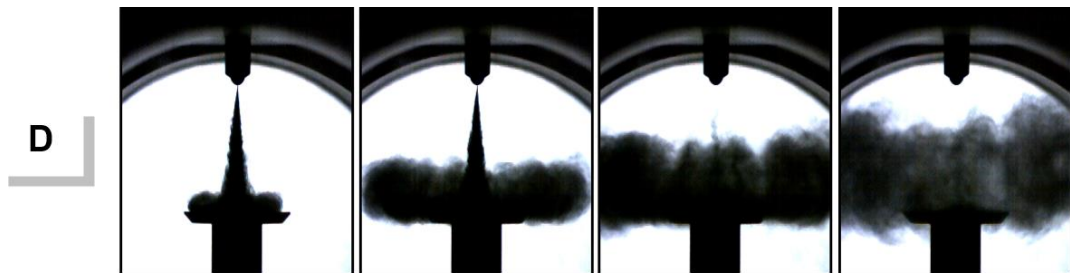
t_{asoi} = 1.0 msec t_{asoi} = 3.0 msec t_{asoi} = 5.0 msec t_{asoi} = 8.0 msec

(d) L_w = 30 mm, D_d = 30 mm, P_{inj} = 170 MPa, P_a = 3 MPa

Figure 3-9 Shadowgraphic images of 30-mm impingement spray
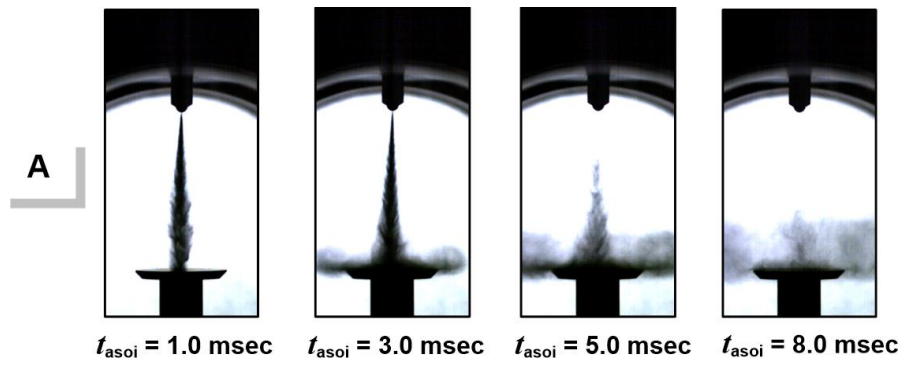
A

t_{asoi} = 1.0 msec t_{asoi} = 3.0 msec t_{asoi} = 5.0 msec t_{asoi} = 8.0 msec

(a) L_w = 50 mm, D_d = 30 mm, P_{inj} = 40 MPa, P_a = 1 MPa

B

t_{asoi} = 1.0 msec t_{asoi} = 3.0 msec t_{asoi} = 5.0 msec t_{asoi} = 8.0 msec

(b) L_w = 50 mm, D_d = 30 mm, P_{inj} = 40 MPa, P_a = 3 MPa

C

t_{asoi} = 1.0 msec t_{asoi} = 3.0 msec t_{asoi} = 5.0 msec t_{asoi} = 8.0 msec

(c) L_w = 50 mm, D_d = 30 mm, P_{inj} = 170 MPa, P_a = 1 MPa

D

t_{asoi} = 1.0 msec t_{asoi} = 3.0 msec t_{asoi} = 5.0 msec t_{asoi} = 8.0 msec
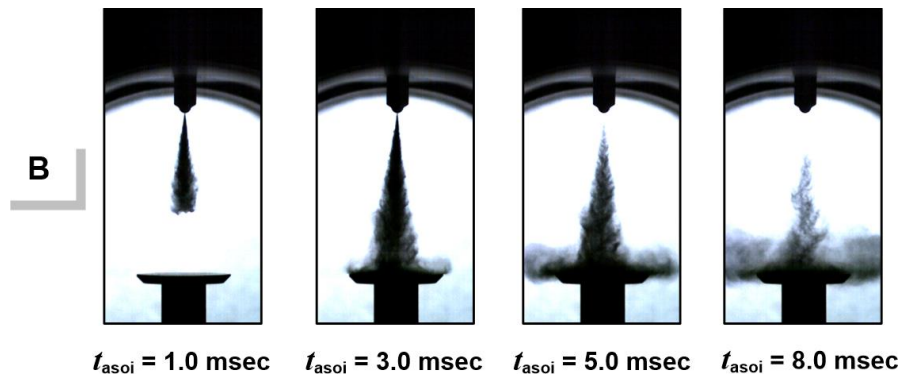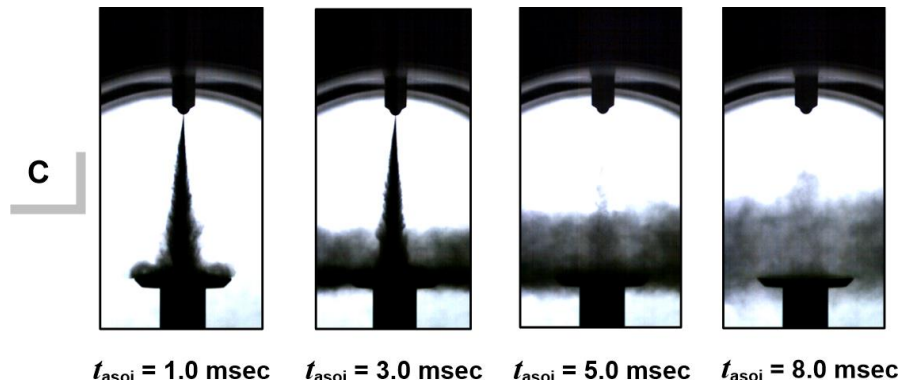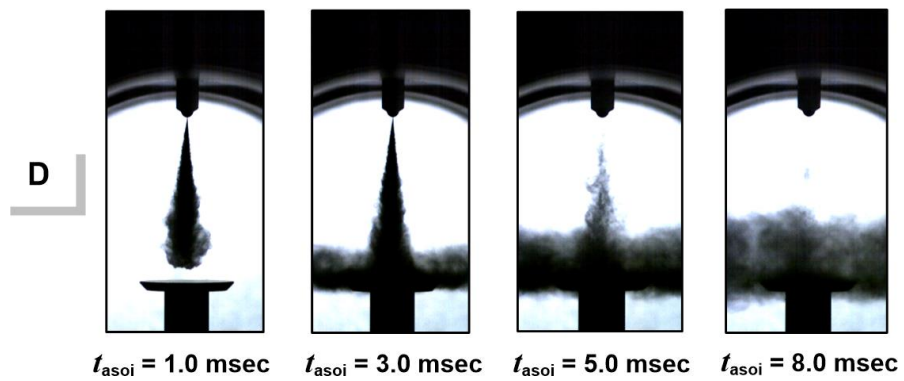
(d) L_w = 50 mm, D_d = 30 mm, P_{inj} = 170 MPa, P_a = 3 MPa

Figure 3-10 Shadowgraphic images of 50-mm impingement spray

77

t_{asoi} = 1.0 msec t_{asoi} = 3.0 msec t_{asoi} = 5.0 msec t_{asoi} = 8.0 msec

(a) L_w = 70 mm, D_d = 30 mm, P_{inj} = 40 MPa, P_a = 1 MPa

t_{asoi} = 1.0 msec t_{asoi} = 3.0 msec t_{asoi} = 5.0 msec t_{asoi} = 8.0 msec

(b) L_w = 70 mm, D_d = 30 mm, P_{inj} = 40 MPa, P_a = 3 MPa

t_{asoi} = 1.0 msec t_{asoi} = 3.0 msec t_{asoi} = 5.0 msec t_{asoi} = 8.0 msec

(c) L_w = 70 mm, D_d = 30 mm, P_{inj} = 170 MPa, P_a = 1 MPa

t_{asoi} = 1.0 msec t_{asoi} = 3.0 msec t_{asoi} = 5.0 msec t_{asoi} = 8.0 msec

(d) L_w = 70 mm, D_d = 30 mm, P_{inj} = 170 MPa, P_a = 3 MPa
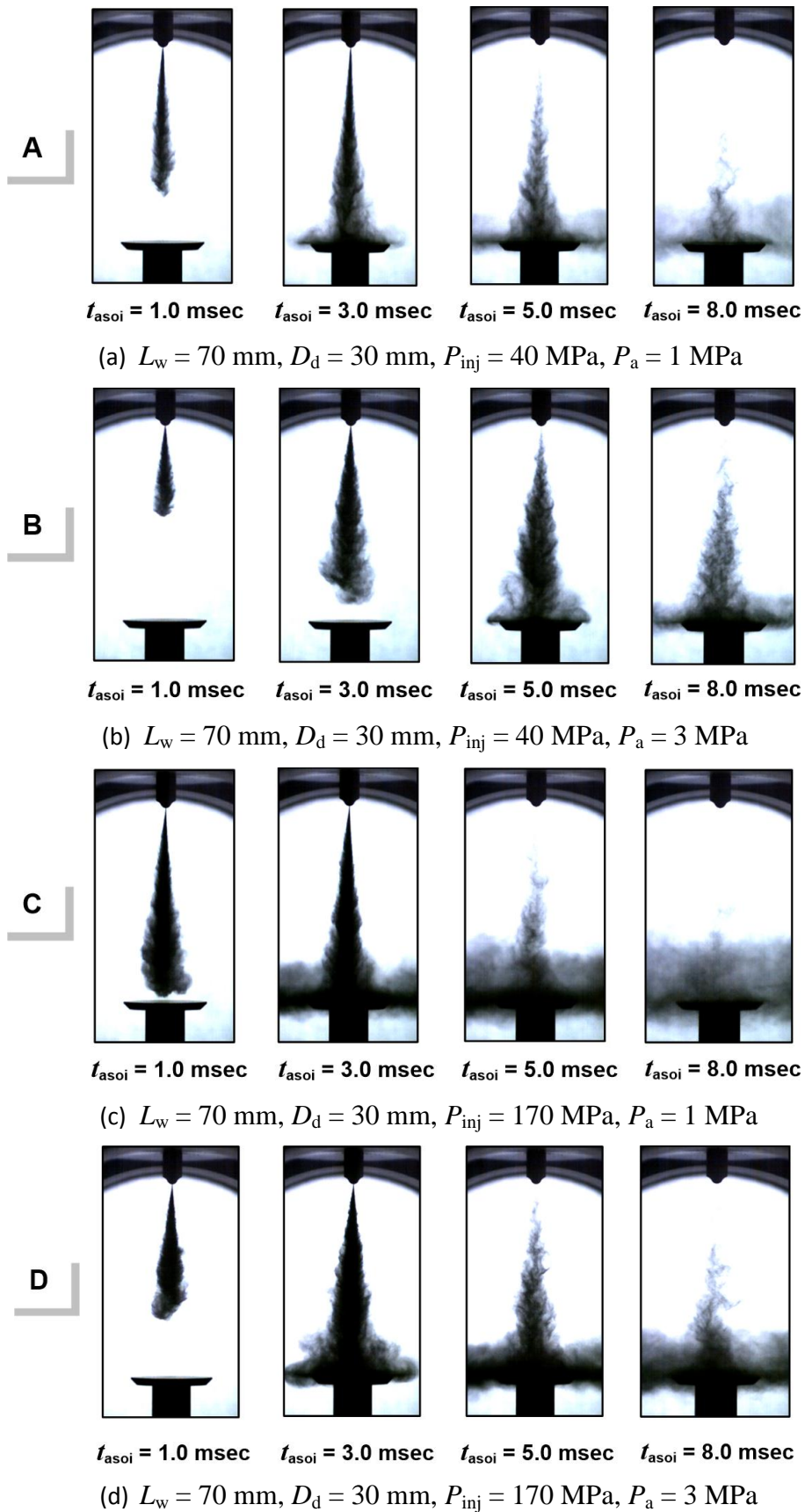
Figure 3-11 Shadowgraphic images of 70-mm impingement spray

In general, almost the same trend of spray impingement occurred regardless of injection pressure and impingement distance. It could be observed that the core of the injected spray impinged on the middle of the disk. In addition, under low ambient pressure, the injected fuel jet did not developed to a complete spray before it impinged on the wall. Thus the dense core region of the spray impinged on the wall. Similar impinging characteristics also appeared in Katsura et al. **[3]**, Park and Lee **[5]** and Andreassi et al. **[1]**. In accordance with them, impingement at normal wall caused to radial movement and upwards directions of spray. The movements of spray also have been agreed with the numerical model analysis done by Andreassi et al. **[1]**. The results show some similarities between numerical model and images captured through experimental works. The momentum of the core was larger than the fuel droplets in a completely developed spray. This high momentum seemed to be the main reason for less adherence at a short impingement distance. It was considered that fuel adherance, re-bound and fuel film splash were caused mainly by the core of the injected spray. It became the main reason that the disk diameter or disk area had little effect on the adhering fuel mass, because the diameter of the spray core was smaller than the impingement disk (except $D_d = 20$ mm).

Figure 3-12 shows the relationship between adhered mass ratio and height of post impingement spray (H) at elapsed times of 3 msec, 5 msec and 8 msec. Height of the post impingement spray was defined as height or thickness of the lateral spray after it impinged on the disk. It changed with impingement distance and elapsed time. Further, adhered mass ratio decreased monotonically as the height of post impingement spray increased.

At 3 msec after injection, the height of the post impingement spray changed to a range of 1 mm to 18 mm. Even though the impingement distances were different, the small height of the post impingement spray resulted in high adhered mass ratio. Since the small height of post impingement spray meant a spray with less re-bound and less splash of fuel film on the disk, much of the spray remained on the disk. While at 5 msec after injection, the height of the post impingement spray increased from 4 mm to 26 mm, which was slightly higher than at 3 msec after the start of injection. The high height of the post impingement spray corresponded to the rolling up motion that was caused by the re-bound of spray. This was previously explained for **Fig. 3-9**. At 8 msec after injection, the height of the post impingement spray increased from 8 mm to 28 mm.
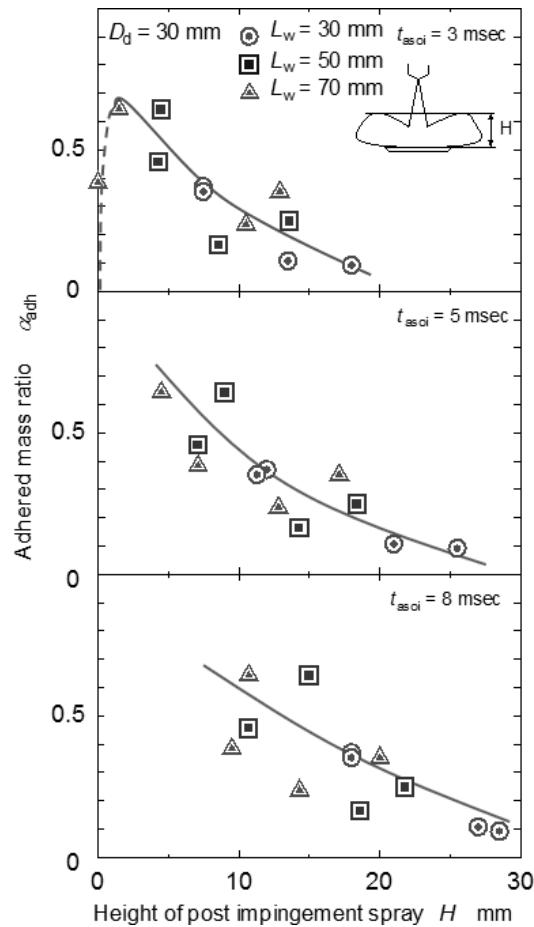
Figure 3-12 Relation of adhered mass ratio and height of post-impingement spray

Generally, there were similar decreasing trends of adhering mass ratio with a height increase of the post impingement spray under different elapsed time conditions. Since secondary atomization and re-bound of spray caused high height of post impingement spray, adhering mass ratio decreased with an increase of the height. In other words, thin fuel thickness corresponding to a low adhered mass ratio could easily promote secondary atomization and re-bound of spray droplets. It result high height of post impingement spray. On the contrary, a thick fuel film corresponding to high adhering mass ratio could easily capture spray droplets. This resulted in thicker fuel film and lower height of post impingement spray.

Re-bound and splash of spray only occurred during impingement. However, the height of the post impingement spray increased with elapsed time because the post impingement spray had upward velocity. Then the relationship between the adhered mass ratio and the height of the post impingement spray just after the finish of impingement were most important. According this consideration, heights of the post impingement spray at 5 msec and 8 msec were more important than the

result of 3 msec. More detail discussion of the impingement height was performed later in Chapter 6.

3.8 Summaries

From the experimental results of the impingement sprays, the effects of the impingement distance, the injection pressure and ambient pressure on adhered mass ratio were investigated. The following results were obtained:

1. Lower injection pressure such as 40 MPa resulted in more adhered fuel mass for all impingement distances.
2. Adhered mass ratio was inversely proportional to injection pressure.
3. At a short impingement distance such as 30 mm, the adhered fuel mass was unaffected by ambient pressure, because spray impinging at this distance had sufficient velocity to splash fuel film and reduce adherance. While, at a long impingement distance such as 90 mm, a decrease of adhered fuel mass was clearly observed.
4. Adhered fuel mass ratio had the potential to decline after reaching its peak when impingement velocity decreased beyond a critical velocity. However, it might be insufficient to justify this mechanism.
5. As the height of post impingement spray increased, less adhered fuel on the disk was obtained.

References

[1]   Andreassi, L., Ubertini, S. and Allocca, L., Experimental and numerical analysis of high pressure diesel spray-wall interaction, *Int. Journal of Multiphase Flow,* vol. 33, pp. 742-765, 2007.

[2]   Ko, K. and Arai, M., Diesel Spray Impinging on a Flat Wall, Part 1: Characteristics of Adhered Fuel Film in an Impingement Diesel Spray, *Atomization and Spray*, vol. 12(5&6), pp. 737-751, 2002.

[3]   Katsura, N., Saito, M., Senda, J. and Fujimoto, H., Characteristics of a Diesel Spray Impinging on A Flat Wall, *SAE paper*, no. 890264, pp. 191-207, 1989.

[4]   Ko, K. and Arai, M., Diesel Spray and Adhering Fuel on an Impingement Wall, *SAE paper*, no. 2002-01-1628, pp. 115-128, 2002.

[5]   Park, S.W. and Lee, C.S. Macroscopic and Microscopic characteristic of a fuel spray impinged on the wall, Experiments in Fluids 37, *Springer-Verlag*, pp. 745-762, 2004.

Chapter 4

Impingement area and wall inclination effect on adhered fuel mass

4.1 Introductory remarks

When spray impinged on the piston wall especially at low temperature condition of the wall, there might be a possibility of fuel adhering to the wall. This might cause to effect on unburnt HC and soot emissions [1]. Saito and Kawamura [2], observed the growth of adhering fuel film on the wall, and they reported the diameter of fuel film became smaller with increase of wall temperature. Montajir et al. [3] investigated the effect of combustion chamber geometry. They found that cavity size was affected the fuel film formation. Since the evaporation of heated fuel film influenced on the exhaust emissions, knowing the behavior of adhering fuel film on the surface wall was important.

As well known, the spray impinges on the cavity wall is not always in vertical position to the wall. In a real diesel engine, the spray tended to impinge on the curvature surface of the cavity wall. Thus, the effect of inclination angle on the impinging spray was important. Ebara et al. [4, 5] conducted the experiment on the inclined wall surface and they estimated the spray penetration under the wall effect. Guerrassi and Champoussin [6] performed the study on the inclined wall and reported their inclined model was similar to the photograph images. However, they did not pay attention on the adhering fuel mass under the effect of inclined wall. For more detailed understanding on the effect of inclined wall on the adhering fuel, more experimental work needs to be done. Further due to the downsizing of diesel engine, size of piston surface area as well as piston cavity volume was reduced. Thus the impingement area of spray became narrow. Also, in the real practical diesel engine, there was no flat wall surface. Take into this consideration, impingement area effect and inclination effect became importance for this study.

In this chapter, adhesion characteristics of diesel fuel spray impinging on a flat wall disk were investigated experimentally. Various sizes of disk and inclined angles were tested in order to observe the behavior of impinging spray. The fuel mass adhered to the disk surface on normal and inclined wall was evaluated. Moreover, effect of injection pressure on thickness of the liquid film was estimated. Furthermore, general trend of adhered fuel mass was explained by

using of modified adhered mass ratio concept which combined with disk diameter and inclination angle effect. In addition, model of adhering fuel was introduced based on the results obtained. Thus, this model could be useful in understanding the behavior of adhering fuel on the piston or cavity wall for the non-evaporated condition. Finally, the effect of the inclination angle on the velocity field of post-impingement spray was discussed.

4.2 Adhered fuel mass of vertically impinged diesel spray

4.2.1 Adhered fuel mass on the critical area of disk

Diesel spray impinged to the center of circular impingement disk. Its adhered mass was evaluated with the surface area (A_d) of impingement disk.

$$A_d = \frac{\pi}{4} D_d^2 \qquad (4\text{-}1)$$

Relationship between impingement disk surface area (A_d) and adhered mass ratio (α_{adh}) was investigated as the start of this chapter. The summary of the results are shown in **Fig. 4-1**. Experiment conditions were based on an impingement distance of (a) 30 mm and (b) 90 mm. Injection pressure varied from 40 to 170 MPa with ambient pressure of 1.0 MPa. Both of **Figs. 4-1 (a)** and **(b)** showed almost the same trend of adhered fuel mass.

At the impingement distance of 30 mm, the adhered mass ratio increased with an increase of the impingement disk area up to 300 mm^2 ($D_d \simeq 20$ mm). However, beyond this impingement disk area, adhered mass ratio tended to saturate. These phenomena seemed similar to all injection pressures where the saturated situation of adhered mass ratio began at around 500 mm^2 ($D_d \simeq 25$ mm).

While at the impingement distance of 90 mm, the adhered mass ratio proportionally increased with the area up to 500 mm^2 ($D_d \simeq 25$ mm). However, between impingement disk area of 700 mm^2 ($D_d \simeq 30$ mm) to 2000 mm^2 ($D_d \simeq 50$ mm), the adhered mass ratio closed to constant. The saturated tendency of adhering mass ratio was also observed at this impingement distance.
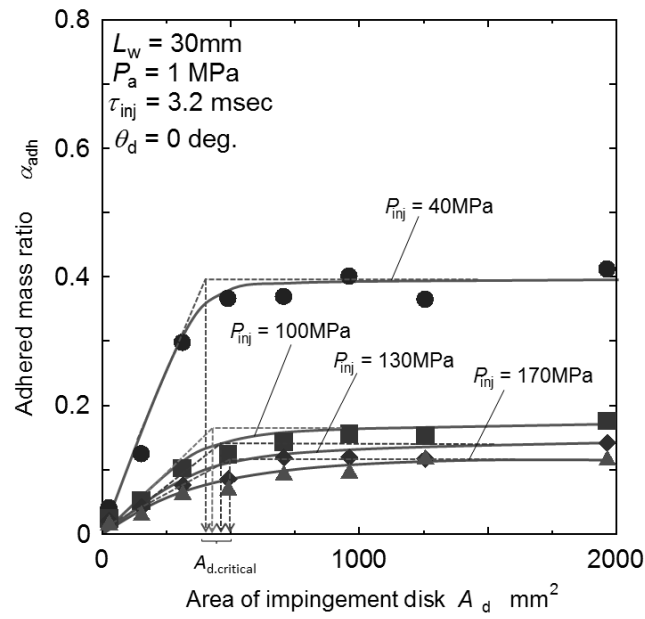
(a) $L_w = 30$ mm
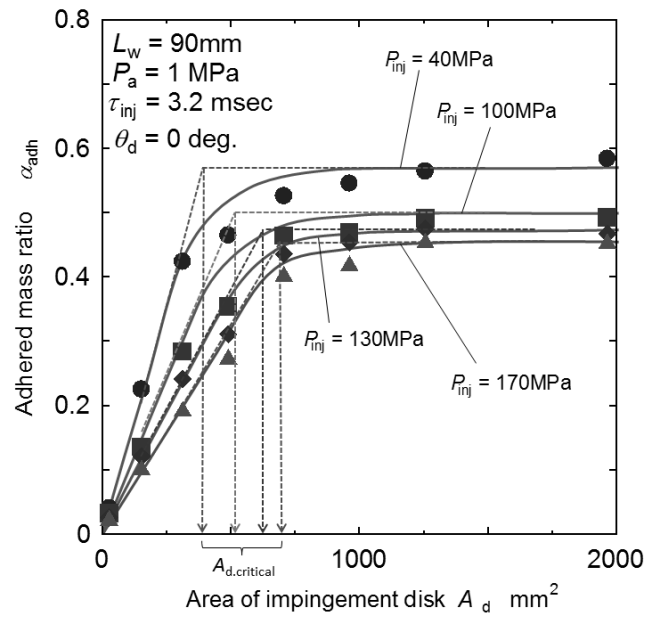
(b) $L_w = 90$ mm

Figure 4-1 Relationship between impingement disk area and adhered fuel mass ratio

According to Ko and Arai **[7]** as discussed earlier in Chapter 1, the larger diameter of fuel film formed after the impingement compared to the spray width at impingement point. It shows that the slipping phenomena occurred on the post-impingement spray. However, the spray diameter remained almost constant after some elapsed time. Referring to the results obtained in **Figs. 4-1 (a)** and **(b)**, the saturated trends of adhered mass ratios were somehow correlated to the post-

impingement of fuel film diameter. This correlation between fuel film diameter and adhering fuel mass could be explained later by the models in **Fig. 4-2**.

Regardless of injection pressures and impingement distances, it was found that the adhered fuel mass became constant with increasing the area of disk. The effects of injection pressure on the adhered mass ratio were slightly small especially for injection pressures beyond 100 MPa. Lee and Park **[8]** had investigated the effect of injection pressure on the macroscopic spray behavior and atomization characteristics of high-pressure spray. They measured the Sauter mean diameter by using phase Doppler particle analyzer. For each injection pressures they measured, they found that the Sauter mean diameter were not changed and almost constant between axial distance from 30 mm to 100 mm down from nozzle tip. It was reported that injection pressure might not influence much on the droplet size of primary spray. Then, adhered fuel mass that was changed by the impingement distance was mainly affected by velocity or momentum change of impinging spray. Detailed effects of injection pressures and impingement distances on adhering mass ratio were discussed in the Chapter 3.

As shown in both **Figs. 4-1 (a)** and **(b)**, the critical area of disk ($A_{d.critical}$) was defined as an area at a coincident point between linear and saturated lines of each injection pressure. The physical meaning of critical area of disk was the fuel adhesion area that remained on the disk. Moreover as explained later in **Fig. 4-3**, the diameter of the fuel adhesion area was larger than spray width. It means that fuel droplets adhered on not only spray impact area but also surface area where spray droplets and adhered fuel film were travelling.

Figure 4-2 shows the adhering fuel model on impingement disk of different sizes. The model is divided into three sub-models according the size (area) of impingement disk. The first condition (**Fig. 4-2(1)**) of impinging diesel spray shows that the size of the impingement disk diameter ($D_{d.1}$) is larger than the critical diameter of adhesion ($D_{d.critical}$). This condition represents that the mass of adhering ($m_{adh.1}$) is equivalent to critical adhered mass ($m_{adh.critical}$). It corresponded to the saturated trend of adhered mass ratio. In the second condition of impinging diesel spray, it shows that the impingement disk diameter ($D_{d.2}$) coincides with the critical diameter of adhesion. Thus, the mass of adhering ($m_{adh.2}$) means the critical adhered mass. While in the third condition of impinging diesel spray, the impingement disk diameter ($D_{d.3}$) is smaller than the critical diameter of adhesion. Therefore, the mass of adhering ($m_{adh.3}$) is less than the critical adhered mass. According to the linear relationship between adhered mass and disk area, it can be considered that adhered mass of this condition is equivalent to a critical adhered

mass modified by the ratio of impingement disk area over the critical area ($A_{d.3}/A_{d.critical}$). Above consideration is clearly explained by following equations.

$$m_{adh.1} = m_{adh.critical} \qquad (4\text{-}2)$$

$$m_{adh.2} \equiv m_{adh.critical} \qquad (4\text{-}3)$$

$$m_{adh.3} = \left(\frac{A_{d.3}}{A_{d.critical}}\right) \cdot m_{adh.critical} \qquad (4\text{-}4)$$

However, this concept of impingement mass of spray applied only for smaller diameter disk than critical diameter of disk on the normal wall conditions. The concept of impingement mass of spray for the inclined wall was different and discussed later in **Fig. 4-12**.
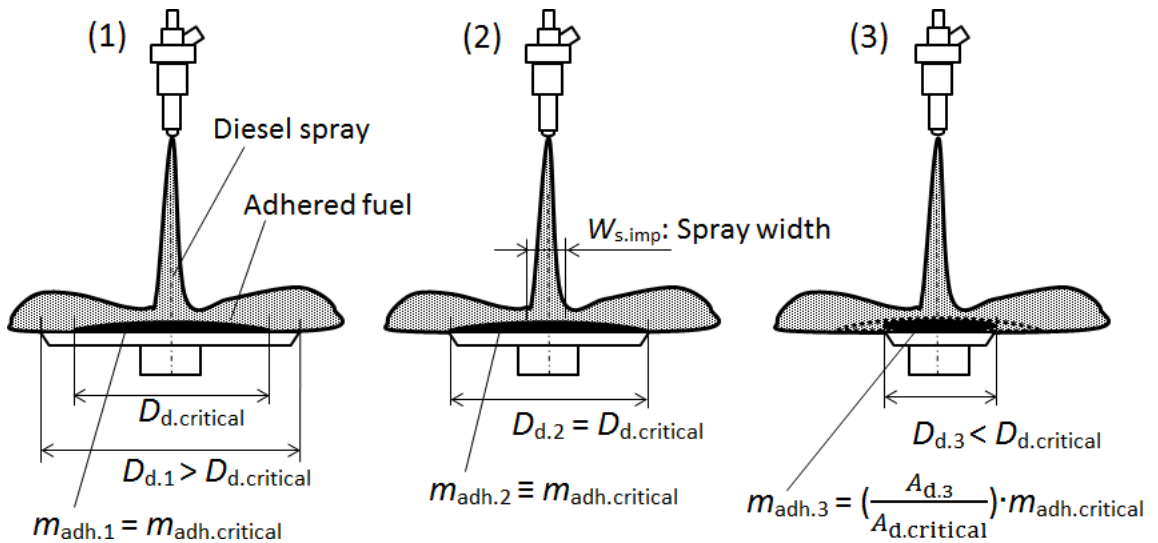
Figure 4-2 Models of adhering fuel on various sizes of disk

4.2.2 Spray width on the critical area of disk

Effects of impingement distances and injection pressures on critical diameter of disk ($D_{d.critical}$), and spray width just before impingement ($W_{s.imp}$) are shown in **Fig. 4-3**. It was measured on spray photograph at impingement point and average value of it was taken in the figure. Experiment conditions were almost the same as the conditions of **Fig. 4-1**, but the impingement distance was changed. Spray width just before impingement was defined as the width of spray just before

impingement as shown in **Fig. 4-2**. Spray angle is easily calculated from the impingement distance and spray width. For example, $L_w = 50$ mm and $W_{s.imp} = 13$ mm means a spray angle of 15 deg. and it is almost maximum spray angle of impingement sprays of this report. The critical diameter of the disk was derived through the critical area of disk ($A_{d.critical}$) as shown in **Equation (4-5)**.

$$D_{d.critical} = \left(\frac{4 \cdot A_{d.critical}}{\pi}\right)^{0.5} \qquad (4\text{-}5)$$

Physical meaning of $D_{d.critical}$ is the equivalent diameter of adhesion area. Regardless of injection pressure, the critical diameter of disk increased from an impingement distance of 30 mm to 50 mm. While beyond the impingement distance of 70 mm, the critical diameter tended to decrease slowly up to 90 mm impingement distance.

The spray width just before impingement tended to increase with increasing of impingement distance. It was estimated in a range from 2 mm to 26 mm. These results were closed with those suggested by Ko and Arai **[7]**. They reported that the spray width at the impingement point was in a range from 2 mm to 10 mm. However, in their study, the impingement distance was limited only to 70 mm, which was slightly shorter than this report. At the impingement distance of 30 mm, the sprays showed their widths from 2 mm to 6 mm which were much narrower than the critical diameter. However, as the impingement distance increased up to 90 mm, the spray width grew to the wider width between 19 mm to 25 mm which was closer to the critical diameter of the disk. It seemed at the much longer impingement distance than 90 mm, the critical diameter might be influenced by the spray width just before impingement. In other words, critical diameters in this experimental study were independent to the spray width.
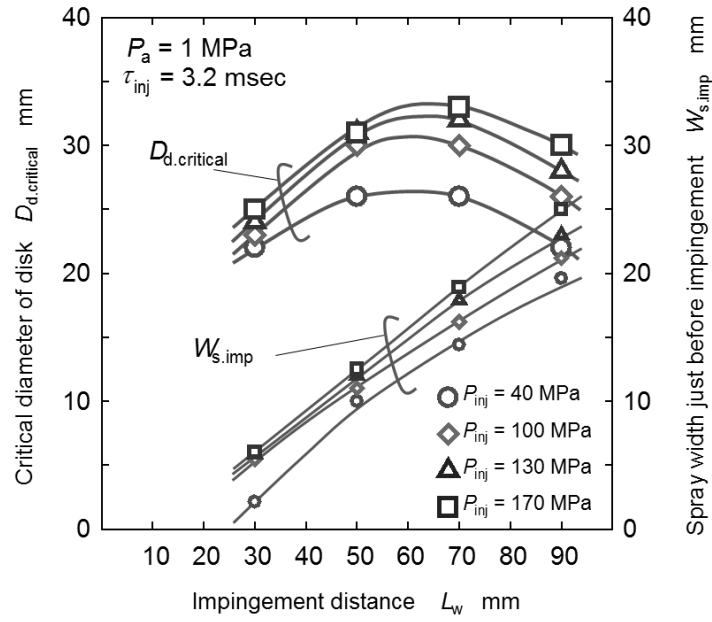
Figure 4-3 Effects of impingement distance and injection pressure on $D_{\text{d.critical}}$ and $W_{\text{s.imp}}$

4.2.3 Critical thickness of liquid film

Figure 4-4 shows the relationship between injection pressure and liquid film thickness for an impingement distance of 30, 50, 70 and 90 mm. Based on the critical area of disk ($A_{\text{d.critical}}$) in **Fig. 4-1** and critical adhered fuel mass ($m_{\text{adh.critical}}$), the critical thickness of liquid film could be obtained from the following equation,

$$t_{critical} = \frac{m_{\text{adh.critical}}}{\rho_{\text{f}} \cdot A_{\text{d.critical}}} \tag{4-6}$$

where, ρ_{f} is the density of diesel fuel.

When the impingement disk was located at 90 mm from nozzle, the critical liquid film thickness decreased almost linearly with increasing of injection pressure. This trend is clearly observed in the impingement distance of 70 mm. In the case of $L_{\text{w}} = 50$ mm, the thickness dramatically decreased at an injection pressure from 40 to 130 MPa, and slightly decreased at an injection pressure more than 130 MPa. However, in the case of $L_{\text{w}} = 30$ mm, the thickness of liquid film decreased with an increase of injection pressures up to 100 MPa, while it slightly decreased at an injection pressure of over 100 MPa. It seemed that there are two kinds of different mechanisms in the thickness decrease for $L_{\text{w}} = 30$ mm. On the

other hand, for L_w = 50, 70 and 90 mm, a single kind of mechanism of the thickness decrease might dominate the trend.

Regardless of injection pressures and impingement distances, the critical liquid film thickness was estimated to be 0.007 mm (7 μm) to 0.032 mm (32 μm). These results were in good agreement with those suggested by Ko and Arai [7]. They reported that the adhered thickness of fuel film for diesel spray injected by a classical jerk-type injection system was in the range from 10 to 30 μm. Considering the results for L_w = 30 mm and injection pressures higher than 100 MPa, the thicknesses of liquid film were in 7 μm - 12 μm, which were in the range of droplet size of diesel spray. Thin fuel film thickness such as 12 μm seemed to allow direct interaction between impinging droplets and the impingement wall surface even though the droplet impinged on the surface of fuel film. It seems that the extremely low adhered mass ratio at beyond P_{inj} = 100 MPa was mainly caused by direct rebound of spray droplets. However, in the case of impingement distance longer than 50 mm, the thickness of liquid film increased up to 32 μm, which was much thicker than the droplet size of diesel spray. The thick fuel film seems suitable to capture fuel droplets impinging on the fuel film surface. High adhered mass ratios in these situations seemed the result of this effect. However with an increase of injection pressure, splash of thick fuel film was promoted by high velocity of impingement spray.

According to the report of Bai and Gosman [9], splash might occurred in high Weber number condition due to high impingement velocity. Andreassi et al. [10] carried out an experimental and numerical analysis of high injection pressure diesel spray impingement. Their experimental and numerical analysis was based on injection pressure up to 120 MPa at various ambient pressures and temperatures. They also adopted the splash model in their numerical analysis. They reported that splash height of the secondary droplets were almost similar between numerical and experimental data. From their reports, the splash might be promoted by high velocity of impingement spray. As for the impingement conditions of **Fig. 4-4**, velocity of impingement spray increased with injection pressure increase, and its velocity range was almost similar to the references mentioned above. Thus, it seemed that decrease trend of adhered mass with injection pressure increase was mainly caused by the splash of fuel film.
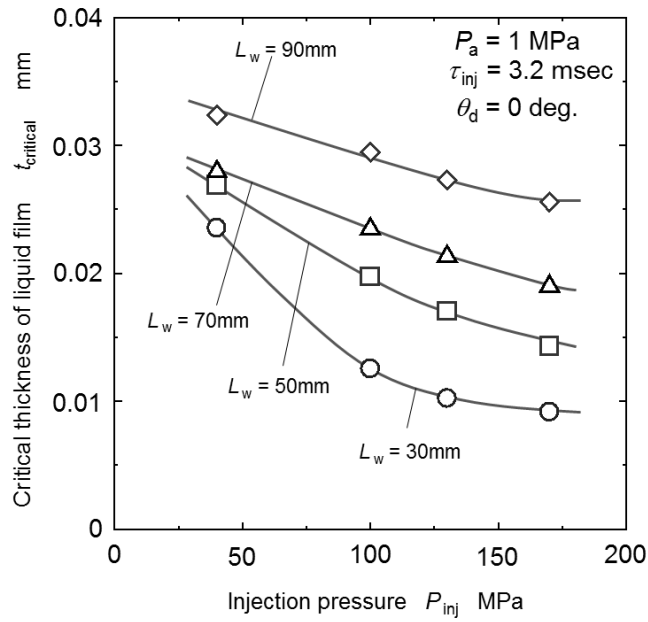
Figure 4-4 Relationship between injection pressure and critical liquid film thickness

4.3 Modified adhered mass ratio on impingement disk of various sizes

The adhered mass ratio for disk size of $D_d > D_{d.critical}$ is shown in **Fig. 4-5**. There are four sizes of disk diameter greater than the critical diameter. They are disk diameters of 30, 35, 40 and 50 mm. Since the sizes of $D_d > D_{d.critical}$ were maintained, adhering mass for each disk diameter was equivalent to critical adhering mass as mentioned previously in **Fig. 4-2**. Therefore, as resulted in **Fig. 4-5**, regardless of injection pressures and impingement distances, adhered mass ratios of disk diameter 30, 35, 40 and 50 mm were close to each other.

This trend could be further applicable to situations of smaller diameter disk than the critical. Here, a modification area factor k is introduced, and modified adhered mass ratio α'_{adh} is derived as follows.

$$m_{adh} = k \cdot m_{adh.critical} ; \qquad (4\text{-}7a)$$

where k is the area factor

$$k = 1 \quad \text{at } D_d \geq D_{d.critical} \qquad (4\text{-}7b)$$

$$k = \left(\frac{A_d}{A_{d.critical}}\right) \quad \text{at } D_d < D_{d.critical} \qquad (4\text{-}7c)$$

$$\alpha'_{adh} = \frac{m_{\text{adh.critical}}}{m_{\text{inj}}} = \frac{m_{\text{adh}}}{k \cdot m_{\text{inj}}} = \frac{\alpha_{\text{adh}}}{k} \qquad (4\text{-}8)$$

Figure 4-6 shows modified adhered mass ratio for impingement distance of 30 mm. Since adhesion area factor k took unit value in impingement conditions from $D_d = 30$ to 50 mm, close values of modified adhered mass ratio were obvious as shown in **Fig. 4-5**. In other words, there was no impingement disk diameter effect on adhered mass ratio. When the impingement disk diameter was less than 30 mm, **Equations (4-7a)** and **(4-7c)** was used to obtain the modified adhered mass ratio. It is clearly observed that the modified adhered mass ratios were close each other for all sizes of impingement disk (except $D_d = 6$ mm). Physical meaning of it was that thickness of adhered fuel mass was almost constant even though the disk diameter was less than critical diameter. Modified adhered mass ratio of disk diameter 6 mm scattered far from the line. This is caused smaller disk diameter than impingement spray width. Since 6 mm disk was smaller than the width of impingement spray, it seemed that different mechanism of adhering for 6 mm disk diameter might dominate the phenomena, and impingement spray model shown by **Fig. 4-2** did not match to this condition.

Figure 4-7 shows the modified adhered mass ratio with adhesion area factor of k, at an impingement distance of 90 mm. In this longer impingement distance, the modified adhered mass ratios were still close to each other for various sizes of disk diameter. Since $k = 1$ was clear for disk diameter larger than $D_d = 30$ mm, modified adhered mass ratios for these conditions consisted to the adhered mass ratios shown in **Fig. 4-5**. Using the area factor k, this trend could be applicable for wider conditions including smaller diameter of impingement disk. Scattered results of $D_d = 6$ mm was caused by the same reason of **Fig. 4-6**. Another off-line data by $D_d = 25$ mm were little strange and no reasonable explanation could be made (it might come from experimental error). Generally, **Fig. 4-6** and **Fig. 4-7** show that the modified adhered mass ratios were uniquely defined in the conditions even though the impingement disk diameter was smaller than the critical diameter.
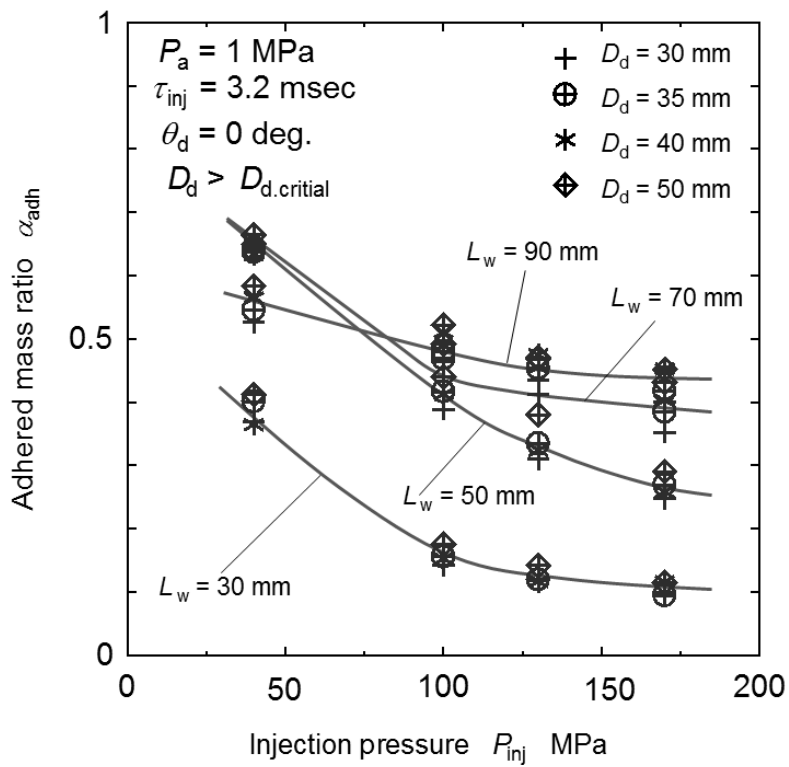
Figure 4-5 Adhered mass ratio for disks of $D_d > D_{d.critical}$
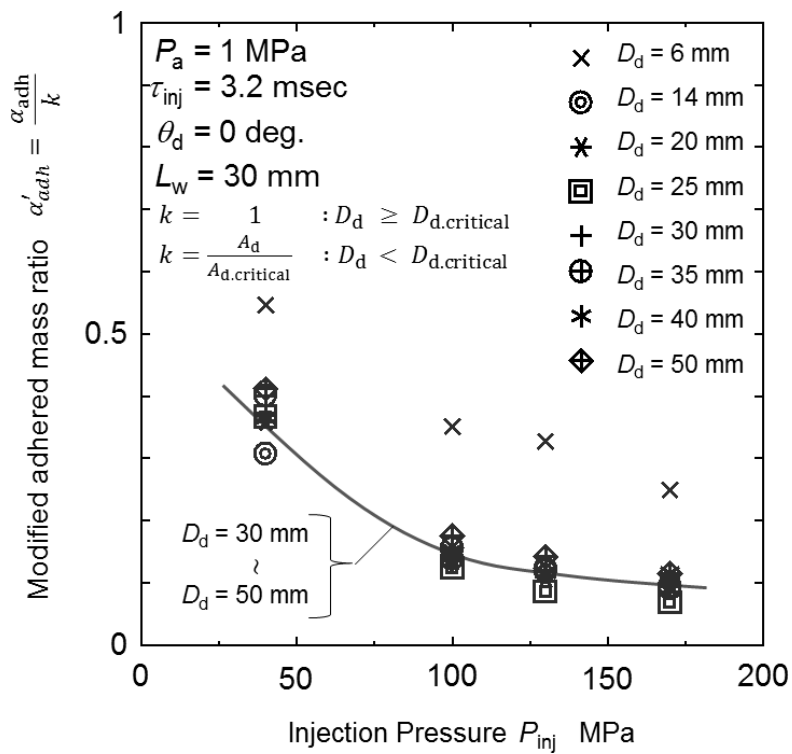
Figure 4-6 Modified adhered mass ratio with adhesion area factor for various impingement disk diameters at $L_w = 30$ mm
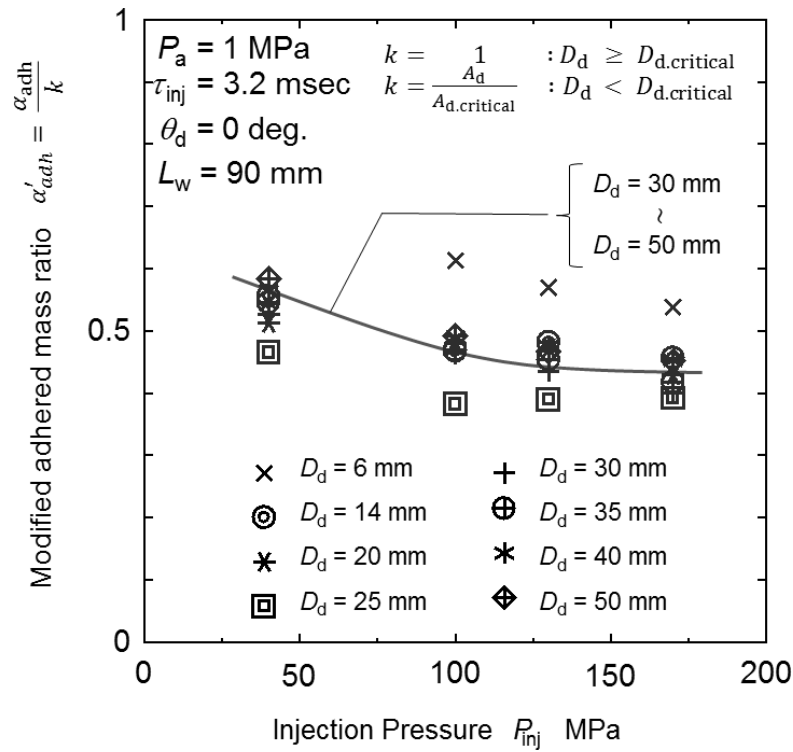
Figure 4-7 Modified adhered mass ratio with adhesion area factor for various impingement disk diameters at $L_w = 90$ mm

4.4 Effect of inclination angle on adhered fuel mass ratio

4.4.1 Adhered fuel mass on the inclined wall

In a direct injection diesel engine, diesel spray injected through injector impinged to the wall of piston cavity or cylinder wall. Impingement axis of diesel spray was usually inclined to the wall. In other words, the diesel spray was not necessarily to impinge vertically to the wall. **Figure 4-8** shows shadow images of impingement spray at $L_w = 30$ mm. Injection pressure of diesel spray was 130 MPa. Images of inclination angle 0, 10 and 20 deg. at 0.75 and 1.5 msec from start of injection are shown in the figure. After impingement, spray was penetrating along the surface of impingement disk. Spray tip penetration to the downhill direction became longer with an increase of inclination angle. It means that radial downhill component of the spray velocity became promoting the downhill penetration with an increase of the angle. Promotion of downhill penetration was also observed in long impingement distance condition such as $L_w = 90$ mm.

94
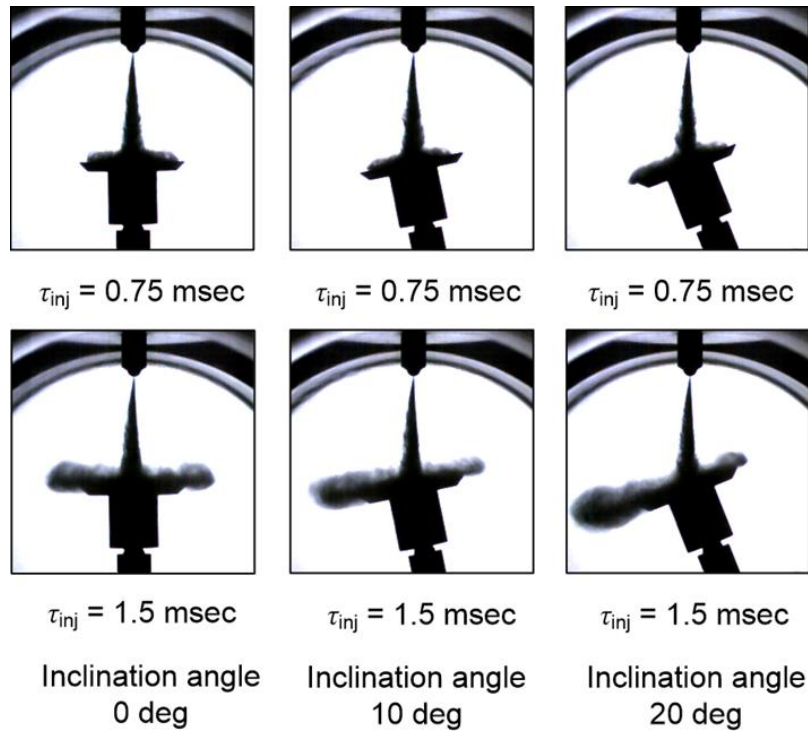
Figure 4-8 Shadowgraphic images of impingement spray ($L_{\mathrm{w}} = 30$ mm and $P_{\mathrm{inj}} = 130$ MPa)

Further explanation of **Fig. 4-8** could be introduced in schematic diagram shown in **Fig. 4-9**. It shows the spray velocity at impingement to an inclination disk. Here, impingement velocity (V_{imp}) of diesel spray and its two components are indicated. Normal component ($V_{\mathrm{imp.n}}$) and radial component ($V_{\mathrm{imp.r}}$) of impinging velocity are derived as follows.

$$V_{\mathrm{imp.n}} = V_{\mathrm{imp}} \cdot \cos\theta_{\mathrm{d}} \qquad (4\text{-}9)$$

$$V_{\mathrm{imp.r}} = V_{\mathrm{imp}} \cdot \sin\theta_{\mathrm{d}} \qquad (4\text{-}10)$$

Where θ_{d} is the inclination angle of impingement disk.
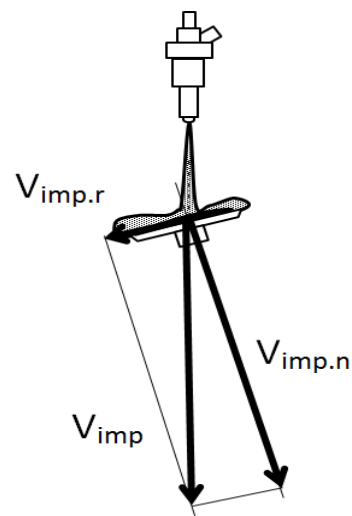
Figure 4-9 Velocity components of impingement diesel spray

To clarify a trend of adhered mass on inclined wall, adhered fuel mass ratio on it was evaluated as the same way as vertical impingement using the special apparatus shown in **Fig. 2-6** (Chapter 2). Effect of inclination angle of the disk on adhered fuel mass ratio was investigated. Some of the results are shown in **Fig. 4-10 (a)** and **(b)**. These figures were based on 30 mm of the disk diameter which was nearly equivalent to the critical diameter in **Fig. 4-3**. As for $L_w = 50$ mm (**Fig. 4-10 (a)**), adhered fuel mass ratio of $P_{inj} = 40$ MPa decreased with increasing the inclination angle of the disk. The ratios for injection pressures more than $P_{inj} = 100$ MPa slightly decreased with increasing the angle. Non-linear decreasing with inclination angle was the characteristic feature of it. The case of further away from the nozzle ($L_w = 90$ mm) is shown in **Fig. 4-10 (b)**. Adhered mass ratios showed obviously non-linear decrease trends with inclination angle.

Normal velocity component shown by **Equation (4-9)** decreased with an increase of inclination angle. It might enhance the adhesion of fuel because low velocity usually showed increased trend of adhesion. However, with inclination of the disk, adhered mass ratio decreased as shown in **Figs. 4-10 (a)** and **(b)**. This decrease trend did not match with the enhancement effect of normal velocity decreasing with increasing the inclination angle. It might be related with the impingement flow caused by the radial velocity component derived in **Equation (4-10)**. Impingement flow change shown in **Fig. 4-8** might result less impingement and less adhered mass of fuel. Mechanism of this effect will be explained later in **Fig. 4-12**.

(a) $L_w = 50$ mm　　　　　　　　　(b) $L_w = 90$ mm
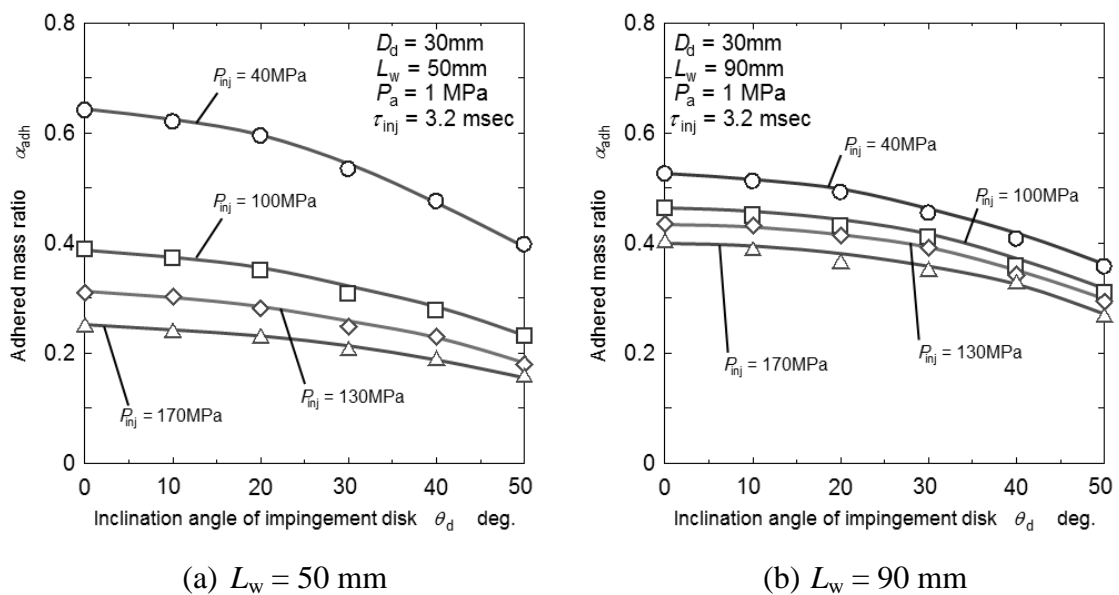
Figure 4-10 Relationship between inclination angle and adhered mass ratio

4.4.2 Modified adhered mass ratio with correction factor angle

A correction factor of $\cos \theta_d$ was introduced to explain the above results. And modified adhered mass ratio α''_{adh} for inclination disk was introduced by **Equation (4-11)**.

$$\alpha''_{adh} = \frac{\alpha_{adh}}{\cos \theta_d} \qquad (4\text{-}11)$$

The correction factor of $\cos \theta_d$ was obtained through the experimental results that the curvature trends in **Fig. 4-10** were closed to the function of $\cos \theta_d$. Modified adhered mass ratios (α''_{adh}) were calculated for various inclination angles as shown in **Fig. 4-11**. As the result, it was clearly observed that the modified adhered mass ratios (α''_{adh}) were close each other for all inclination angles regardless of injection pressures and impingement distances. It means that **Equation (4-11)** was reasonable for inclination modification of adhered mass ratio. Further, trends similar to **Fig. 4-5** appeared even though these results consisted of various inclination angles. It shows a possibility of more general modified adhered mass ratio such as $\alpha'''_{adh} = \alpha_{adh}/(k \cdot \cos \theta_d)$. It will be discussed in the Chapter 5 of this thesis.
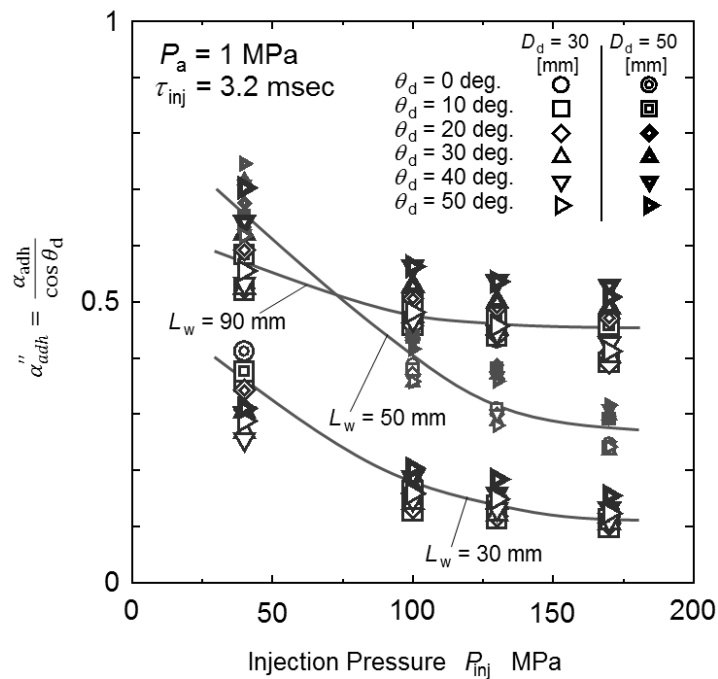
Figure 4-11 Modified adhered mass ratio for various inclination angles

97

In general, the impingement phenomena of diesel spray on inclined disk could be described as shown in **Fig. 4-12**. This figure shows that there were two flow patterns of spray movement on an inclined disk. They were non-impingement flow and impingement flow of spray. Basically, the non-impingement flow of spray was located on the radial side of the downhill section where the diesel spray flowed away in the manner shown here. In this flow, in accordance with **Equation (4-10)**, the radial component of velocity increased with an increase of inclination angle. Therefore, the droplets in the spray might be swept by this flow. Non-impingement mass could be supposed by **Equation (4-12)**.

$$\Delta m_{\text{non-imp}} = \Delta m_{\text{inj}} \cdot (1 - \cos\theta_{\text{d}}) \qquad (4\text{-}12)$$

On the other hand, impingement on inclined disk was mainly referred to the impingement flow of diesel spray as shown in **Fig. 4-12**. The impingement part of spray mainly located in the center area of the disk. Thus, it is supposed that the adhered mass of fuel was mainly caused by impingement mass derived by **Equation (4-13)**.

$$\Delta m_{\text{imp}} = \Delta m_{\text{inj}} \cdot \cos\theta_{\text{d}} \qquad (4\text{-}13)$$

Then $\cos\theta_{\text{d}}$ can be considered as substantial impingement mass factor on the inclined disk. It leads to phenomenological background of modified adhered mass ratio for impingement diesel spray on inclined disk. According to the above consideration, modified adhered mass ratio defined by **Equation (4-11)** and impingement mass obtained by **Equation (4-13)** can be related using following equation.

$$\alpha''_{adh} = \frac{\alpha_{\text{adh}}}{\cos\theta_{\text{d}}} = \frac{m_{\text{adh}}}{m_{\text{inj}} \cdot \cos\theta_{\text{d}}} = \frac{m_{\text{adh}}}{m_{\text{imp}}} \qquad (4\text{-}14)$$
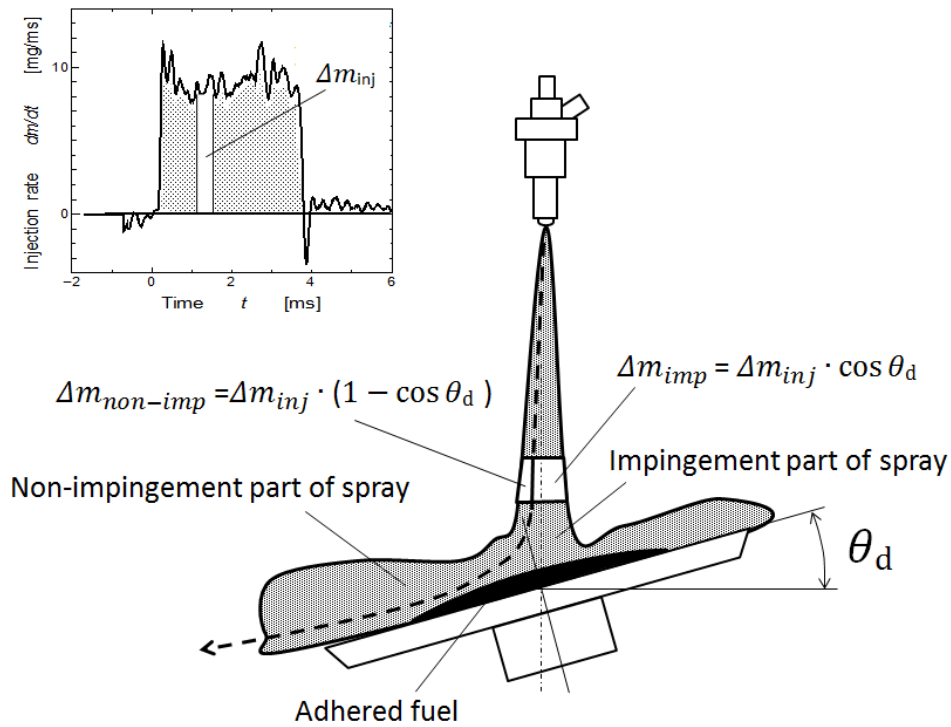
Figure 4-12 Model of impingement and non-impingement part of diesel spray

4.5 Flow analysis of post impingement spray

4.5.1 Effect of inclination angle on velocity field of post-impingement spray

The effect of inclination angle on velocity field of the post-impingement diesel spray was investigated. **Figure 4-13** shows tomographic images and vector maps for 0 deg., 20 deg. and 40 deg. of inclination angle and injection pressure of 150 MPa. Here, radial distance was taken from the geometric impingement center even though inclination injection. Impingement wall distance was kept at 30 mm for all inclination angle, and elapsed time from start of injection was $t_{inj} = 0.22$ ms for all three cases.

Spray tip location of 20 deg. impingement tip was slightly shifted to downward location than 0 deg. Further, the spray tip for 40 deg. obviously developed more than those of previous two images. At the impingement center, there was no correlative vectors and looked like stagnate. Rolling up motion at the tip showed unique feature corresponding the inclination angle of impingement. Its front became leaving to backward direction with inclination angle increasing. Regardless of inclination angle, spray density (image intensity) of the post-impingement spray was lower than impinging spray to the bar. In those figures,

99

incident directions of laser light were illustrated. By considering the incident direction, laser light was less interrupted and became illuminated directly to the post-impingement spray with an increase of inclination angle, because optical path length inside the post-impingement spray became shorter with inclination angle increase. For example, the post-impingement spray density at 40 deg. was obviously lower than the pre-impingement and impinging spray, and it was not the results of light absorption. Therefore, after impingement, spray density became low due to 3D dispersion of the spray. Also fuel adhering on the wall was another reason of low density spray, because the absolute mass of post-impingement spray decreased by its adhesion.

Referring to the **Fig. 4-8**, the shadowgraph images for inclination wall almost similar with the tomographic images here even though the start of injection time was different. It was clearly observed from both images in **Fig. 4-13** and **Fig. 4-8**, at inclination angle of 20 deg., the spray penetrated to the downhill faster that lower inclination angle. It was confirmed that by increasing of the inclination angle, the spray penetration to downhill direction was promoted by spray velocity (lower image of **Fig. 4-13 (b) and (c)**).
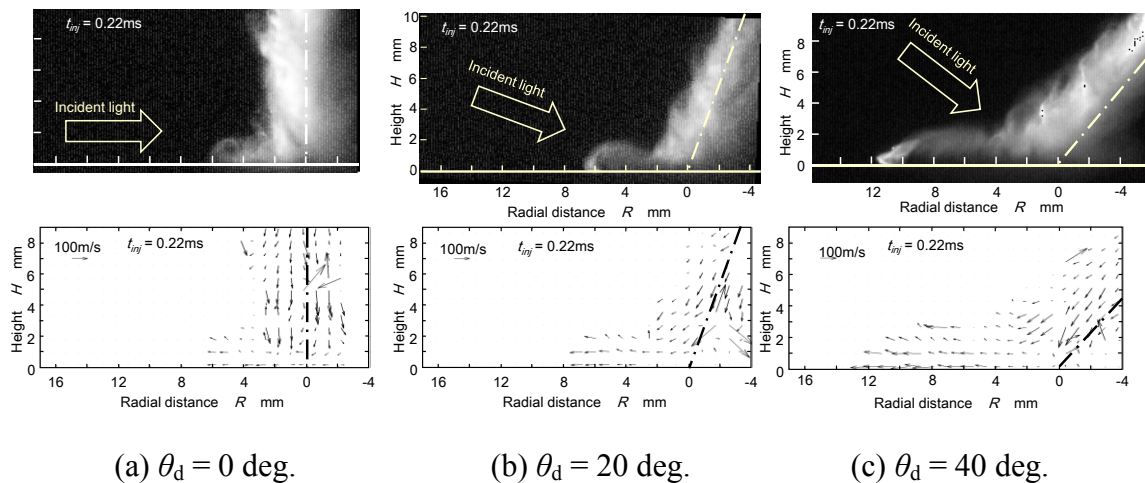
$$(a)\ \theta_d = 0\ deg. \qquad (b)\ \theta_d = 20\ deg. \qquad (c)\ \theta_d = 40\ deg.$$

Figure 4-13 Tomographic images of post-impingement spray for various impingement angle and its velocity field

Figure 4-14 shows another tomographic images of post-impingement diesel spray for 0 deg., 20 deg. and 40 deg. The tip of the post-impingement spray for 0 deg. was always a shape like "whale melon" as shown in **Fig. 4-14 (a)**. On the other hand, for 20 deg., the tip near the impingement wall was a shape like "dolphin rostrum" as shown in the upper image of **Fig. 4-14 (b)**. The tip like "dolphin rostrum" frequently appeared. The dolphin rostrum was caught up by the

following part of the post-impingement spray shown in lower image of **Fig. 4-14 (b)**. It was caused by velocity deceleration of the tip due to momentum loss with wall friction. For 40 deg. of inclination angle (**Fig. 4-14 (c)**), the tip like "dolphin rostrum" always appeared after impingement, and the tip was not caught up by the main body of the post-impingement spray.

(a) $\theta_d = 0$ deg.   (b) $\theta_d = 20$ deg.   (c) $\theta_d = 40$ deg.
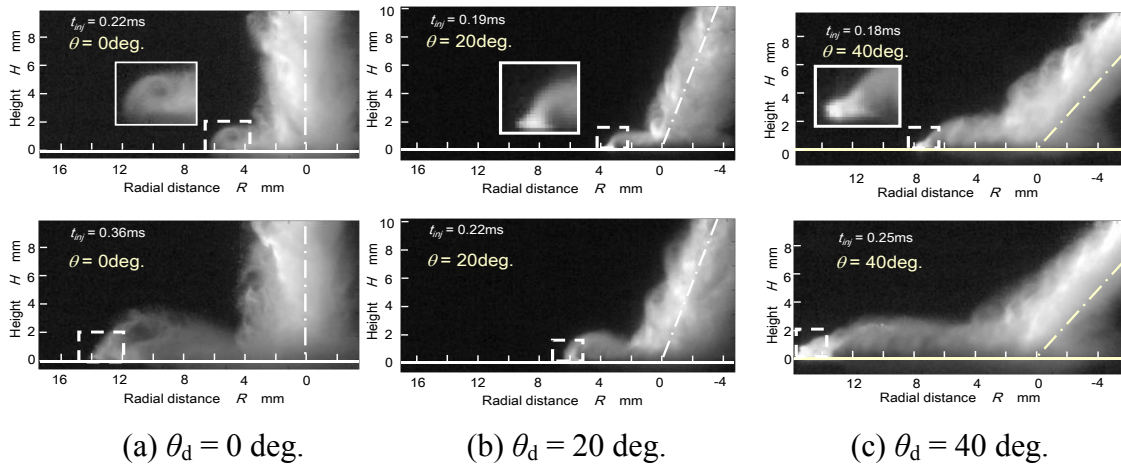
Figure 4-14 Tomographic of dolphin nose for various impingement angles

4.5.2 The post-impingement spray under steady state condition

Based on instantaneous velocity field, mean velocity field could be evaluated. In the case of post-impingement diesel spray, the main body of the post-impingement spray showed almost steady state feature, and time averaging seemed to be possible there. Here, the main body means the part of post-impingement spray near the impingement point and including no tip part of the post-impingement spray. The tip of the post-impingement spray was developing to the radial direction, and then the spray tip had to be excluded in evaluation of mean velocity field. As for $\theta_d = 0$ deg., the velocity fields from $t_{inj} = 0.49$ ms to $t_{inj} = 0.54$ ms were selected. After $t_{inj} = 0.54$ ms, velocity map had some erroneous vectors due to shade effect and was not used for velocity averaging. In the case of $\theta_d = 20$ deg., the velocity in the period from $t_{inj} = 0.42$ ms to $t_{inj} = 0.46$ ms was averaged. The velocities from $t_{inj} = 0.28$ ms to $t_{inj} = 0.35$ ms for $\theta_d = 40$ deg. were used for the mean velocity field.

Figure 4-15 shows the mean velocity fields of impingement diesel spray. Radial component profiles of the velocity vector were also illustrated. The spray periphery was obtained from average tomographic image of the steady state post-impingement spray. Over $R = 14$ mm, the periphery was unclear due to low spray

101

density by diffusion of the spray.

In the case of $\theta_d = 0$ deg., the whole spray from $R = 0$ mm to 4 mm moved to the impingement wall. In this radial region (0 mm < R < 4 mm), there were some upward vectors. It means that the spray might rebound after impinging to the wall, or structure of droplet cluster was deformed with impingement. Discontinuity of the spray flow between the impinging spray and the post-impingement spray seems to appear there. In the radial region apart from impingement point (4 mm < R < 14 mm), the post-impingement spray near the wall moved to radial direction, but upper part of the post-impingement spray (H > 2 mm) hardly moved. It means that the most of mass flow of the post-impingement spray appeared near the wall. On the radial component profile at around $R = 12$ mm, it could be observed that upper part of the spray slightly moved to backward direction.

Regarding $\theta_d = 20$ deg., the impinging spray in a region from $R = 0$ mm to $R = 2$ mm was bended to radial direction and flowed along the wall. It means that continuous flow of the spray was maintained there. Thus it seems that the substantial spray mass impinging to the wall decreased as compared with the impinging spray mass of $\theta_d = 0$ deg. The velocity of post-impingement spray near the wall was higher than that of upper part of it as well as the post-impingement spray at 0 deg. As for the upper part of the post-impingement spray at $R = 12$ mm, the spray moved to backward direction more clearly compared with 0 deg.

As for 40 deg., the most of impinging spray smoothly flowed to radial direction along the impingement wall as compared with 20 deg. It means that non-impingement part of the spray increased with an increase of inclination angle. According to the result obtained in **Fig. 4-10**, it was found that adhered fuel mass decreased with an increase of inclination angle. By considering the result of flow patterns of various inclination angles, it was concluded that adhered fuel mass decreased because the non-impinging part of the spray increased with an increase of inclination angle. This discussion could be the evidence for the model illustrated in **Fig. 4-12**.

Averaged velocity (t_{inj} = 0.49ms~0.54ms)

(a) θ_d = 0 deg.

Averaged velocity (t_{inj} = 0.42ms~0.46ms)

(b) θ_d = 20 deg.

Averaged velocity (t_{inj} = 0.28ms~0.35ms)
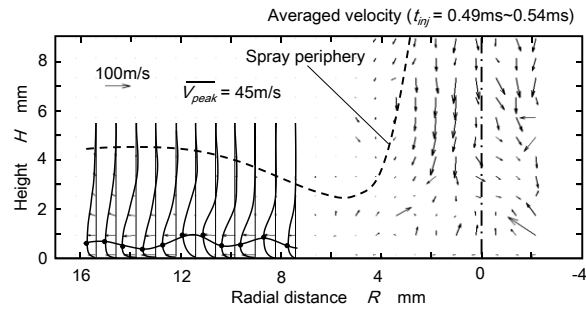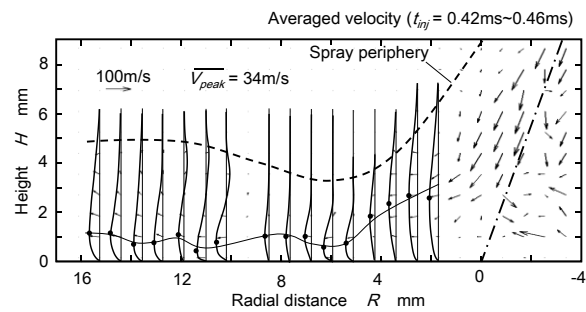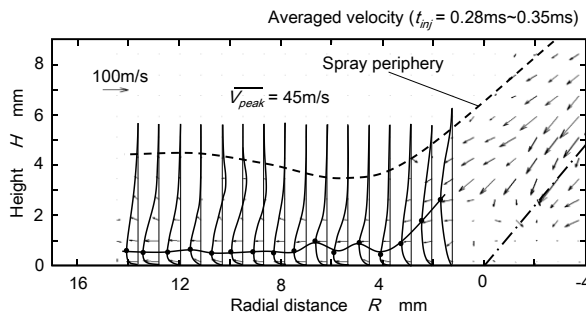
(c) θ_d = 40 deg.

Figure 4-15 Mean velocity distribution of the post-impingement diesel spray

A peak velocity in radial component profile of the velocity could be evaluated, and the height of peak velocity position was shown by solid line. From R = 8 mm to R = 16 mm, averaged thickness of the layer from wall surface to the peak velocity position was around 1 mm and did not change even though inclination angle of the impingement wall was changed. In other word, a very thin mass flow layer was formed near the impingement wall. The peak velocities from R = 8 mm to R = 16 mm were averaged. The averaged velocities were 45 m/s for 0 deg., 35 m/s for 20 deg. and 45 m/s for 40 deg. There was also no big difference of averaged velocities among inclination angles.

By considering the layer thickness and the averaged velocity, it seems that heat transfer coefficient between the post-impingement spray and the impingement

wall was hardly changed even though inclination angle of the impingement disk was different. When the heat transfer problem for evaporations of post-impingement spray was considered, this thin layer could be considered as a layer of heat transfer from the wall to post-impingement spray. It suggests that heat transfer process was controlled by a droplet cloud sub-layer of post-impingement spray. However in this PIV analysis, flow velocity of adhered fuel film was difficult to detect. Then flow vector of adhered fuel mass might be needed for further discussion of heat transfer mechanism between droplet sub-layer and wall.

4.6 Summaries

To clarify the characteristics of the adhesion fuel on the flat and inclined walls, effects of impingement disk size and its inclination angle on adhered mass ratio were investigated. Adhesion behavior on the critical area of disk was discussed. Further, the effect of inclination angle on adhered fuel mass was obtained. In addition, the correction angle factor was introduced and discussed precisely. Then, the following results could be obtained.

1. Regardless of injection pressure and impingement distances, it was found that the adhered fuel mass became constant with increasing the diameter of the impingement disk.
2. Thickness of liquid film tended to decrease with increasing of injection pressure. However, decreasing trends were different based on the impingement distance.
3. Two concepts of impingement mass of spray were introduced which is based on the disk diameter (adhesion area factor of k) and inclination angle (inclination angle factor of $\cos \theta_d$).
4. Using the adhesion area factor of k, adhered mass trend was uniquely expressed by the modified adhered mass ratio even though the impingement disk diameter was smaller than the critical diameter of adhesion.
5. Adhered fuel mass ratio decreased with an increase of the inclination angle of disk.
6. Using the substantial impingement mass factor of $\cos \theta_d$, adhered mass trend on inclination disk was uniquely expressed by the modified adhered mass ratio.
7. According to the flow pattern result of PIV, substantial impinged mass of fuel decreased due to the non-impinging part of the spray increased with an increase of inclination angle of wall.

References

[1] Tsunemoto, H. et al., Process of Mixture Formation of Impinging Spray on the Wall in a Hole Type Nozzle, *JSAE*, vol. 27, no. 2, pp. 39-45, 1996.

[2] Saito, A. and Kawamura, K., Behavior of Fuel Film on a Wall at Fuel Spray Impinging, *Proc. of ICLASS 1997,* pp. 54-61, 1997.

[3] Montajir, R.M., Tsunemoto, H., Ishitani, and Minami, T., Fuel spray behavior in a small DI diesel engine: effect of combustion chamber geometry, *SAE Paper*, no. 2000-01-0946, 2000.

[4] Ebara, T. and Arai, M., Estimation of Spray Penetration under a Wall Effect, *ILASS-Japan*, pp. 213-218, 1996.

[5] Ebara, T., Amagai, K., and Arai, M., Penetration Model of a Diesel Spray along a Wall , *COMODIA 98*, pp. 423-428, 1998.

[6] Guerrassi, N. and Champoussin, J.C., Experimental study and modelling of diesel spray/wall impingement, *SAE Paper*, no. 960864, 1996.

[7] Ko, K. and Arai, M., Diesel Spray Impinging on a Flat Wall, Part 1: Characteristics of Adhered Fuel Film in an Impingement Diesel Spray, *Atomization and Spray*, vol. 12(5&6), pp. 737-751, 2002.

[8] Lee, C. S. and Park, S. W., An experimental and numerical study on fuel atomization characteristics of high-pressure diesel injection sprays, *Fuel*, vol. 81, pp. 2417–2423, 2002.

[9] Bai, C. and Gosman, A. D., Development of methodology for spray impingement simulation, *SAE Technical Paper*, 1995.

[10] Andreassi, L, Ubertini, S., and Allocca, L., Experimental and numerical analysis of high pressure diesel spray-wall interaction, *Int. Journal Multiphase Flow*, vol. 33, pp. 742–765, 2007.

Chapter 5

Weber number correlation on adhesion fuel

5.1 Introductory remarks

In the spray-wall interaction research, most common and popular parameter discussed by many researchers was the droplet Weber number [1, 2, 3, 4, 5]. In their studies, the droplet Weber number was used as the non-dimensional value for estimating the impingement droplet stability. Various phenomena such as stick, spread, splash and rebounding as introduced by Naber and Reitz [1], occurred when droplets impinged on a wall surface. Since the stability of impinging droplet was concerning those droplet-wall interaction phenomena, Weber number of droplet was used as controlling factor of these classification. Nagaoka et al. [6], used the Weber number to define the post-impingement droplet size and velocity. Mundo et al. [7], used the Weber number for developing their own impingement criteria. Weber number also was used as to define the spray and film interaction criteria in the numerical experiments [3, 4, 5].

Since each droplet in fuel spray during impingement was difficult to analyze directly, Weber number of average spray droplet was expected to be the most representative dimensionless number for stochastic analysis of impingement phenomena of a diesel spray. Spray contained droplets of various sizes. The Sauter mean diameter was one of the representative mean diameter of spray, and Weber number based on Sauter mean diameter was usually adopted as the average Weber number of spray.

In this chapter, adhered fuel mass was characterized with not only injection pressure and impingement distance, but also size of impingement disk. Moreover, effect of Weber number of impinging droplet, impingement disk size, and inclination angle of disk on adhering fuel mass was investigated. Relationship between adhered mass and Weber number which was obtained with impingement velocity and the Sauter mean diameter of spray were evaluated. To evaluate quantitatively the Weber number effect on adhered mass, modified adhered mass ratio concerning diameter of impingement disk and its inclined angle was introduced. Finally empirical relationships among adhered mass ratio, thickness of adhered fuel film and Weber number were derived from the experimental data

obtained in Chapter 3 and 4. Also, this empirical relationship would be useful tool for the engine designer when designing the diesel engine.

5.2 Impingement velocity of droplet and its Weber number

Various evaluation indexes concerning injection fuel spray are shown in **Fig. 5-1**. Evaluation indexes were injection velocity (V_{inj}), Sauter mean diameter (D_{SMD}) of spray, and Weber number (We_{inj}) of droplet which diameter was represented by D_{SMD} of spray. The D_{SMD} of spray was calculated based on the **Equations (2-4)** and **(2-5)** which described earlier in Chapter 2. Even though there were several published works with D_{SMD} value, but the D_{SMD} was obtained from different experimental conditions from our study. Thus, it was suggested that calculated D_{SMD} from Hiroyasu equations as it was presented our experimental conditions. The relationship among these indexes was summarized as the start of this chapter. **Figure 5-1** shows that the mean diameter of spray was from 7 to 10 μm under different injection pressures. The mean diameter of spray decreased with an increase of injection pressure. According to Arai [7], the D_{SMD} of a traditional type diesel spray was ranging into 25 to 35 μm, but here D_{SMD} less than 10 μm was estimated because of high injection pressure.
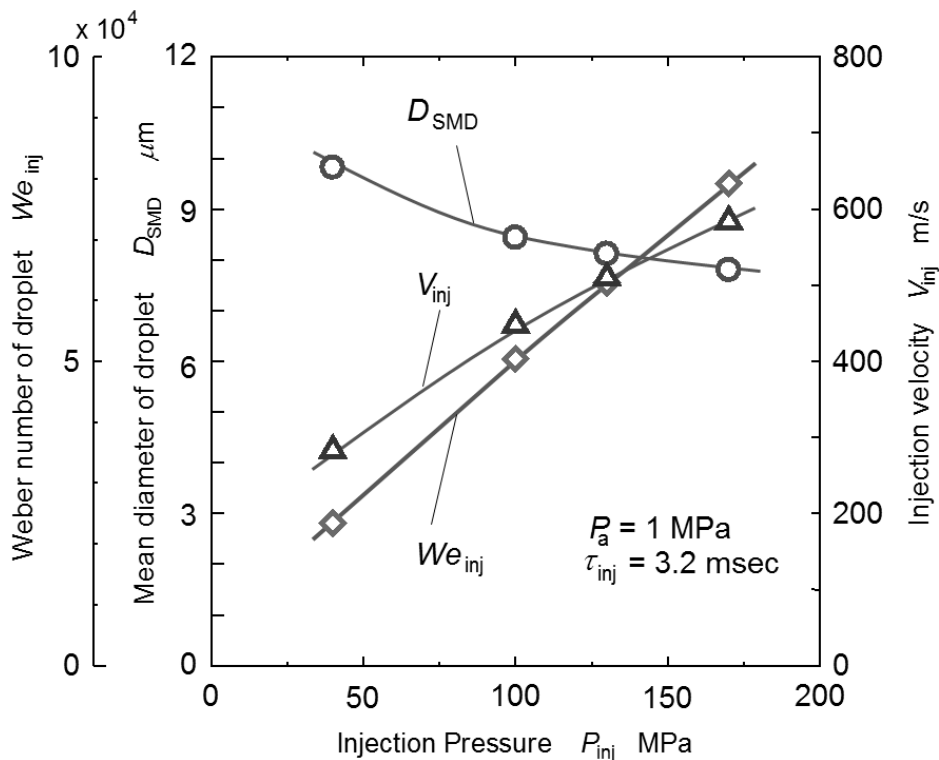
Figure 5-1 Various evaluation indexes of fuel spray

107

Weber numbers of droplet were in a range of from 2×10^4 to 8×10^4 under injection velocities from 280 to 620 m/s. Injection velocity was proportional to square root of the injection pressure ($\sqrt{P_{\text{inj}}}$). While Weber number of droplet was the power of two of the injection velocity as shown in **Equation (2-6)** (Chapter 2). It means that We_{inj} was almost proportional to the injection pressure.

The effect of impingement distance and injection pressure on Weber number (We_{d}) at impingement point are shown in **Fig. 5-2**. This Weber number was obtained through **Equation (2-7)** (Chapter 2). Regardless of injection pressure, the Weber number at impingement point decreased almost linearly with an increase of impingement distance. While the impingement distance beyond 70 mm, the We_{d} tended to decrease slowly. It seems that there were two kinds of decreasing trends of We_{d} over the impingement distance. Through the **Equation (2-7)**, the We_{d} was the power of two of the impingement velocity. It means, they depended the decrease of impingement droplet velocity that was estimated by the movement of spray tip.
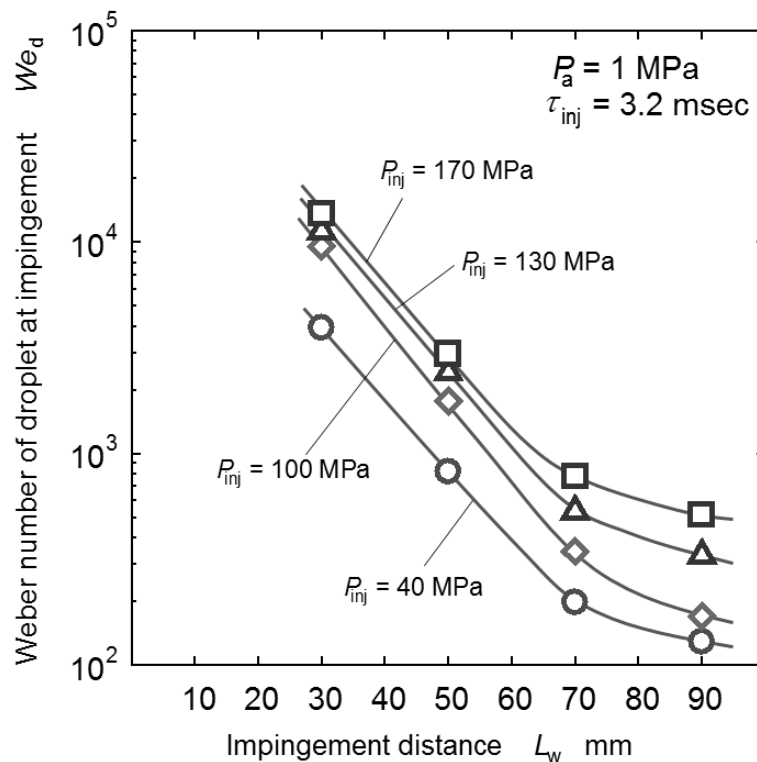
Figure 5-2 Effects of impingement distance and injection pressure on We_{d}

Table 5-1 shows summaries of injection velocities and Weber numbers at impingement points. Regardless of injection pressures and impingement distances, We_{d} could be estimated from D_{SMD} and impingement velocity. Concerning the

results for $L_w = 30$ mm, We_d increased from 3930 to 13600 by an increase of the injection pressure. Since at closer distance to nozzle tip, higher the impingement velocity, We_d was the highest among the tested impingement distances. According to the breakup model by Senda et al. [5], secondary breakup of impinging droplet and build-up of adhered fuel film occurred, and it was classified into three sub-models according the Weber number of impinging droplet. Since their model was represented on non-vaporizing spray condition which similar to this study condition, the Weber number criterion was chosen to establish the impact regimes in this study. They reported that, for $We < 80$, impinging droplets were hardly re-bounded from fuel film surface and caused no break up of the film. Meanwhile, for $80 \leq We < 600$, impingement droplets were re-bound and liquid film remaining on the wall were broken up into large droplets. While for $We \geq 600$, impingement droplets or liquid film were broken up into small droplets.

The We_d at $L_w = 30$ mm was fallen into the category of $We \geq 600$. It seemed that results of low adhered mass ratio at $L_w = 30$ mm obtained in the Chapter 4 was mainly caused by direct re-bound of small broken droplets. In the case of impingement distance of 90 mm, the We_d was fallen into the category of $80 \leq We < 600$ and impinging droplets might be re-bounded or remaining as a fuel film. In the cases of impingement distances of 50 mm and 70 mm, droplets in a size range of D_{SMD} were under the category of $We \geq 600$ but other smaller droplets were in a range of $80 \leq We < 600$, then both of the droplets re-bound and build-up of fuel film might be mixed in the droplet-wall interaction. The adhered mass ratio increased by increased of impingement distance up to 70 mm and began to decline when it reached to a distance of 90 mm (as discussed in Chapter 3). Since the adhered mass ratio tend to decline after reached impingement distance of 90 mm, the category of Weber number reflected to this distance seemed to be suitable. The combination effect of D_{SMD} and impingement velocity were the main factor of fuel mass adherence on the wall as described by the range of Weber number above.

According to the results obtained on Chapter 4, thickness of liquid film for impingement distance longer than 50 mm increased up to 32 μm, which was much thicker than the mean droplet size of diesel spray. It seemed that weak breakup behavior at impingement distance beyond 50 mm was suitable for fuel adhering on a thick fuel film. High adhered mass ratios in these situations seemed to be the result of this effect.

Table 5-1 Droplet velocity and Weber number at impingement point

Injection pressure P_{inj}, MPa	Injection velocity V_{inj}, m/s	Injection Weber number We_{inj}, ($\times 10^4$)	Mean diameter of droplet D_{SMD}, μm	Impingement velocity and impingement Weber number							
				30 mm		50 mm		70 mm		90 mm	
				V_{imp} m/s	We_d	V_{imp} m/s	We_d	V_{imp} m/s	We_d	V_{imp} m/s	We_d
40	283	2.34	9.82	116	3930	53	821	26	198	21	129
100	448	5.04	8.44	195	9550	84	1770	37	344	26	170
130	510	6.29	8.12	216	11280	100	2420	47	534	37	331
170	584	7.92	7.80	242	13600	113	2970	58	781	47	513

5.3   Modified adhered mass ratio of vertical impingement

5.3.1   Adhered mass ratio of vertical impingement

Relationship between impingement disk surface area (A_d) and adhered mass ratio (α_{adh}) was investigated. The summary of the results are shown in **Fig. 5-3**. Experiment conditions were based on vertical impingement and an impingement distance of 50 mm. Injection pressure varied from 40 to 170 MPa with ambient pressure of 1.0 MPa. The results suggested almost the same trend of adhered fuel mass under conditions of various injection pressures. It also suggested that the adhered mass ratio increased with an increase of the impingement disk area up to 500 mm^2 ($D_d \simeq 25$ mm). However, beyond this impingement disk area, adhered mass ratios tended to saturate. These phenomena seemed similar in all injection pressures, where the saturated situation of adhered mass ratios began at around 700 mm^2 ($D_d \simeq 30$ mm). A critical area of disk ($A_{d.critical}$) was defined as an area at coincident point between linear and saturated lines for each injection pressure. Physical meaning of this critical area was the fuel adhesion area that remained on the disk. Critical areas or diameters of disks under other impingement distances were also obtained as same as **Fig. 5-3**. Details of them were already explained in the Chapter 4.
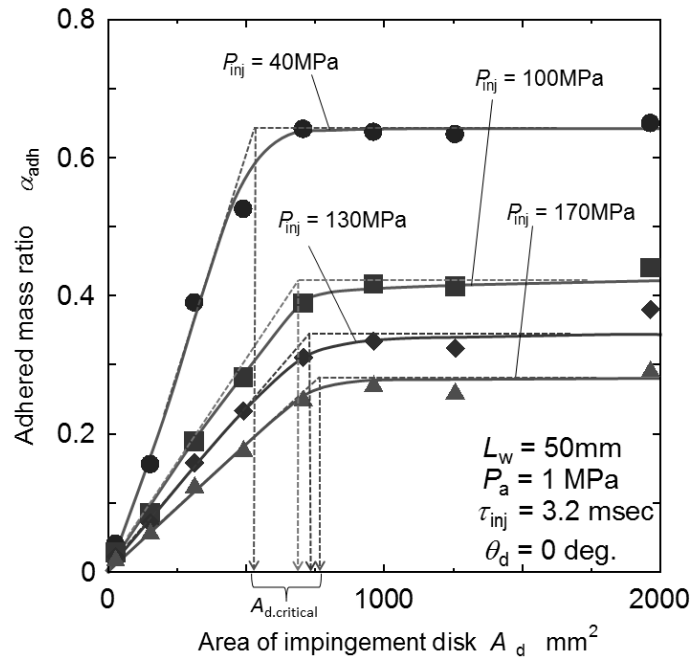
Figure 5-3 Relationship between impingement disk area and adhered fuel mass ratio

5.3.2   Relationship between modified adhered mass ratio and Weber number

Effects of Weber number (We_d) of impinging droplet on adhered mass ratio were summarized as shown in **Fig. 5-4**. In general, the adhered mass ratio seemed to decrease with an increase of Weber number. However as impingement disk diameter changing from 6 mm to 50 mm, adhered mass ratios were widely scattered even though We_d was not changed. Disk size dependance was clearly observed on the smaller disk sizes such as 6 mm and 14 mm. As disk diameter approaching to the critical disk diameter, weaker dependance of disk size on adhered mass ratio was observed. As for adhered mass ratios for impingement disk sizes more than 30 mm, it seemed that those were less scattered and closed to each other in a group.
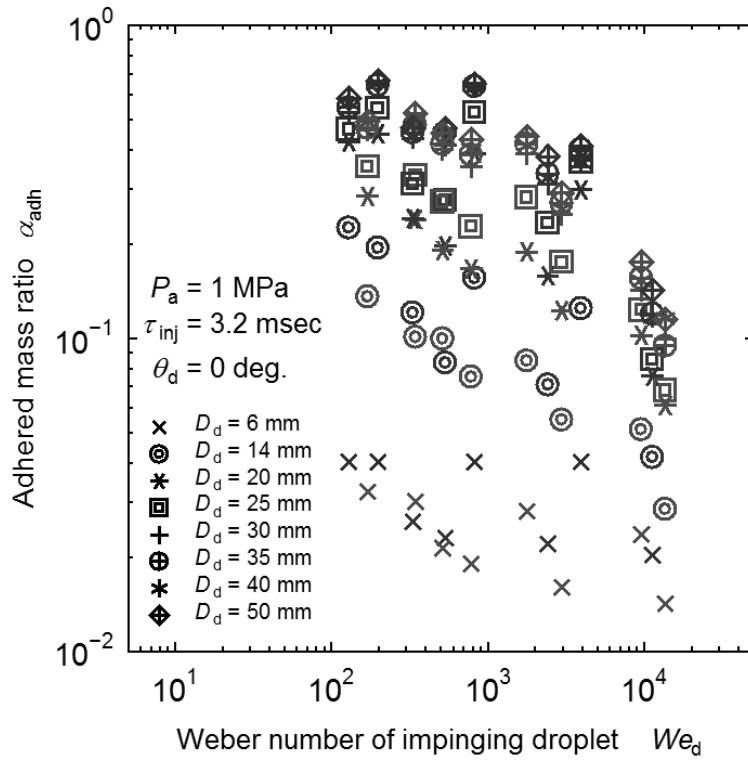
Figure 5-4 Weber number of impinging droplet and adhered mass ratio

The adhered mass ratio was modified by using adhesion area factor " k ". This factor was introduced in the Chapter 4. The modified adhered mass ratio α'_{adh} was derived as follows.

$$m_{adh} = k \cdot m_{\text{adh.critical}} \; ; \quad \text{where " } k \text{ " is the adhesion area factor} \quad (5\text{-}1a)$$

$$k = 1 \quad \text{at } D_\text{d} \geq D_{\text{d.critical}} \quad\quad\quad (5\text{-}1b)$$

$$k = \left(\frac{A_d}{A_{d.critical}}\right) \quad \text{at } D_\text{d} < D_{\text{d.critical}} \quad\quad (5\text{-}1c)$$

$$\alpha'_{adh} = \frac{m_{\text{adh.critical}}}{m_{\text{inj}}} = \frac{m_{\text{adh}}}{k \cdot m_{\text{inj}}} = \frac{\alpha_{\text{adh}}}{k} \quad\quad (5\text{-}2)$$

Figure 5-5 shows the relationship between Weber number of impinging droplet and modified adhered mass ratio mentioned above. By using of **Equation (5-1c)**, the modification of adhered mass ratio could be obtained when the disk diameter was smaller than the critical diameter. Since adhesion area factor " k " took a value less than unity in impingement conditions from $D_\text{d} = 6$ to 25 mm,

112

adhered mass ratios of these conditions were successfully modified and plots of their modified adhered mass ratios were gathered to a unique plots group. In other words, disk diameter dependance could be compensated by the adhesion area factor " k ".

The modified adhered mass ratio was apparently affected only by Weber number (We_d) of impinging droplet. The modified adhered mass ratio tended to uniquely decrease with an increase of We_d. However, it was divided into two decreasing trends. First decreasing trend of modified adhered mass ratio was in a We_d range of 100 to 1000. The first decreasing trend of modified adhered mass ratio was very small till it looks like a constant over the increase of We_d. It seems that $We_d = 1000$ was a transient condition of these two decreasing trends. The modified adhered mass ratio decreased rapidly when We_d was over this transient Weber number. The second decreasing trend appeared in a We_d range of 1000 to 15000. It was clear that the modified adhered mass ratio was uniquely correlated by the Weber number for all conditions where impingement phenomena on the disk smaller than the critical diameter were included.

As according to discussion in Chapter 1 and 2, SMD was the volume-surface mean diameter of spray, and it was considered that SMD was representative of evaporation rate of spray. As for the feature of wall impingement, mass of droplet, number of droplet and droplet diameter were most important parameters of spray adhesion. In this sense, mode diameter was sometimes more important than SMD, because mode diameter was representative of peak number diameter of the spray. Generally, mode diameter was around half of SMD and Weber number based on mode diameter was also around half of Weber number obtained here. It means that transition Weber number of mode diameter should be the half of this study and was more close tendency with classification shown in **Fig. 1-11** (Chapter 1).
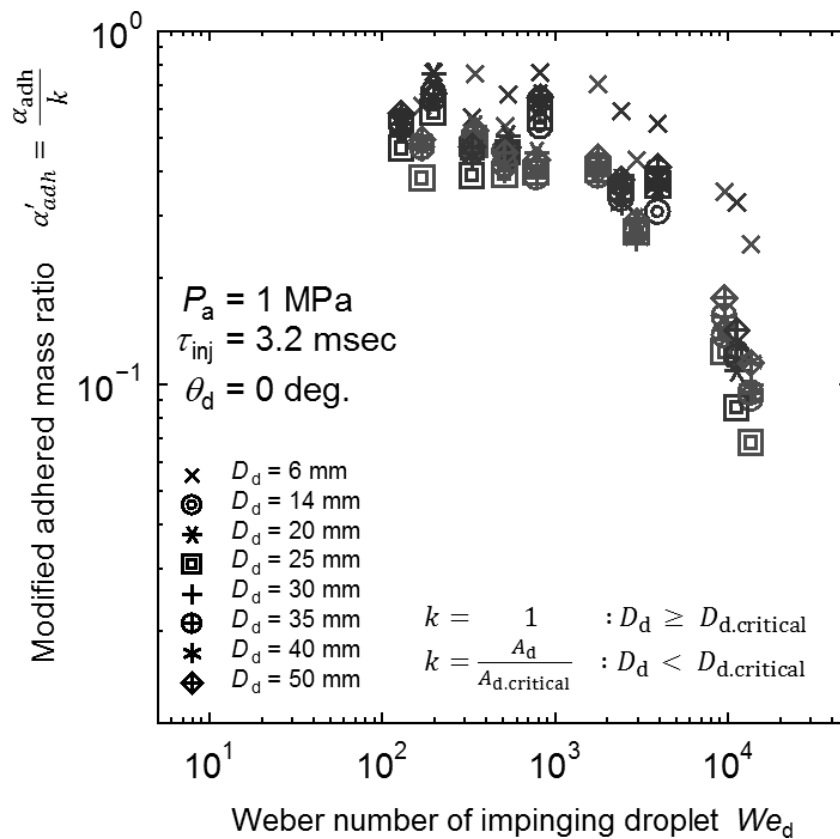
Figure 5-5 Relationship between We_d and adhered mass ratio modified by adhesion area factor

5.4 Modified adhered mass ratio of inclined impingement

5.4.1 Adhered mass ratio of inclined impingement

To clarify a trend of adhered mass on an inclined wall, adhered fuel mass ratio on it was evaluated as same as vertical impingement. One of the typical results is shown in **Fig. 5-6**. This figure was based on $L_w = 50$ mm, which was the same impingement distance of the condition in **Fig. 5-3**. However, disk size condition was limited in $D_d = 50$ mm, and it was for larger diameter than critical diameter indicated by the results of **Fig. 5-3**. It means that the adhesion area factor " k " was kept unity. Adhered fuel mass ratio of $P_{inj} = 40$ MPa decreased with increasing the inclination angle of the disk. Also, the ratios for injection pressures more than $P_{inj} = 100$ MPa decreased with an increase of the angle. It seemed that regardless of injection pressure was low or high, same effect of inclination angle on adhered mass ratio appeared.
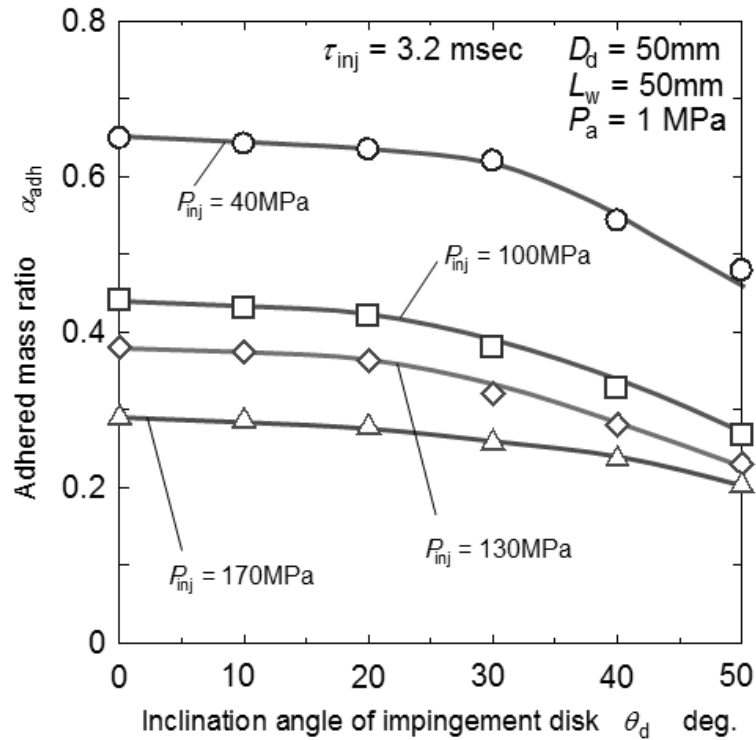
Figure 5-6 Relationship between inclination angle and adhered mass ratio

5.4.2 Modified adhered mass ratio of inclined impingement and its Weber number

As discussed in the Chapter 4, the inclination angle factor of $\cos \theta_d$ was introduced to explain the above results. The modified adhered mass ratio α''_{adh} for inclination disk was introduced by **Equation (5-3)**.

$$\alpha''_{adh} = \frac{\alpha_{adh}}{\cos \theta_d} \qquad (5\text{-}3)$$

In **Figure 5-7**, relationships between Weber number (We_d) of impinging droplet and modified adhered mass ratio α''_{adh} were summarized. This figure was based on $D_d = 30$ and 50 mm. The modified adhered mass ratios α''_{adh} were close to each other even though their conditions included all inclination angles and all injection pressures. It means that **Equation (5-3)** was reasonable modification of adhered mass ratio on inclined impingement. Further, transient condition of $We_d = 1000$ was clearly observed. It was almost similar to the transient condition in **Fig. 5-5**.
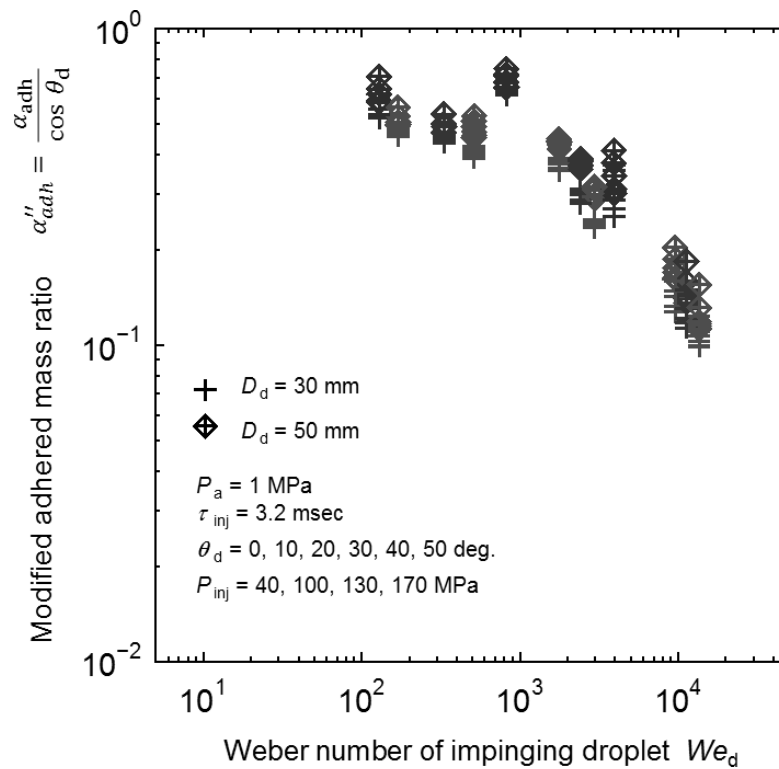
Figure 5-7 Relationship between We_d and modified adhered mass ratio for various inclination angles

Results obtained in **Fig. 5-7** could be expressed in more sophisticated way when the Weber number based on the normal impingement velocity ($We_{d.n}$) was used. **Figure 5-8** shows the relationship between Weber number ($We_{d.n}$) and modified adhered mass ratio for various inclination angles. Using $We_{d.n}$, Weber number dependance of modified adhered mass ratio (α''_{adh}) was more clearly observed than **Fig. 5-7** where We_d was used. It means that the droplet-wall interaction process of inclination impingement was not completely controlled by impingement Weber number (We_d) but it directly controlled by normal impinging Weber number ($We_{d.n}$) of droplet. In other words, approaching velocity of droplet to the impingement surface was more fundamental factor of adhesion. Although the $We_{d.n}$ was influenced by the normal impingement velocity ($V_{imp.n}$), in $We_{d.n}$, the data of We_d was also included. Thus the critical $We_{d.n}$ for the decrease of the modified adhered mass ratio might similar that for We_d which is 1000. Even though the transient Weber number for both conditions (We_d and $We_{d.n}$) was almost same at 1000, the decreasing trends of modified adhered mass ratio and transient Weber number were more clearly observed when used of $We_{d.n}$ compared to that We_d. **Figure 5-9** was the same results of **Fig. 5-8** but the plots of injection pressure of 40 MPa were eliminated. It was clearly observed that no off-line plots

116
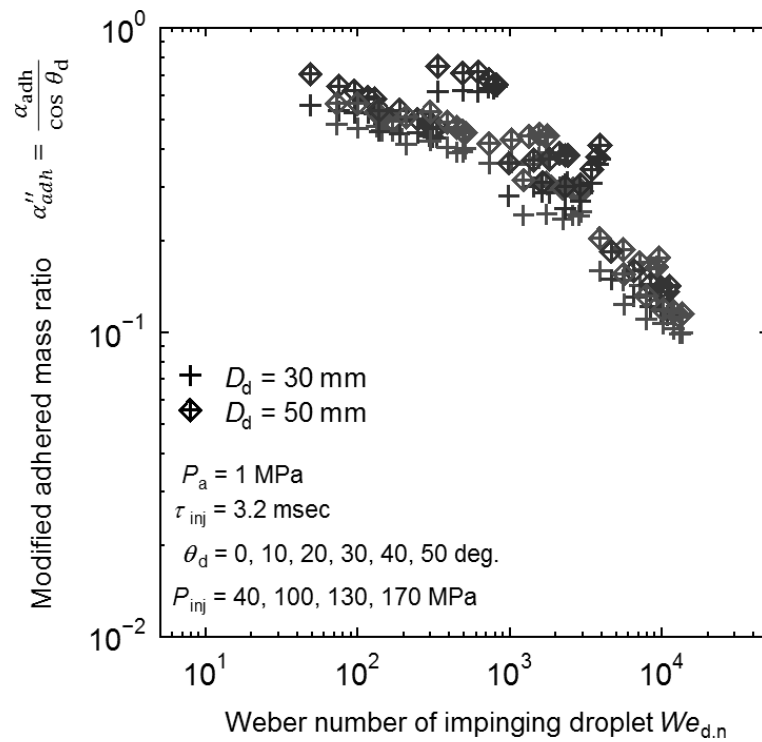
Figure 5-8 Relationship between $We_{d.n}$ and modified adhered mass ratio for various inclination angles (Injection pressures were 40, 100, 130, and 170 MPa)

$$\alpha_{adh} = 0.85 \cdot \cos\theta_d \cdot (We_{d.n})^{-0.11}$$

$$\alpha_{adh} = 27 \cdot \cos\theta_d \cdot (We_{d.n})^{-0.61}$$
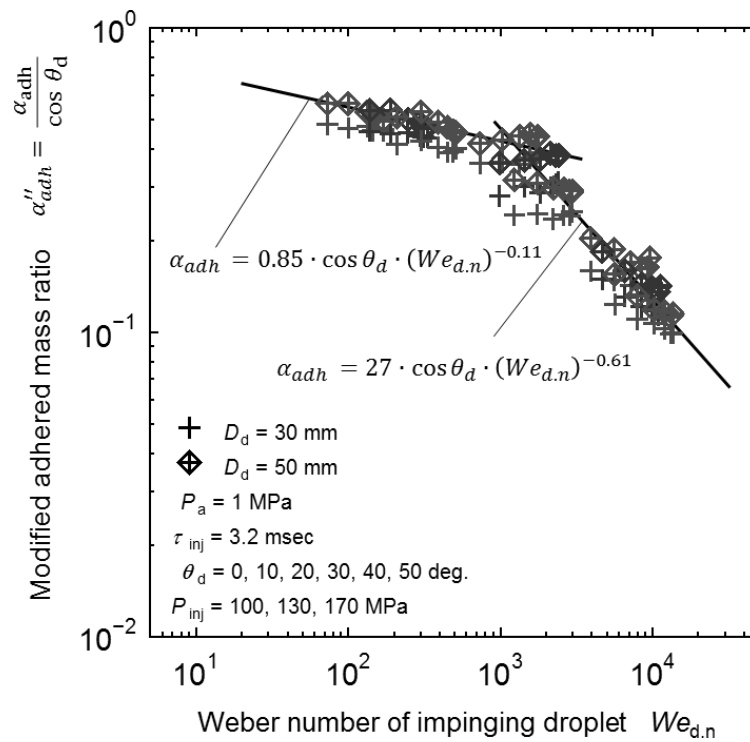
Figure 5-9 Relationship between $We_{d.n}$ and modified adhered mass ratio for various inclination angles (Injection pressures were 100, 130, and 170 MPa)

were there. It means that the adhesion mechanism for injection pressure of 40 MPa was somewhat different as compared to other injection pressures. It was because of smaller $We_{d.n}$ for 40 MPa injection at longer impingement distances of $L_w = 70$ mm and 90 mm.

In **Figure 5-9**, Weber number ($We_{d.n}$) dependance of modified adhered mass ratio was more sophistically indicated as compared with **Fig. 5-7** and **Fig. 5-8**. It strongly suggested that the decreased trends of modified adhered mass ratios (α''_{adh}) for various inclination angles were mostly influenced by the increase of $We_{d.n}$. It means that approaching velocity to the wall was more dominant velocity than the impingement velocity under the condition of inclined wall impingement. There were two correlation lines drawn in **Fig. 5-9** and following two equations were derived.

$$\alpha_{adh} = 0.85 \cdot \cos\theta_d \cdot (We_{d.n})^{-0.11} \qquad (5\text{-}4)$$

$$\alpha_{adh} = 27 \cdot \cos\theta_d \cdot (We_{d.n})^{-0.61} \qquad (5\text{-}5)$$

Figure 5-9 also shows that the adhered mass ratios could be summarized in two different ranges of $We_{d.n}$. It could be separated by the transient $We_{d.n}$ of around 1000. **Equation (5-4)** was based on a range before transient condition of $We_{d.n} = 1000$. While the plots for these $We_{d.n}$ being larger than 1000, were correlated by **Equation (5-5)**. In the case of inclination impingement, it was clear that two kinds of modification were needed to mention the impingement phenomena. One was the inclination angle factor "$\cos\theta_d$", which was corresponding to the real impingement part of spray without escaping (refer to the Chapter 4). The other was "$We_{d.n}$", which was concerning the real approaching velocity of droplet. In later figure, in order to discuss in details the non-dimensional film thickness of adhered fuel, effect of injection pressure of 40 MPa will again adopted together with other factor such as various impingement disk diameters, impingement distances and inclination angles.

5.5 Combined modified adhered mass ratio and thickness of adhered fuel film

Finally, from the above discussions, the combined modified adhered mass ratio α'''_{adh} could be introduced by **Equation (5-6)**.

$$\alpha_{adh}''' = \frac{\alpha_{\text{adh}}}{k \cdot \cos \theta_{\text{d}}} \qquad (5\text{-}6)$$

The combined modified adhered mass ratio could be defined as a unique adhered mass ratio in which adhesion area factor " k " and inclination angle factor "$\cos \theta_{\text{d}}$" were combined. Thus, it could show the combined behavior of adhered mass ratio under various impingement disk sizes and inclination angles.

Relationships between $We_{\text{d.n}}$ and combined modified adhered mass ratio were summarized in **Fig. 5-10**. The plotted data in the figure were results of various combinations of impingement distances, disk diameters, inclination angles and injection pressures. The trend similar to **Fig. 5-9** appeared even though these plots consisted of the results with various parameters as mentioned above. There were two correlation lines drawn in **Fig. 5-10** and following two equations were derived.

$$\alpha_{\text{adh}} = 0.85 \cdot k \cdot \cos \theta_{\text{d}} \cdot (We_{\text{d.n}})^{-0.11} \qquad (5\text{-}7)$$

$$\alpha_{\text{adh}} = 27 \cdot k \cdot \cos \theta_{\text{d}} \cdot (We_{\text{d.n}})^{-0.61} \qquad (5\text{-}8)$$

These equations were well correlated to the data with r-squared value of 0.83. This value shows the experimental data was well fitted on the derived equations. Even though k factor was added in **Fig. 5-10**, plotted data were almost distributed on the same plot as **Fig. 5-9** except some points which will explained later. Thus, fitting values were not changed between **Equations (5-4)** - **(5-5)** and **Equations (5-7)** - **(5-8)**. Also plotted data in **Fig. 5-10** was not changed much due to this reason.
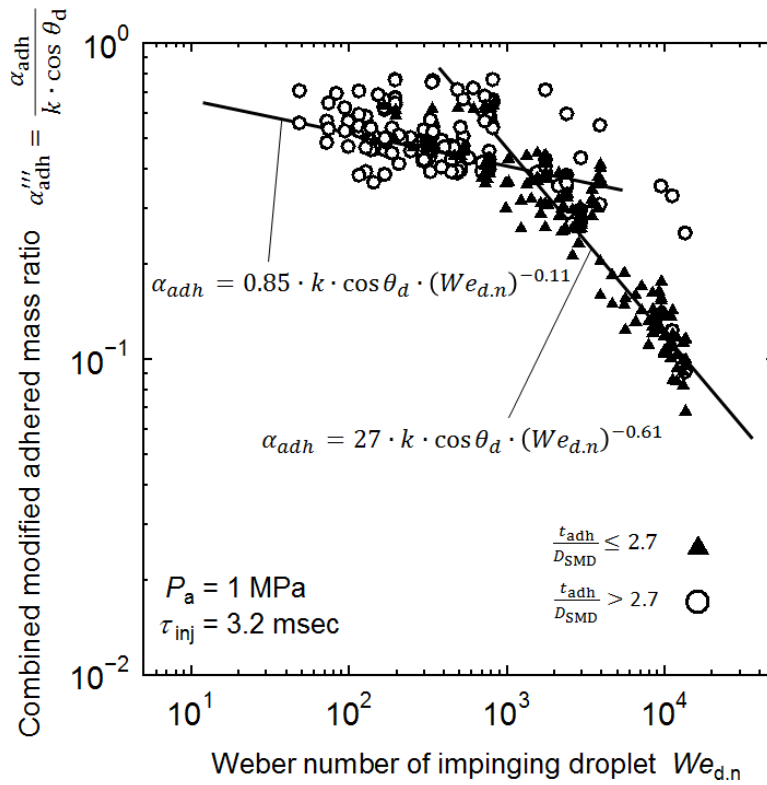
Figure 5-10 Combined modified adhered mass ratio for various impingement disk diameters, inclination angles and injection pressures

Two decreasing trends were basically separated by the transient Weber number of $We_{d.n} = 1000$. However these two trends were mixed in the range near the transient Weber number. It could be explained by using non-dimensional film thickness of adhered fuel (t_{adh}/D_{SMD}). The physical meaning of (t_{adh}/D_{SMD}) was non-dimensional thickness of adhered fuel film to the mean diameter of spray. Since D_{SMD} changed with injection pressure, the values of D_{SMD} were based on each injection pressure for all given data. The thickness of adhered fuel (t_{adh}) was obtained by the equations below.

For $D_d \geq D_{d \cdot critical}$:

$$t_{adh} = \frac{m_{adh}}{\rho_l} \cdot \frac{1}{\frac{\pi}{4}(D_{d.critical})^2} \qquad (5\text{-}9)$$

For $D_d < D_{d \cdot critical}$:

$$t_{adh} = \frac{m_{adh}}{\rho_l} \cdot \frac{1}{\frac{\pi}{4}(D_d)^2}$$ (5-10)

As for the inclined impingement, the critical disk diameter was not measured and it was assumed as the same as normal impingement.

In **Figure 5-10**, plots shown by symbol "○" were corresponded to the adhered film thickness of t_{adh}/D_{SMD} being larger than 2.7. It suggested that the film was thicker than around 30 μm. These plots were correlated by the relationship indicated by **Equation (5-7)**. It means that impingement of lower Weber number droplet produced thick film and adhered fuel mass was little influenced by the Weber number. On the contrary, plots by symbol "▲" represent the adhered mass results where the thickness of the film was less than around 30 μm ($t_{adh}/D_{SMD} \leq$ 2.7). Weber number dependance in these plots appeared strongly and adhered fuel mass ratio decreased rapidly with an increase of $We_{d.n}$. Since high Weber number and thin fuel film were suitable conditions for re-bound of impinging droplet, not only general adhered mass ratio but also absolute value of adhered mass became lower values in these conditions. By used the non-dimensional thickness of adhered fuel film to the mean diameter of spray, the different between transient Weber number was clearly observed. From our calculation, the critical value of 2.7 shows the different between modified adhered mass ratio on low Weber number and high Weber number. Thus this critical value of 2.7 was expected to differentiate between the region of low and high Weber number. These plots were well correlated by the relationship shown by **Equation (5-8)**.

Most of the off-line plots in **Fig. 5-10** corresponded to the results of 40 MPa injection. Also there were some other data plotted far from the correlation lines. Even though, both of **Equation (5-7)** and **Equation (5-8)** were still possible to evaluate the adhered mass ratio as same as **Equation (5-4)** and **Equation (5-5)**. Further, **Equation (5-4)** and **Equation (5-7)** were corresponding the adhered mass ratio when non-dimensional thickness of fuel film was thicker than 2.7, and **Equation (5-5)** and **Equation (5-8)** were representative equations with high Weber number and thin fuel film condition.

5.6 Summaries

In order to clarify the characteristics of adhesion in vertical and inclined impingements, effects of Weber number of impinging droplet, impingement disk size, and its inclination angle on adhered mass ratio were investigated. From the adhering fuel mass and modification of the adhered mass ratio, the empirical equations were estimated. Furthermore, the characteristics of adhering fuel according to the Weber number of impinging droplet were discussed. Then, the adhering fuel and thickness of adhering fuel were discussed in detail on the basis of the results. Further, the main results were summarized as follows.

8. Combined modified adhered mass ratio was introduced to summarize the adhered mass with combinations of various impingement distances, disk sizes, inclination angles and injection pressures.
9. Weber number of $We_{d.n}$ which was calculated by approaching velocity of droplet to the impingement wall was more dominant factor than the Weber number obtained by droplet absolute velocity.
10. The impingement of lower Weber number droplet produced thick film and adhered fuel mass was little influenced by the Weber number.
11. There were two decreased trends which were separated by the transient Weber number ($We_{d.n} = 1000$). The modified adhered mass ratio rapidly decreased in a range of Weber number higher than this transient Weber number.
12. The adhered mass ratio could be correlated by using relationships shown by **Equation (5-7)** and **Equation (5-8)**.

References

[1]   Naber, J.D. and Reitz, R.D, Modeling spray/wall impingement, *SAE Paper*, no. 880107, 1988.

[2]   Wachters, L.H.J. and Westerling, N.A., The heat transfer from a hot wall to impinging water drops in the spheroidal state, *Chem. Eng. Sci.,* vol. 21, no. 11, pp. 1047-1056, 1966.

[3]   Senda, J., and Fujimoto, H.G., Multidimensional modeling of impinging sprays on the wall in diesel engines, *Applied Mechanics Review*, no. 94, pp. 341–348, 1994 (Japenese).

[4]   Senda, J., Kobayashi, M., Iwashita, S. and Fujimoto, H., Modeling of diesel spray impinging on flat wall, *SAE Technical Paper*, no. 941894, 1994.

[5]   Senda, J., Kobayashi, M., Iwashita, S. and Fujimoto, H., Modeling of diesel spray impinging on flat wall, *The Japan Society of Mechanical Engineers*, vol. 52, no. 4, pp. 119–138, 1999.

[6]   Nagaoka, M., Kawazoe, H., and Nomura, N., Modeling Fuel Spray Impingement on a Hot Wall for Gasoline Engines, *SAE International*, no. 940525, 1994.

[7]   Mundo, C.., Sommerfeld, M., and Tropea, C., On the modeling of liquid sprays impinging on surfaces, *Atomization and Sprays*, vol. 8, no. 4, pp. 625–652, 1998.

Chapter 6

Ambient pressure effect on adhered fuel mass

6.1 Introductory remarks

Wall impingement of fuel spray is known as the main contributor to a DI diesel engine with small combustion cavity. Recently, a high boost intake pressure and high exhaust gas recirculation (EGR) were adopted in diesel engine systems for high performance and reduction of NOx and PM.

In ultra-high boost engine, compressed gas density in combustion chamber became 4 or 5 times higher than that in naturally aspirated (NA) engine [1, 2, 3, 4]. It seems that a diesel spray behavior in high gas density surroundings might differ from that in a conventional diesel engine. Generally, spray tip penetration decreased with an increase of ambient pressure or density of surroundings. It resulted a decrease of the spray velocity at the combustion cavity wall. Then wall impingement behavior including fuel adhesion on the combustion cavity wall might be affected greatly by ambient pressure. Therefore, under high gas density condition, precise investigation of impingement fuel spray is needed. On the contrary, when the early injection strategy was adopted, fuel injection under low surrounding pressure and long impingement distance dominated the mixture formation process with fuel adhering. Further low and high surrounding densities seemed to affect different ways to the adhering mechanism, and have received fundamental interest as the basic research.

In this chapter, effect of ambient pressure and atmospheric pressure on adhered fuel mass ratio of normal impingement diesel spray was investigated experimentally. Also, effects of injection pressure and impingement distance were investigated. Concerning the trend of adhered mass ratio, shadowgraph image and Weber number of impingement spray droplet were discussed. Finally ambient pressure effect was considered using Jet number and empirical equations of adhered mass ratio were introduced.

6.2 Spray droplet velocity and Weber number

Relationship between mean diameter (D_{SMD}) and droplet initial Weber number (We_{inj}) of injected spray under various ambient pressure conditions are

shown in **Fig. 6-1**. The mean diameter of spray droplet (D_{SMD}) varied from 3 μm to 15 μm with an increase of ambient pressure even though injection pressure was kept constant (P_{inj} = 150 MPa). This diameter increase was due to sudden velocity decrease of injected liquid before its complete atomization [5]. According to Arai [6], D_{SMD} of traditional type diesel spray was ranging between 25 μm to 35 μm, but here D_{SMD} less than 15 μm was estimated because of the high injection pressure.
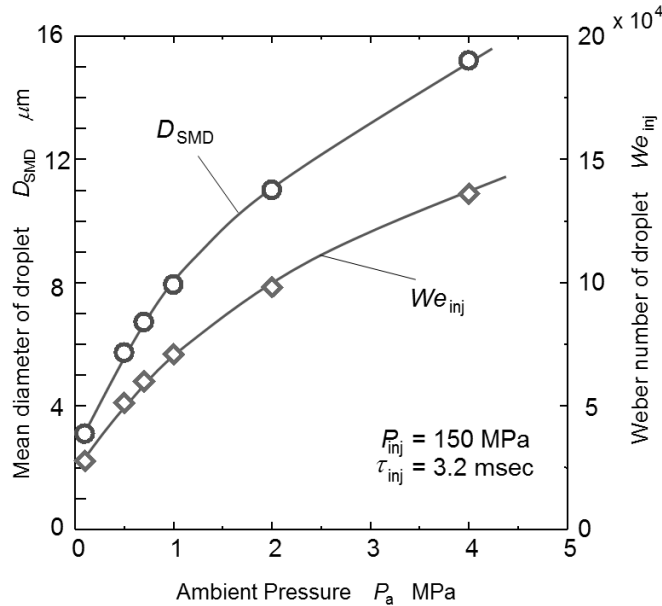
Figure 6-1 Relationship between D_{SMD} and We_{inj}

Weber number of droplet (We_{inj}) just after injection was calculated by using of **Equation (2-6)** (Chapter 2). We_{inj} increased with an increase of ambient pressure. For injection pressure of 150 MPa, Weber numbers of droplet were in a range of from 2.5×10^4 to 1.4×10^5. As for other injection conditions, D_{SMD} and We_{inj} were also calculated with the same data treatment. As the results, similar increasing trends of D_{SMD} and We_{inj} with an increase of ambient pressure were obtained.

Effects of ambient pressure and injection pressure on Weber number (We_d) at impingement point are shown in **Fig. 6-2**. This Weber number was obtained through **Equation (2-7)** (Chapter 2). Spray-wall interaction could be discussed using an average Weber number of impingement spray and impingement velocity that varied with ambient pressure and impingement distance. The combined ambient pressure effects on impingement velocity and D_{SMD} resulted whole tendency of We_d.

At the impingement distance of 30 mm (**Fig. 6-2 (a)**), Weber number slightly decreased with ambient pressure increase from 0.5 MPa to 0.7 MPa and decreased

125

almost smoothly with further increase of the ambient pressure. It seemed that the decreasing trend of We_d was dominated by spray velocity decay due to an increase of ambient pressure.

(a) $L_w = 30$ mm   (b) $L_w = 90$ mm
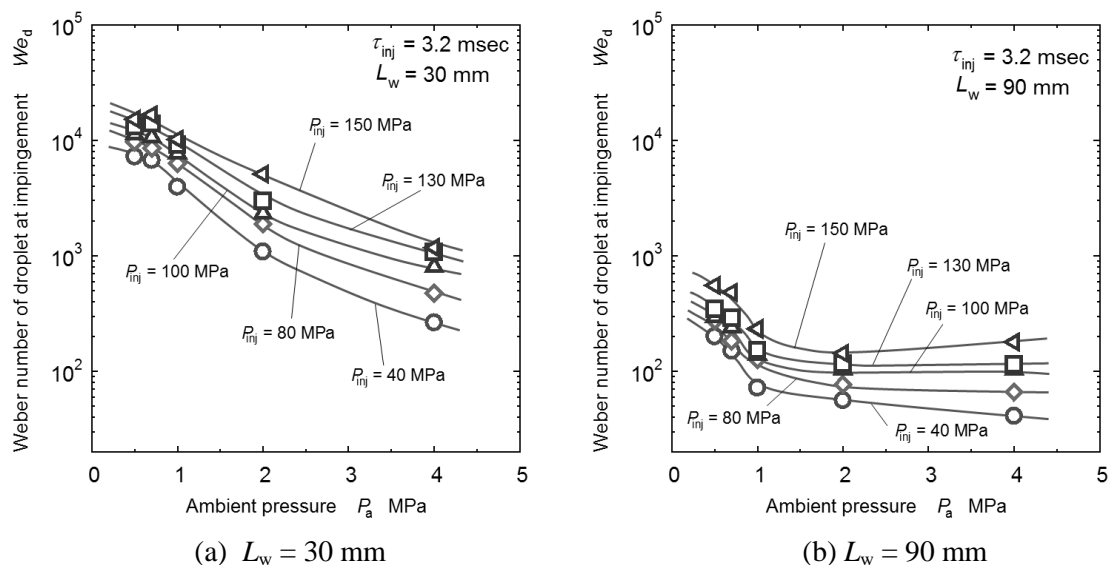
Figure 6-2 Effects of ambient pressure on We_d

As according from the result obtained in **Fig. 3-5** (Chapter 3), one of the influenced factor of adhering was the impingement velocity where the adhered mass ratio was slightly decreased during 70 mm – 90 mm impingement distance at injection pressure lower than 100 MPa. It seemed that lower velocity than critical resulted to less adhering. To explain this, here, effect of impingement velocity was combined with the effect of droplet mean diameter D_{SMD}. It could be clearly observed the We_d at ambient pressure 1 MPa for 90 mm impingement distance was much lower than at 30 mm impingement distance.

At the impingement distance of 90 mm (**Fig. 6-2 (b)**), We_d also tended to decrease at ambient pressure from 0.5 MPa to 1.0 MPa. In these conditions, the ambient pressure effect on We_d decreasing was more clearly observed than 30 mm impingement.   However when ambient pressure increased beyond 1 MPa, it showed almost constant tendency. Since the impingement droplet velocity was low enough at 90 mm impingement and not much different under high ambient pressure conditions (2 MPa and 4 MPa), no obvious effect of the ambient pressure on We_d was obtained. Concerning the Weber number for $P_{inj} = 150$ MPa at $L_w = 90$ mm, We_d showed slightly increasing trend in a range from 2 MPa to 4 MPa. This We_d slight increasing was caused with the D_{SMD} increase with ambient pressure.

Table 6-1 shows summaries of spray velocities and Weber numbers at impingement points. This table included the results of two different ambient pressures. They were ambient pressures of 0.5 MPa and 4 MPa. Concerning the results for $P_a = 0.5$ MPa and $L_w = 30$ mm, We_d increased from 7220 to 15200 with an increase of the injection pressure. As for $P_a = 4$ MPa and $L_w = 30$ mm, as increasing the injection pressure, We_d increased from 264 to 1180. According to Ohta et al. [7], as ambient pressure increasing, spray tip penetration decreased. It meant that the velocity of disintegrated spray droplet decreased by the effect of high density surroundings. Then higher the ambient pressure and longer the impingement distance, We_d became low. As for the 40 MPa injection, $We_d = 41$ was estimated at the condition of $P_a = 4$ MPa and $L_w = 90$ mm.

According to the breakup model by Senda and Fujimoto [8], secondary breakup of impinging droplet and build-up of adhered fuel film occurred, and it was classified into three sub-models according the Weber number of impinging droplet. They reported that, for $We < 80$, impinging droplets were hardly re-bounded from fuel film surface and caused no break up of the film. Meanwhile, for $80 \leq We < 600$, impingement droplets were re-bounded and liquid film remaining on the wall was broken up into large droplets. While for $We \geq 600$, impingement droplets or liquid film were broken up into small droplets.

Table 6-1 Droplet velocity and Weber number at impingement point

Ambient Pressure P_a, MPa	Injection Pressure P_{inj}, MPa	Injection Velocity V_{inj}, m/s	Injection Weber Number We_{inj}, ($\times 10^4$)	Mean diameter of droplet D_{SMD}, μm	Impingement velocity and impingement Weber number							
					30 mm		50 mm		70 mm		90 mm	
					V_{imp} m/s	We_d	V_{imp} m/s	We_d	V_{imp} m/s	We_d	V_{imp} m/s	We_d
	40	283	1.69	7.09	185	7220	121	3090	66	919	31	200
	80	400	3.00	6.31	227	9690	147	4060	79	1170	38	274
0.5	100	448	3.64	6.10	249	11300	153	4250	84	1280	40	295
	130	510	4.54	5.86	276	13300	174	5280	89	1380	44	344
	150	548	5.12	5.72	299	15200	192	6280	105	1880	57	554
	40	283	4.50	18.8	22	264	13	95	11	68	9	41
	80	400	8.00	16.8	31	474	17	144	15	112	12	66
4	100	448	9.70	16.2	41	803	19	174	16	123	15	103
	130	510	12.1	15.6	48	1070	23	245	17	134	16	114
	150	548	13.6	15.2	51	1180	29	381	21	200	20	179

We_d : [ ] < 80 $80 \leq$ [ ] < 600 $600 \leq$ [ ]

Figure 6-2 and **Table 6-1** show that values of impingement Weber number were varied widely with injection pressure, ambient pressure and impingement

distance. All three categories of Weber number mentioned above appeared in the present experiment. It means the spray impingement behavior and adhered fuel mass ratio might be changed with various mechanisms mentioned above.

6.3 Adhered mass ratio and impingement disk size

Relationships between impingement disk diameter (D_d) and adhered mass ratio (α_{adh}) are shown in **Fig. 6-3**. Injection pressure was 130 MPa with ambient pressures of 1 MPa (**Fig. 6-3 (a)**) and 4 MPa (**Fig. 6-3 (b)**). At the ambient pressure of 1 MPa (**Fig. 6-3 (a)**), adhered mass ratio increased with an increase of impingement disk diameter up to $D_d = 30$ mm. However, beyond this impingement disk diameter, adhered mass ratio tended to saturate. These phenomena seemed similar in all impingement distances, where the saturated feature of adhered mass ratio began at around $D_d = 30$ mm. Even though at high ambient pressure conditions (**Fig. 6-3 (b)**), the similar saturating tendency of adhering mass ratio was observed. However adhered mass ratio of $L_w = 90$ mm was lower than those of $L_w = 50$ mm and 70 mm. It seems that adhesion mechanism at $L_w = 90$ mm was somewhat different from other impingement conditions.

(a) $P_a = 1$ MPa   (b) $P_a = 4$ MPa
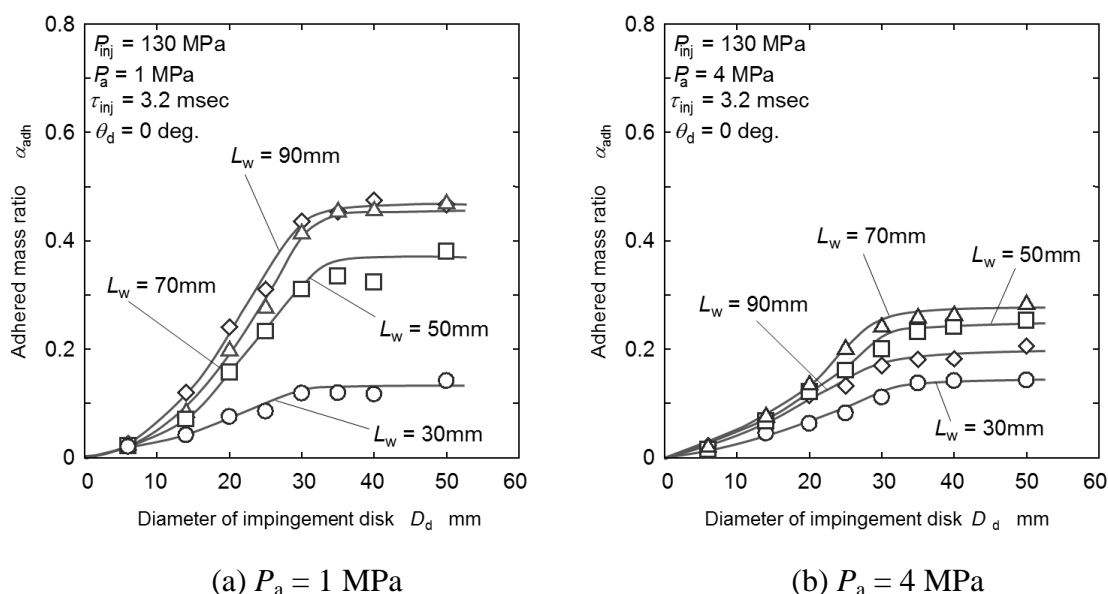
Figure 6-3 Relationship between impingement disk diameter and adhered fuel mass ratio ($P_{inj} = 130$ MPa)

Similar results under the conditions of 1 MPa ambient pressure were already obtained in Chapter 4. As discussed in Chapter 4, a critical diameter was the

smallest disk size where saturated trend of adhered mass ratio was observed, and suggested that the critical diameter was around 30 mm. When the ambient pressure changed from 1 MPa to 4 MPa (**Fig. 6-3 (b)**), no obvious difference of critical diameter was observed. Here, impingement disk diameter was set on 50 mm. According to the above results, it means that disk size did not affect the results of this chapter.

6.4 Ambient pressure effect on adhered mass ratio

Effects of ambient pressure on adhered mass ratio for various impingement distances are shown in **Fig. 6-4**. At the impingement distance of 30 mm (**Fig. 6-4 (a)**), the adhered mass ratio decreased slightly from ambient pressure of 0.1 MPa to 1.0 MPa. However, adhered mass ratio remained almost constant between ambient pressure of 1 MPa to 4 MPa. These phenomena seemed similar to all injection pressures.

At the impingement distance of 50 mm (**Fig. 6-4 (b)**), the 40 MPa injection showed highest adhered mass ratio among them. The adhered mass ratio under 40 MPa injection decreased with increase of ambient pressure from 0.1 MPa to 2 MPa. Then it slightly decreased under the ambient pressure from 2 MPa to 4 MPa. However under the injection pressure beyond 80 MPa, the adhered mass ratio tended to be almost constant between ambient pressures of 2 MPa and 4 MPa.

Further, when impingement distance changed to 70 mm (**Fig. 6-4 (c)**), the adhered mass ratio tended to decrease with ambient pressure from 0.1 MPa to 2 MPa regardless of injection pressure. Also, adhered mass ratio continued to decrease more for ambient pressure from 2 MPa to 4 MPa. While at an impingement distance of 90 mm (**Fig. 6-4 (d)**), the adhered mass ratio showed somewhat different trend from the results of impingement distance 70 mm. It decreased monotonously with an increase of ambient pressure from 0.1 MPa to 4 MPa. As for ambient pressure of 0.1 MPa and 1 MPa, the adhered mass ratio of L_w = 90 mm showed higher values than at L_w = 70 mm. However, as ambient pressure increasing up to 4 MPa, the adhered mass ratio at L_w = 90 mm was lower than at L_w = 70 mm. At long impingement distances such as 70 mm and 90 mm (**Fig. 6-4 (c)** and **(d)**), ambient pressure effect on adhered fuel mass strongly appeared on the decreasing trend. Generally under long impingement condition, adhered fuel mass in high ambient pressure condition such as 4 MPa was half of that under 1 MPa condition.
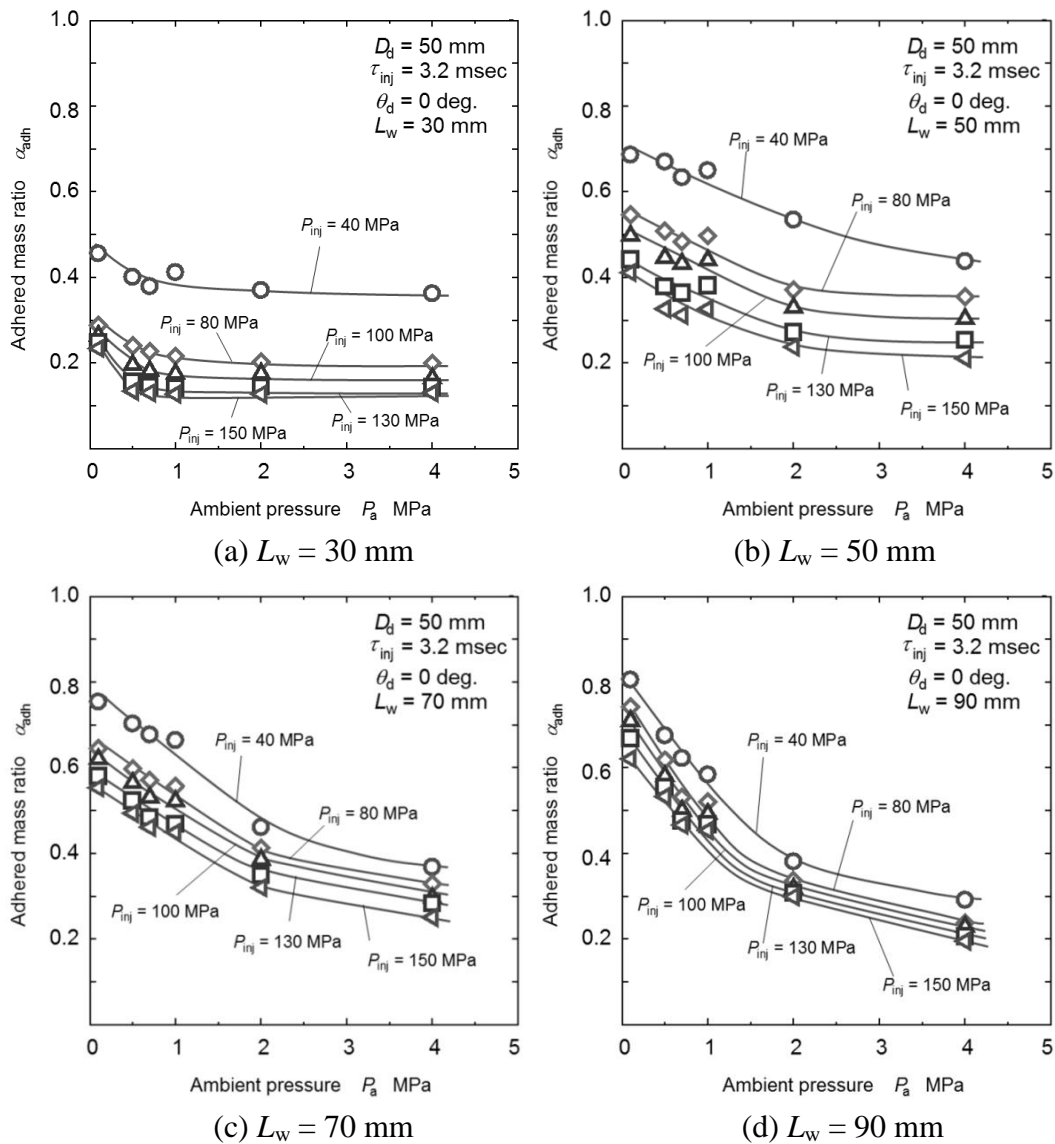
Figure 6-4 Effect of ambient pressure on adhered mass ratio

Moreover, the effects of ambient pressure and impingement distance on adhered mass ratio are shown in **Fig. 6-5**. As for the ambient pressure effect, the trends appeared in **Fig. 6-5 (a)** and **(b)** were almost similar even though the injection pressures were far different. Both results suggested that effect of ambient pressure on adhered mass ratio at $L_w = 30$ mm was uniquely different from the results obtained at other longer impingement distances.

As for $P_{inj} = 130$ MPa (**Fig. 6-5 (a)**), low adhered mass ratio at $L_w = 30$ mm seemed to be caused by secondary atomization on the impingement disk, because injection velocity was high and its decay was not so much at 30 mm impingement distance. At the impingement distances of 50 mm and 70 mm, the effect of

ambient pressure on adhered mass ratio was almost similar. However at $L_w = 90$ mm, the adhered mass ratio tended to decrease below that of 70 mm.

As for low injection pressure case of $P_{inj} = 40$ MPa (**Fig. 6-5 (b)**), it shows that the adhered mass ratio was higher than **Fig. 6-5 (a)** for all impingement conditions. The adhered mass ratio at $L_w = 70$ mm tended to decrease below $L_w = 50$ mm when the ambient pressure increased beyond 1 MPa. While, the adhered mass ratio at $L_w = 90$ mm tended to decrease more when the ambient pressure increased beyond 2 MPa. Generally, lower velocity at longer impingement distances and more dispersed spray at higher ambient pressure conditions became the reason of above adhered mass decreasing.

Ko and Arai **[9, 10, 11]** also reported adhered fuel mass ratio using jerk injection system which injection pressure might be lower than 40 MPa. They showed impingement distance effect in a range of ambient pressures from 0.1 MPa to 1.5 MPa, and suggested the increasing trend of adhered mass ratio with an increase of impingement distance. Similar tendencies with impingement distance were observed in **Fig. 6-5** under ambient pressures of 0.5 MPa and 1 MPa. Then in a range of ambient pressure lower than 1 MPa, it could be concluded that increasing trend of adhered mass ratio with impingement distance appeared under wide injection pressure condition which included jerk injection and common rail injection systems. While at higher ambient pressures such as 2 MPa and 4 MPa, some of other effects appeared under long impingement distance conditions.

(a) $P_{inj} = 130$ MPa   (b) $P_{inj} = 40$ MPa
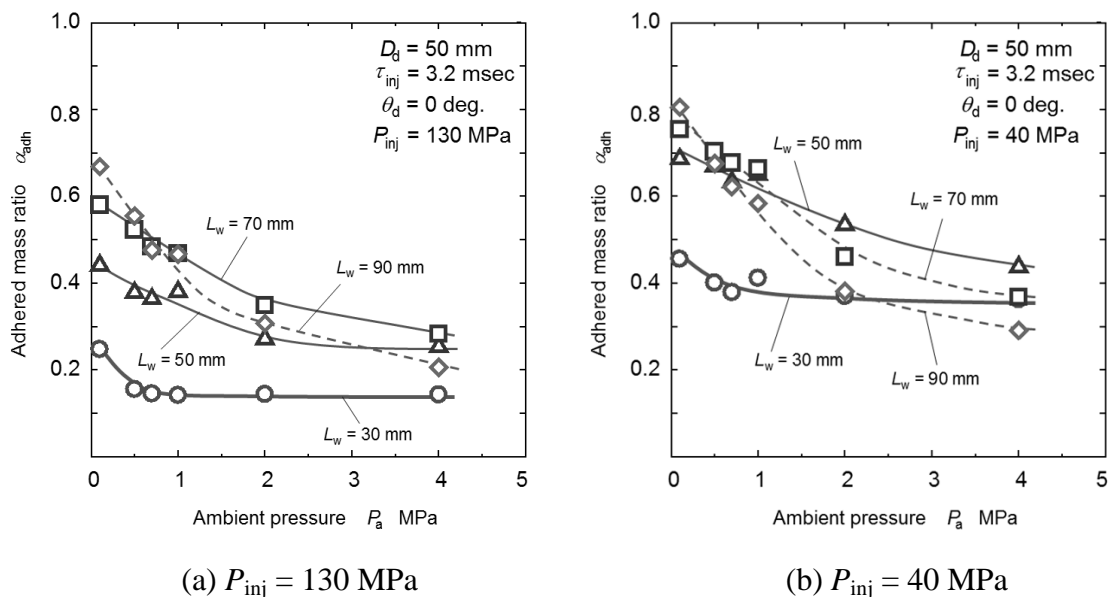
Figure 6-5 Effects of ambient pressure and impingement distance on adhered mass ratio

6.5 Impingement spray behavior and height of impingement spray

### 6.5.1 Ambient pressure effects on 130 MPa injection spray

Figure 6-6 shows shadowgraphic images of 130 MPa injection spray under various impingement distances. Images were noted by the time after impingement start. The time after impingement start (t_{ais}) could be obtained as follows.

$$t_{ais} = t_{asoi} - t_{is} \qquad (6\text{-}1)$$

Where t_{asoi} was elapsed time after start of injection and t_{is} was the time impingement. Since the frame rate of high-speed camera was 2000 frame/sec, these times had some undefinable error of 0.2 msec. Ambient pressure conditions of 0.5 MPa and 4 MPa was chosen here as the examples. Ambient pressure of 0.5 MPa was the special case of low ambient pressure, where re-bounded spray movement was slightly restricted by surroundings. And it movement was strongly suppressed under high ambient density condition such as 4 MPa.

Two series of photographs for the short impingement (L_w = 30 mm) are shown in **Fig. 6-6 (a)**. As for the photo-series of P_a = 0.5 MPa shown as upper images in **Fig. 6-6 (a)**, impingement started approximately at t_{is} = 0.5 ms. Typical impingement phenomena were clearly observed. The impinged spray expanded to the lateral side direction. On the other hand, as for P_a = 4 MPa (lower images in **Fig. 6-6 (a)**), impingement started at around t_{is} = 1 ms which was later than the impingement of P_a = 0.5 MPa. Delayed start of impingement means a lower velocity impingement due to high ambient pressure effect. Impinged spray was also expanded to the lateral side. Further, rolling up motion was clearly observed at the tip of post-impingement spray. Owing to this motion, thickness or height of post-impingement spray grew-up with the time elapsed.

D_d = 50 mm , L_w = 30 mm t_{ais} = time after impingement start
P_{inj} = 130 MPa , P_a = 0.5 MPa t_{asoi} = time after start of injection
t_{is} = 0.5 ms t_{is} = impingement time $t_{ais} = t_{asoi} - t_{is}$
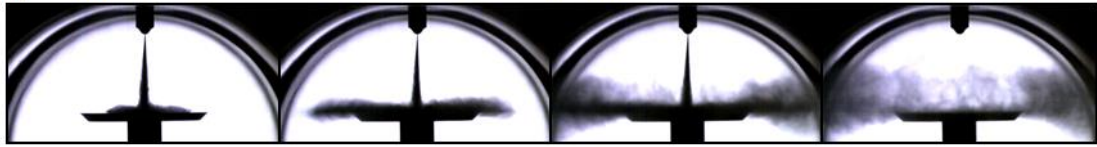
t_{ais} = 0 ms t_{ais} = 1 ms t_{ais} = 3 ms t_{ais} = 5 ms

P_{inj} = 130 MPa , P_a = 4 MPa

t_{is} = 1 ms
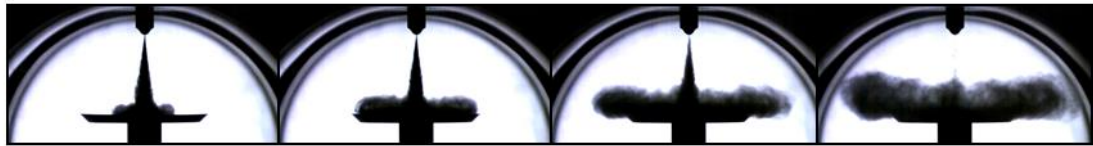
t_{ais} = 0 ms t_{ais} = 1 ms t_{ais} = 3 ms t_{ais} = 5 ms

(a) L_w = 30 mm

D_d = 50 mm , L_w = 50 mm t_{ais} = time after impingement start
P_{inj} = 130 MPa , P_a = 0.5 MPa t_{asoi} = time after start of injection
t_{is} = 1 ms t_{is} = impingement time $t_{ais} = t_{asoi} - t_{is}$
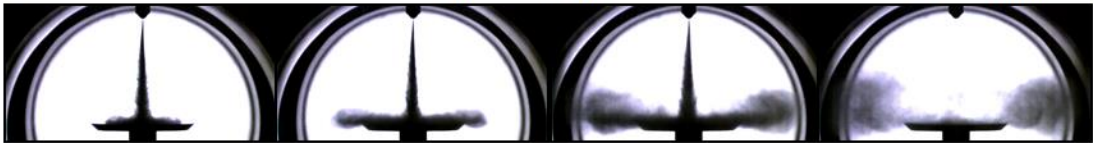
t_{ais} = 0 ms t_{ais} = 1 ms t_{ais} = 3 ms t_{ais} = 5 ms

P_{inj} = 130 MPa , P_a = 4 MPa

t_{is} = 1.5 ms

t_{ais} = 0 ms t_{ais} = 1 ms t_{ais} = 3 ms t_{ais} = 5 ms

(b) L_w = 50 mm

D_d = 50 mm , L_w = 70 mm t_{ais} = time after impingement start

P_inj = 130 MPa , P_a = 0.5 MPa t_{asoi} = time after start of injection

t_{is} = 1 ms t_{is} = impingement time $t_{ais} = t_{asoi} - t_{is}$
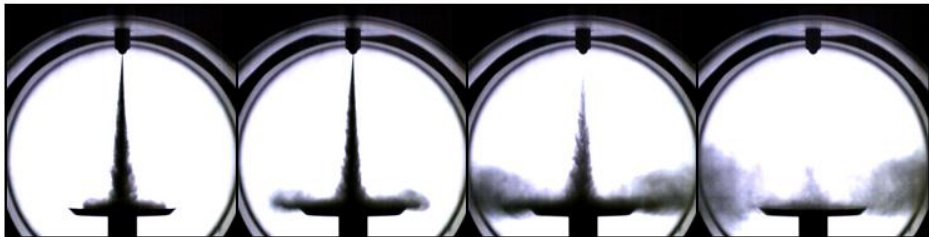
t_ais = 0 ms t_ais = 1 ms t_ais = 3 ms t_ais = 5 ms

P_inj = 130 MPa , P_a = 4 MPa

t_{is} = 2.5 ms
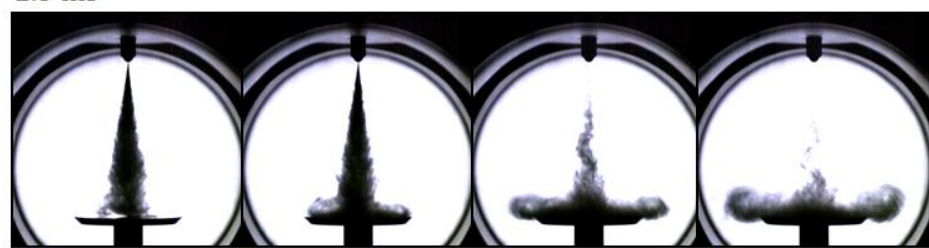
t_ais = 0 ms t_ais = 1 ms t_ais = 3 ms t_ais = 5 ms

(c) L_w = 70 mm

D_d = 50 mm , L_w = 90 mm t_{ais} = time after impingement start

P_inj = 130 MPa , P_a = 0.5 MPa t_{asoi} = time after start of injection

t_{is} = 1.5 ms t_{is} = impingement time $t_{ais} = t_{asoi} - t_{is}$
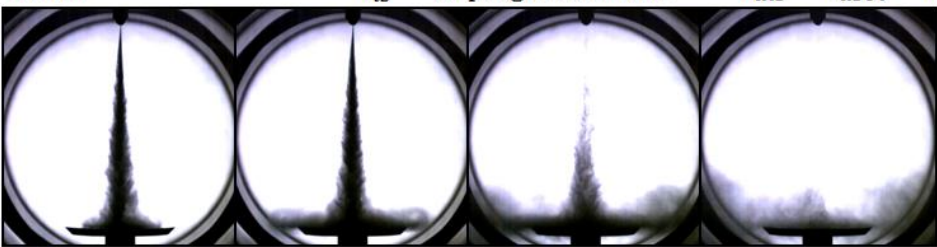
t_ais = 0 ms t_ais = 1 ms t_ais = 3 ms t_ais = 5 ms

P_inj = 130 MPa , P_a = 4 MPa

t_{is} = 4 ms
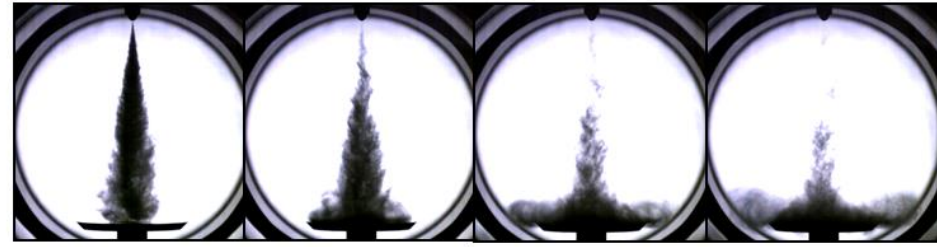
t_ais = 0 ms t_ais = 1 ms t_ais = 3 ms t_ais = 5 ms

(d) L_w = 90 mm

Figure 6-6 Shadowgraphic images of 30, 50, 70 and 90-mm impingement spray
with effects of ambient pressure (P_inj = 130 MPa)

The impingement phenomena at impingement distance of 50 mm are shown in **Fig. 6-6 (b)**. Impingement started approximately at t_{is} = 1 ms for P_a = 0.5 MPa. The impinged spray expanded to the lateral side direction. Besides, for P_a = 4 MPa, impingement started at around t_{is} = 1.5 ms. Impinged spray was also expanded to the lateral side. Further, the rolling up motion was more clearly observed than L_w = 30 mm (**Fig. 6-6 (a)**).

Figure 6-6 (c) shows the impingement phenomena at 70 mm distance. It showed the similar trend as L_w = 50 mm, but the rolling up motion appeared weaker due to longer impingement distance. When impingement distance increased to 90 mm, as shown in **Fig. 6-6 (d)**, more time was needed for spray to arrive at the wall. At ambient pressure of 0.5 MPa, the impingement time was around 1.5 ms. While at P_a = 4 MPa, the impingement time was around 4 ms. The impingement started approximately after the end of fuel injection. The spray seemed to impinge weakly for both ambient pressure conditions.

In order to understand the behavior of impingement spray, height of impingement spray was evaluated. **Figure 6-7** was the height of impingement spray corresponding **Fig. 6-5 (a)** and **Fig. 6-6** (P_{inj} = 130 MPa). Height of impingement spray (H) was defined as height or thickness of the lateral spray at the side end of disk as indicated in the figure. It was measured at 1 msec after start of impingement (t_{ais}). This definition was different from the definition used in Chapter 3 (**Fig. 3-12**). However time after start of impingement could represent the impingement behavior more clearly than the fixed elapsed time from injection start, because t_{is} (**Equation (6-1)**) took various times according ambient pressure and impingement distance.

A thicker line of L_w = 30 mm showed a smooth trend and was different from the other impingement distance cases. At ambient pressures of 0.5 MPa and 1 MPa, the height of impingement spray increased according to an increase of impingement distance. At these ambient pressures, impingement Weber numbers higher than 600 were estimated except 90 mm impingement. Then it shows that there was a possibility that impingement droplet or liquid film broken up into small droplets and tended to rise up the height of impingement spray.

As for P_a = 2 MPa, the height of impingement spray for L_w = 30 mm was highest among four tested impingement distances. Further, the height of impingement spray at L_w = 90 mm was higher than the L_w = 50 mm and 70 mm. However at P_a = 4 MPa, the height of impingement spray decreased with an increase of impingement distances. Higher the ambient pressure, injected fuel became fully developed to a complete spray before it impinged on the wall. It

means that a dense core region of spray did not impinge on the wall at a longer impingement distance. Thus, at higher ambient pressure condition as 4 MPa, the height of impingement spray decreased with an increase of impingement distance. Similar impinging characteristics were also reported by Park and Lee [12] and Andreassi et al. [13].
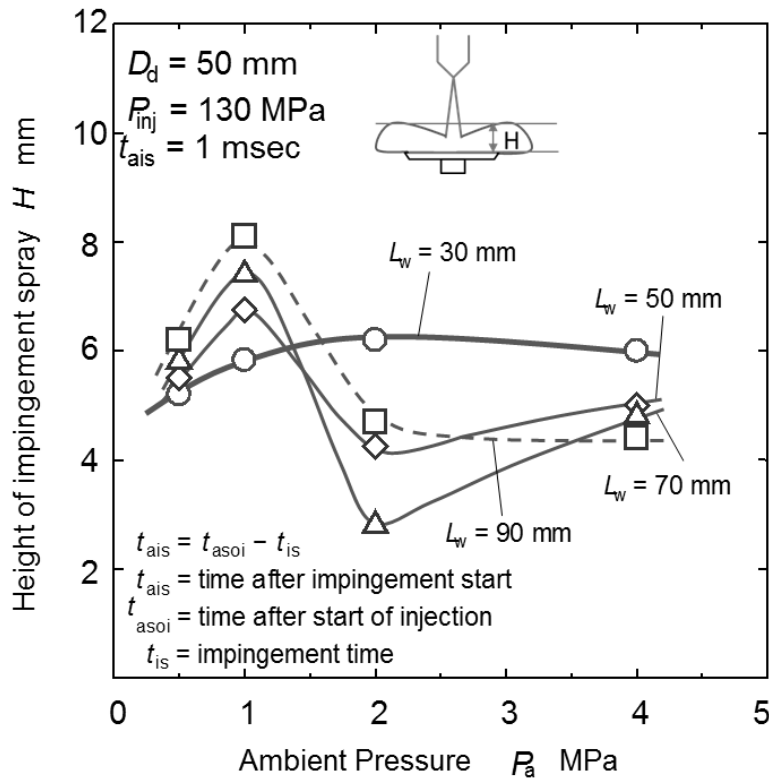
Figure 6-7 Behavior of height of impingement spray at P_{inj} = 130 MPa

6.5.2 Ambient pressure effects on 40 MPa injection spray

Injection pressure of 40 MPa was selected as the example of low injection pressure since at a lower injection pressure caused low spray velocity and its movement was affected strongly by ambient surroundings. **Figure 6-8** shows shadowgraphic images under the low injection pressure of 40 MPa. Here two impingement distances (L_w = 30 mm and L_w = 90 mm) cases are shown for the comparison with **Fig. 6-6** (P_{inj} = 130 MPa). As for P_a = 0.5 MPa at L_w = 30 mm (upper images of **Fig. 6-8 (a)**), the impingement started approximately at 1 ms which was later than P_{inj} = 130 MPa (upper images of **Fig. 6-6 (a)**). At t_{ais} = 1 ms, the height of impinged spray looked like a very thin film. The lateral spray development was also observed but it showed weaker than that of P_{inj} = 130 MPa.

Further, as the time elapsed, there was no upward movement of impinging spray occurred. As for P_a = 4 MPa at L_w = 30 mm (lower images of **Fig. 6-8 (a)**), the rolling up motion appeared slightly. This weaker rolling up motion was resulted from less height of impingement spray as compared to P_{inj} = 130 MPa.

D_d = 50 mm , L_w = 30 mm t_{ais} = time after impingement start
P_{inj} = 40 MPa , P_a = 0.5 MPa t_{asoi} = time after start of injection
t_{is} = 1 ms t_{is} = impingement time $t_{ais} = t_{asoi} - t_{is}$

t_{ais} = 0 ms t_{ais} = 1 ms t_{ais} = 3 ms t_{ais} = 5 ms

P_{inj} = 40 MPa , P_a = 4 MPa
t_{is} = 1 ms

t_{ais} = 0 ms t_{ais} = 1 ms t_{ais} = 3 ms t_{ais} = 5 ms

(a) L_w = 30 mm

D_d = 50 mm , L_w = 90 mm t_{ais} = time after impingement start
P_{inj} = 40 MPa , P_a = 0.5 MPa t_{asoi} = time after start of injection
t_{is} = 1.5 ms t_{is} = impingement time $t_{ais} = t_{asoi} - t_{is}$

t_{ais} = 0 ms t_{ais} = 1 ms t_{ais} = 3 ms t_{ais} = 5 ms

P_{inj} = 40 MPa , P_a = 4 MPa
t_{is} = 7.5 ms

t_{ais} = 0 ms t_{ais} = 1 ms t_{ais} = 3 ms t_{ais} = 5 ms

(b) L_w = 90 mm

Figure 6-8 Shadowgraphic images of 30 and 90-mm impingement spray with effects of ambient pressure (P_{inj} = 40 MPa)

As for $P_a = 0.5$ MPa at $L_w = 90$ mm (upper images of **Fig. 6-8 (b)**), spray impinged weakly at $t_{is} = 1.5$ ms. After then, low height of impingement spray appeared and there was no roll-up motion. Further as for $P_a = 4$ MPa at $L_w = 90$ mm (lower images of **Fig. 6-8 (b)**), the impingement started approximately at $t_{is} = 7.5$ ms. This impingement time was extremely late and far delayed from injection end (injection period = 3.2 ms). It means the extremely low impingement velocity. In this condition, the impinging behavior on the wall was much different. It seems that the spray impinged on the wall with less penetration forces. Moreover as the time elapsed, impinged spray looked like stagnant without expanding to lateral direction and no roll-up motion appeared.

Figure 6-9 was the height of impingement sprays corresponding to $P_{inj} = 40$ MPa. The height of impingement spray was changed in various ways. The height of impingement spray seemed to be lower as compared to $P_{inj} = 130$ MPa (**Fig. 6-7**). It seems to be caused by low Weber number of 40 MPa injection. Weber number of 30 mm impingement was not so low and was changing from 7220 (0.5 MPa) to 264 (4 MPa). It seems to be the main reason of the relatively high height of 30 mm impingement.
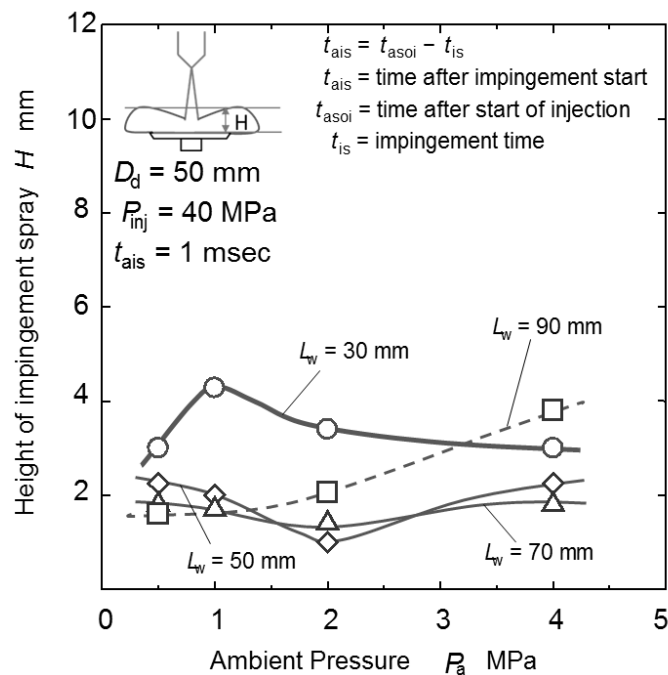
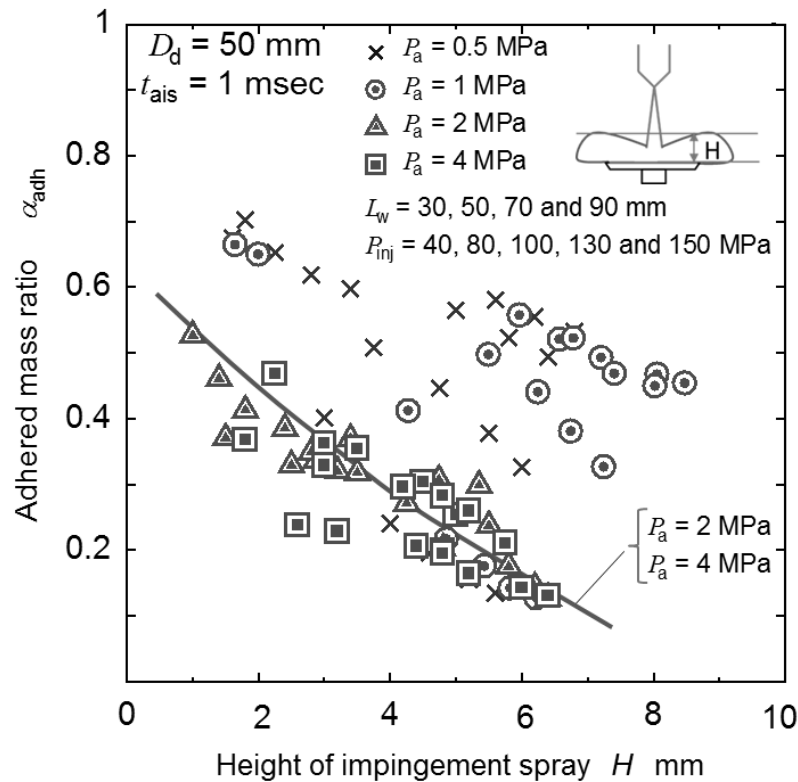**Figure 6-9** Behavior of height of impingement spray ($P_{inj} = 40$ MPa)

While at $L_w = 50$ mm and 70 mm, both heights of impingement sprays were changing in similar ways. They took the minimum at $P_a = 2$ MPa. However, at $L_w = 90$ mm, spray height monotonously increased. At $P_a = 4$ MPa, Weber number

decreased to 41 and the height of 90 mm impingement spray was higher than other impingement distances. Under lower Weber number than 80, when the droplet impinged to the wall, it might stick, but direct impingement hardly occurred because of low impingement velocity or stagnation near the wall. The behavior of stagnated spray near the wall was somewhat different from other spray that developed to lateral side, and height of impingement spray increased by another mechanism such as spray stagnation.

6.5.3 Relationship between adhered fuel mass and height of impingement spray

Figure 6-10 shows the relationship between adhered mass ratio and height of impingement spray. There were many un-certain problem in the definition of height of impingement spray and in practical measurement of it. It was considered that one of the reasons of the complicated results in Sections 6.5.1 and 6.5.2 came from them. Whereas, the relationship between height of impingement spray and adhered fuel mass ratio was simply expressed as shown here. The result shows that the adhered mass ratios scattered at any height of impingement spray. Especially for adhered mass ratios under ambient pressures of 0.5 MPa and 1 MPa, they scattered widely due to complex effects of injection pressure and impingement distance. However they showed decreasing tendency with impingement spray height. Further, adhered mass ratios under ambient pressures of 2 MPa and 4 MPa showed a monotonous decrease with an increase of the height. There were no obvious differences between 2 MPa and 4 MPa.

High height of impingement spray suggested the impingement phenomena with strong rebound of droplets and it resulted less adhesion. Almost similar result was pointed in **Fig. 3-12** (Chapter 3). In Chapter 3, the results were suggested that adhered mass ratio decreased with increasing of height of impingement spray under ambient pressure of 1 MPa. The results shown in **Fig. 6-10** indicated that there was a strong relationship between adhered mass ratio and height of impingement spray under high ambient pressure conditions such as 2 MPa and 4 MPa. In other words, adhered mass ratio of highly rebounded impingement spray was low. When the ambient pressure was low such as 0.5 MPa and 1 MPa, adhered mass ratio was also affected injection pressure and impingement distance as shown in **Fig. 6-7** and **Fig. 6-9**.

Figure 6-10 Relationship of height of impingement spray and adhered mass ratio

6.6 Weber number correlation on adhered mass ratio

In order to evaluate the effects of impinging velocity (V_{imp}) and mean diameter (D_{SMD}) of impinging spray on adhered mass ratio, Weber number (We_d) effects were summarized as shown in **Fig. 6-11**. In general, the adhered mass ratio seemed to decrease with an increase of Weber number. However as ambient pressure changing from 0.5 MPa to 4 MPa, adhered mass ratios were widely scattered. It could be observed that adhered mass ratios for ambient pressures 0.5 MPa - 0.7 MPa and 2 MPa - 4 MPa were divided by the condition of ambient pressure of 1 MPa. In order to establish correction factor for ambient pressure, 1 MPa was adopted as the closest reference which divided two regions of low and high ambient pressure. At the lower ambient pressure, the adhered mass ratio appeared above a dash line, while at higher ambient pressure it appeared below the dash line.
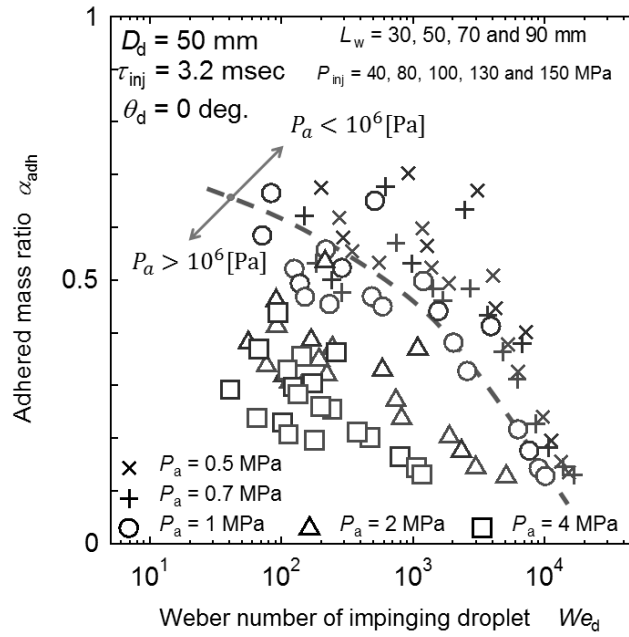
Figure 6-11 Weber number of impinging droplet and adhered mass ratio

A correction factor f_{press} for ambient pressure was introduced by **Equation (6-2)** to explain the above results.

$$f_{press} = \left(\frac{P_a}{P_{a.reference}}\right)^n \qquad (6\text{-}2)$$

According the trend shown in **Fig. 6-11**, $n = 0.5$ (experimental constant) and $P_{a.reference} = 1.0$ MPa were adopted in this study. The reason why $P_a = 1.0$ MPa was used as the reference pressure was that ambient pressure effects on adhered fuel mass ratio shown in previous sections of this chapter was dramatically changed between lower and higher than $P_a = 1.0$ MPa. Then, modified adhered mass ratio β_{adh} with ambient pressure effect was introduced by **Equation (6-3)**.

$$\beta_{adh} = \alpha_{adh} \cdot \left(\frac{P_a}{1 \times 10^6}\right)^{0.5} \qquad (6\text{-}3)$$

Figure 6-12 shows the relationship between Weber number of impinging droplet and modified adhered mass ratio (β_{adh}) mentioned above. The power of -0.5 was chosen by several trial and error to obtain the linear relationship of two correlation lines. The adhered mass ratios were successfully modified and plots of

their modified adhered mass ratios were gathered to a unique plot group. In other words, ambient pressure dependence could be compensated.

The modified adhered mass ratios could be summarized in two different ranges of We_d. First decreasing trend of modified adhered mass ratio was in a We_d range of 40 to 1000. It seems that $We_d = 1000$ was a transient condition of the trend. The modified adhered mass ratio decreased rapidly when We_d was over this transient Weber number. The second decreasing trend appeared in a We_d range of 1000 to 15000. It was clear that the modified adhered mass ratio was uniquely correlated by the Weber number for all conditions where lower and higher ambient pressures than 1 MPa were included. There were two correlation lines drawn in **Fig. 6-12** and following two equations were derived.

$$\alpha_{adh} = 0.85 \cdot \left(\frac{P_a}{10^6}\right)^{-0.5} \cdot We_d^{-0.11} \qquad (6\text{-}4)$$

$$\alpha_{adh} = 27 \cdot \left(\frac{P_a}{10^6}\right)^{-0.5} \cdot We_d^{-0.61} \qquad (6\text{-}5)$$

Here the same empirical constants as in Chapter 5 were used for convenience of future discussion. **Equation (6-4)** was based on a range lower transient condition of $We_d = 1000$. While, the plots for these We_d being larger than 1000 were correlated by **Equation (6-5)**.
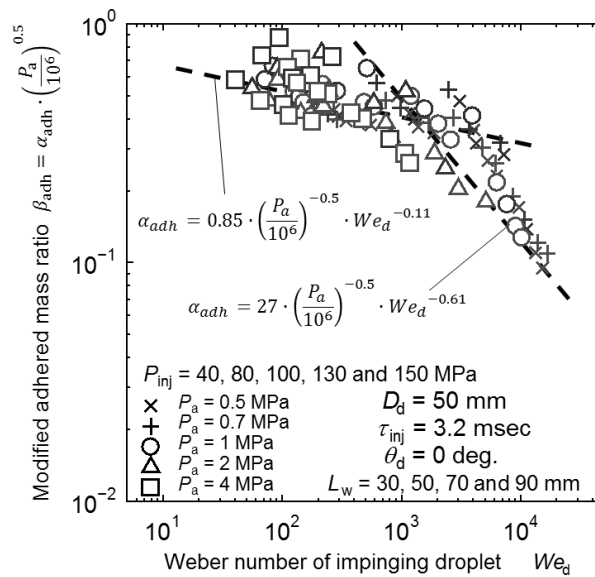
Figure 6-12 Relationship between We_d and modified adhered mass ratio for various ambient pressures

Referring to Chapter 5, in order to obtain the effect of inclination angle and disk size, the other modified adhered mass ratio α'''_{adh} was already introduced as **Equation (6-6)**. (See **Equation (5-6)**).

$$\alpha'''_{adh} = \frac{\alpha_{adh}}{k \cdot \cos \theta_{d}} \qquad (6\text{-}6)$$

Here, k was a modification factor of disk size that was smaller than the critical diameter of disk and θ_{d} was an inclination angle of the disk. Then, using the **Equation (6-6)**, more general modification of adhered mass ratio β'_{adh} was introduced by **Equation (6-7)**.

$$\beta'_{adh} = \frac{1}{k} \cdot \left(\frac{P_{a}}{1\times10^{6}}\right)^{0.5} \cdot \frac{\alpha_{adh}}{\cos \theta_{d}} \qquad (6\text{-}7)$$

Relationships between Weber number ($We_{d.n}$) of droplet and general modified adhered mass ratio $\left(\beta'_{adh}\right)$ were summarized in **Fig. 6-13**. Weber number ($We_{d.n}$) of droplet was defined as the Weber number with normal impingement velocity. Here all the data previously in Chapter 5 were referred in the figure. The plotted data in the figure were results of various combinations of ambient pressures, impingement distances, disk diameters, inclination angles and injection pressures. The trend similar to **Fig. 6-12** appeared even though these plots consisted of the results with various parameters mentioned above. There were two correlation lines drawn in **Fig. 6-13** and following two equations were derived.

$$\alpha_{adh} = 0.85 \cdot k \cdot \left(\frac{P_{a}}{10^{6}}\right)^{-0.5} \cdot \cos \theta_{d} \cdot We_{d.n}^{-0.11} \qquad (6\text{-}8)$$

$$\alpha_{adh} = 27 \cdot k \cdot \left(\frac{P_{a}}{10^{6}}\right)^{-0.5} \cdot \cos \theta_{d} \cdot We_{d.n}^{-0.61} \qquad (6\text{-}9)$$
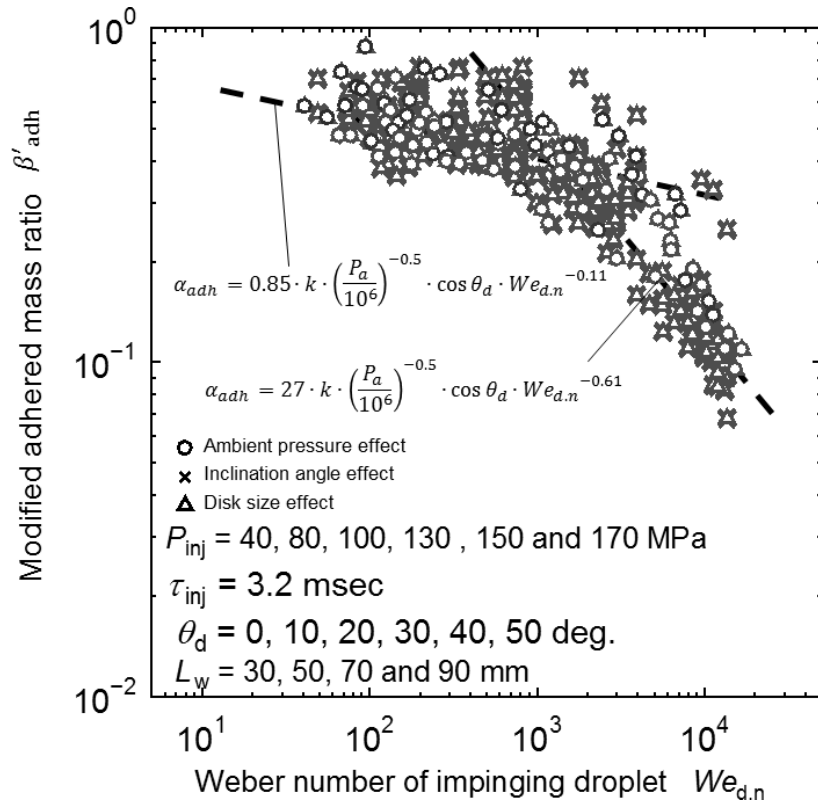
Figure 6-13 General modified adhered mass ratio for various ambient pressures, injection pressures, inclination angles and impingement disk diameters

Then, in order to express more sophistically the ambient pressure effect, Jet number that had the density term of surroundings was introduced here. As for the physical meaning, pressure correction shown in **Fig. 6-2** should be considered as the density effect of surroundings. The physical meaning of the original Jet number proposed by Tanasawa and Toyoda **[14]** was the non-dimensional number of liquid jet stability modified by density effect of surroundings and was expressed as follows.

$$Je = \frac{\rho_l \cdot V_{inj}^2 \cdot D_n}{\sigma} \cdot \left(\frac{\rho_a}{\rho_l}\right)^{0.55} \tag{6-10}$$

Then in this study, a Jet number based on impingement droplet stability was introduced. It was formulated as follows.

$$Je = \frac{\rho_l \cdot V_{imp}^2 \cdot D_{SMD}}{\sigma} \cdot \left(\frac{\rho_a}{\rho_l}\right)^{0.5} \tag{6-11}$$

In original *Je*, $(\rho_a/\rho_l)^{0.55}$ was used as the density effect, but here, exponential index of 0.5 was used to correlate the pressure effect obtained in the present experiment. **Equation (6-8)** and **Equation (6-9)** could be re-arranged using this Jet number. Then final empirical equations were as follows.

For $We_{d.n} < 1000$:

$$\alpha_{adh} = 0.10 \cdot k \cdot \cos\theta_d \cdot \frac{We_{d.n}^{0.89}}{Je} \qquad (6\text{-}12)$$

For $We_{d.n} > 1000$:

$$\alpha_{adh} = 3.2 \cdot k \cdot \cos\theta_d \cdot \frac{We_{d.n}^{0.39}}{Je} \qquad (6\text{-}13)$$

6.7 Summaries

In this chapter, the adhesion characteristics of impinging diesel spray under various ambient pressure, injection pressure and impingement distance were investigated. In addition, empirical equations obtained in Chapter 5 was further enhanced and formulated new empirical equations which accounted ambient pressure effect. Furthermore, the Jet number was introduced as the sophisticated expression. Then, the results was summarized as follows.

1. Higher the ambient pressure and higher the injection pressure, adhered mass fuel tended to decrease.
2. As for long impingement distances such as 70 mm and 90 mm, adhered fuel mass in high ambient pressure condition such as 4 MPa was half of that under 1 MPa condition. However ambient pressure had no effect on the adhered mass under the condition of 30 mm impingement.
3. Height of impingement spray changed in various ways under various ambient pressures. In general, height of impingement spray increased, less adhered fuel on the disk was obtained.
4. Using the correction factor for ambient pressure, adhered mass trend could be expressed by the modified adhered mass ratio.
5. There were two adhered mass ratio trends which were separated by the transient Weber number ($We_{d.n} = 1000$). The modified adhered mass ratio rapidly decreased in a range of Weber number higher than this transient Weber number.

6. The adhered mass ratio could be correlated by using Weber number and Jet number.

References

[1]   Kobayashi, M., Aoyagi,Y., Adachi, T., Murayama, T., Noda, A., Goto, Y. and Suzuki, H., Effects of high boost and high EGR on the super clean diesel engine, *Proc. of COMODIA-2008*, pp. 129-136, 2008.

[2]   Aoyagi, Y., Kunishima, E., Asaumi, Y., Aihara, Y., Odaka, M. and Goto, Y., Diesel Combustion and Emission using High Boost and High Injection Pressure in a Single Cylinder Engine, *JSME International Journal*, Vol. 48, pp. 648-655, 2005.

[3]   Aoyagi, Y., Osada, H., Misawa, M., Kobayashi, M., Noda, A., Goto, Y. and Suzuki, H., Low NOx diesel combustion using of high rate of cooled EGR, *Proc. of 6th Asia-Pacific Conference on Combustion*, pp. 35-42, 2007.

[4]   Osada, H., Aoyagi, Y. and Kazuaki, S., Goto, Y. and Suzuki, H., Reduction of NOx and PM for a heavy duty diesel using 50% EGR rate in single cylinder engine, *SAE International Journal*, no. 2010-01-1120, pp. 65-80, 2010.

[5]   Tabata, M., Arai, M. and Hiroyasu, H., The sauter mean diameter of a diesel spray in an elevated pressure enviroment, *Proc. of ICLASS*, pp. 405-410, 1988.

[6]   Arai, M., Physics behind diesel spray, *Proc. of 12th International Conference on Liquid Atomization and Spray Systems (ICLASS-2012),* CD/contribution 1419, pp. 1-18, 2012.

[7]   Ohta, T., Furuhata, T., Saito, M. and Arai, M., Behavior of diesel free spray in high ambient pressure conditions, *Proc. of ILASS-Asia*, pp. 15-20, 2008.

[8]   Senda, J., and Fujimoto, H.G., Multidimensional modeling of impinging sprays on the wall in diesel engines, *Applied Mechanics Review*, no. 94, pp. 341–348, 1994a (Japenese).

[9]   Ko, K., and Arai, M., Diesel spray impinging on a flat wall, Part 2: Volume and average air-fuel ratio of an impingement diesel spray, *Atomization and Sprays*, vol. 12, no. 5-6, pp. 753–768, 2002.

[10]   Ko, K., and Arai, M., Diesel spray impinging on a flat wall, Part 1: Characteristics of adhered fuel film in an impingement diesel spray, *Atomization and Sprays*, vol. 12, no. 5-6, pp. 737–751, 2002.

[11]   Ko, K., and Arai, M., Diesel spray and adhering fuel on an impingement wall, *SAE paper*, no. 2002-01-1628, 2002.

[12]   Park, S.W. and Lee, C.S., Macroscopic and Microscopic characteristic of a fuel spray impinged on the wall, *Experiments in Fluids*, pp.745-762, 2004.

[13]   Andreassi, L., Ubertini, S. and Allocca, L., Experimental and numerical analysis of high pressure diesel spray-wall interaction, *Int. J. of Multiphase Flow,* pp. 742-765, 2007.

[14]   Tanasawa, Y. and Toyoda, S., On the atomization of liquid jet issuing from a cylindrical nozzle, *Technical Report Tohoku Univ*, no. 19, pp. 135–156, 1955.

Chapter 7

Conclusions

The impinging diesel spray for non-evaporation condition was studied for the fundamental research of adhering fuel on the wall. The investigation in this study involves a single hole injection system for the whole experiment as to simplify the measurement works. Many parameters were considered in this study such as impingement distance, size of impingement disk, inclination angle, injection pressure and also the ambient pressure. As the spray impinged on the dry surface wall, the adhered fuel mass was measured as the main parameter in this study. Then adhered mass ratio was analyzed. From this study, we have drawn the following conclusions which reflected in the objectives of this study discussed earlier in Chapter 1.

(1) Effect of injection pressure and impingement distance

In order to clarify the fundamental of spray impingement, the effect of injection pressure and impingement distance on the adhering mass ratio were analyzed quantitatively. Various injection pressures and impingement distances were considered. Different size of impingement disk was used as an impingement wall. The effect of injection pressure and impingement distance on the wall area was discussed. Also, impingement behavior and height of post-impingement spray was discussed precisely.

As the results, at a low injection pressure such as 40 MPa, the adhered fuel mass obviously obtained higher in all impingement distances. The adhered mass ratio was inversely proportional to injection pressure. Also, at a short impingement distance such as 30 mm, the adhered fuel mass was unaffected by ambient pressure, because spray impinging at this distance has sufficient velocity to splash fuel film and to reduce adherance. While, at a long impingement distance such as 90 mm, a decrease of adhered fuel mass was clearly observed. Adhered fuel mass ratio has the potential to decline after reaching its peak when impingement velocity decreased beyond a critical velocity. Finally, it was found the height of post impingement spray increased, less adhered fuel on the disk is obtained.

(2) Impingement area and wall inclination effect

The liquid film formation on the wall mostly described by an area of fuel film adhered on the wall. Therefore, the relationship of impingement area and adhered mass fuel was analyzed by various sizes of impingement disk. Diesel spray impinged to a normal wall and an inclined wall were considered. Thus the effect of the normal and inclined wall on the adhering fuel mass were discussed. The critical area of disk was introduced. Spray width of spray and critical thickness of liquid film were discussed. Moreover, modified adhered mass ratio was introduced in order to explain the general trend of adhered fuel mass. Also, PIV analysis on inclined wall was discussed as to clarify the velocity flow near the wall.

Regardless of injection pressure and impingement distances, it was found that the adhered fuel mass become constant with increasing the diameter of the impingement disk. Also, thickness of liquid film tended to decrease with increasing of injection pressure. However, decreasing trends are different for various impingement distances. Further, by using the adhesion area factor of k, adhered mass trend was uniquely expressed by the modified adhered mass ratio even though the impingement disk diameter was smaller than the critical diameter of adhesion. Moreover, the adhered fuel mass ratio decreased with an increase of the inclination angle of disk. Using the substantial impingement mass factor of $\cos \theta_d$, adhered mass trend on inclination disk was uniquely expressed by the modified adhered mass ratio. Finally, from the flow pattern of PIV analysis, substantial impinged mass of fuel decreased due to the non-impinging part of the spray increased with an increase of inclination angle of wall.

(3) Weber number correlation on adhesion

In order to clarify the behavior of impinging droplet near the wall, impingement velocity and Weber number of droplet was used. The effect of Weber number of impinging droplet on adhered mass, modified adhered mass ratio concerning diameter of impingement disk and inclined angle was discussed. Also, empirical relationships among adhered mass ratio, thickness of adhered fuel film and Weber number were derived from the experimental works.

As the results, general modified adhered mass ratio was introduced to summarize the adhered mass with combinations of various impingement distances, disk sizes, inclination angles and injection pressures. Weber number of $We_{d.n}$

which was calculated by approaching velocity of droplet to the impingement wall was more dominant factor than the Weber number obtained by droplet absolute velocity. Further, the impingement of lower Weber number droplet produced thick film and adhered fuel mass was little influenced by the Weber number. Also it was observed, there were two decreased trends which were separated by the transient Weber number ($We_{d.n} = 1000$). The modified adhered mass ratio rapidly decreased in a range of Weber number higher than this transient Weber number. Finally, from the results of experimental works, the empirical equations concerning the adhered mass ratio were derived as follows.

a) $\alpha_{adh} = 0.85 \cdot k \cdot \cos\theta_d \cdot (We_{d.n})^{-0.11}$

b) $\alpha_{adh} = 27 \cdot k \cdot \cos\theta_d \cdot (We_{d.n})^{-0.61}$

(4) Ambient pressure effect

For designing high performance small engine, high boost intake pressure was adopted and intake pressure was becoming higher than the conventional engine. Thus, the ambient pressure effect was considered. At first, the effect of Weber number of droplet at impingement on ambient pressure was discussed. Then effect of adhered mass ratio on ambient pressure at various impingement distance was discussed. The shadowgraph images on ambient pressure effect were analyzed. The height of impingement spray was measured from the shadowgraph image. Moreover, relationship between Weber number of impinging droplet with adhered mass ratio and modified adhered mass ratio were discussed. From the above results, ambient pressure effect was considered using Jet number and empirical equations of adhered mass ratio were introduced.

As the results, ambient pressure has no effect on the adhered mass under the condition of 30 mm impingement. However, height of impingement spray changed in various ways under various ambient pressures. Higher the ambient pressure and higher the injection pressure, adhered mass fuel tended to decrease. As for long impingement distances such as 70 mm and 90 mm, adhered fuel mass in high ambient pressure condition such as 4 MPa was half of that under 1 MPa condition. In general, height of impingement spray increased, less adhered fuel on the disk was obtained. By using the correction factor for ambient pressure, adhered mass trend could be expressed by the modified adhered mass ratio. Also, it was obtained that there were two adhered mass ratio trends which were

separated by the transient Weber number ($We_{d.n} = 1000$). The modified adhered mass ratio rapidly decreased in a range of Weber number higher than this transient Weber number. Finally, it was found that the adhered mass ratio could be correlated by using Weber number and Jet number. Then final empirical equations were as follows.

a) For $We_{d.n} < 1000$:

$$\alpha_{adh} = 0.10 \cdot k \cdot \cos\theta_d \cdot \frac{We_{d.n}^{0.89}}{Je}$$

b) For $We_{d.n} > 1000$:

$$\alpha_{adh} = 3.2 \cdot k \cdot \cos\theta_d \cdot \frac{We_{d.n}^{0.39}}{Je}$$

where:

$$Je = \frac{\rho_l \cdot V_{imp}^2 \cdot D_{SMD}}{\sigma} \cdot \left(\frac{\rho_a}{\rho_l}\right)^{0.5}$$

(5) General view of this work

In this work, the characteristics of diesel spray were explained in order to achieve better understanding of the mechanism of spray especially on impinging diesel spray. Adhering fuel mass which was measured in this study was considered as the important factor in wall impingement spray. Several effects performed on adhered mass fuel such as impingement distance, injection pressure, impingement disk area, inclination angle and so on for clarifying the mechanism of adhesion. The concept of critical diameter and critical velocity was proposed in order to investigate the adhesion mechanism. Also, the empirical equation was derived from the experimental data. Furthermore, adhering fuel was considerably affected by Weber number. The adhering fuel mass on a wall has been treated as an important issue throughout this thesis. The results obtained in this study would be useful in diesel engine development and further experimental works.

(6) Future works

As well known, in the practical diesel engine, the combustion process activities consist of several complex processes such as the turbulent spray formation, vaporization of droplets and the combustion of fuel vapor. This combustion process occurred after mixture of fuel and air in certain ratios and

controlled by combustion temperature. Since in this study only focused on non-evaporation process which means not included temperature effect, in future, temperature effect on the wall should be added. In addition, the effect of wall surface roughness should also be considered.

List of publications

Journal papers

1. Akop, M.Z., Zama, Y., Furuhata, T., and Arai, M., Experimental investigations on adhered fuel and impinging diesel spray normal to a wall, *Atomization and Sprays*, Vol. 23, No.3, pp. 211–231, 2013.
2. Akop, M.Z., Zama, Y., Tomohiko, F., and Arai, M., Characteristics of adhesion diesel fuel on an impingement disk wall (Part 1: Effect of impingement area and inclination angle of disk), *Atomization and Sprays*, Vol. 23, No. 8, pp. 725–744, 2013.
3. Akop, M.Z., Zama, Y., Tomohiko, F., and Arai, M., Characteristics of adhesion diesel fuel on an impingement disk wall (Part 2: Droplet Weber number and adhered fuel mass), *Atomization and Sprays*, 2013, Accepted.
4. Akop, M.Z., Zama, Y., Tomohiko, F., and Arai, M., Characteristics of adhesion diesel fuel on an impingement disk wall (Part 3: Ambient pressure effect), *Atomization and Sprays*, 2013, Accepted.
5. Zama, Y., Sugawara, K., Akop, M.Z., Tomohiko, F., and Arai, M., Velocity distribution of post-impingement diesel spray on a wall (Part 1: Effect of impingement angle on flow pattern), Atomization and Sprays, 2013, Accepted.

Conference papers

1. Akop, M.Z., Zama, Y., Furuhata, T., and Arai, M., Effect of impingement distance and injection pressure on adhered fuel mass of diesel spray impinging on an inclined wall, *The 23rd Internal Combustion Engine Symposium (Japan)*, (Sapporo Japan), 2012.
2. Akop, M.Z., Zama, Y., Furuhata, T., and Arai, M., Effect of ambient pressure on adhered fuel mass of diesel spray impinging on a flat wall, *16th Annual Conference of ILASS-Asia*, (Nagasaki Japan), 2013.
3. Zama, Y., Sugawara, K., Akop, M.Z., Furuhata, T., and Arai, M., Velocity measurement of diesel spray impinging on a flat wall, *16th Annual Conference of ILASS-Asia*, (Nagasaki Japan), 2013.